Doctoral Dissertation (Shinshu University)

Development and properties of multifunctional biomedical nanocomposites

March 2018

Juhong Yu

Contents

Abstract

Tissue engineering is a promising alternative for treating bone defects caused by trauma, tumors, congenital malformations, degeneration, aging, or bone diseases. Scaffolds play a crucial role in tissue engineering because they represent an alternative to the conventional implantation of organs and tissues. They can provide an appropriate base for tissue growth and cell proliferation and of which the design can be improved to precisely match the irregular boundaries of bone defects as well as facilitate their clinical application. Shape memory polymers (SMP) are a well-known class of stimuli-responsive materials which can be controlled to hold a secondary shape but recover their permanent shape under an external stimulus. This property can be designed and altered by changing the structure, morphology, and various processing parameters of the polymer during fabrication. Hydroxyapatite (HAP) have been used in the bone tissue engineering field for bone filling due to its similar composition to the natural bone, excellent osteoconductibity and biocompatibility.

The purpose of these investigations is to design a three-dimensional porous nanocomposite scaffold which possesses high compression resistance, good shape memory recovery ratio and high biocompatibility. Good shape memory recovery ratio can lead the nanocomposite scaffold more precisely match the irregular boundaries of bone defects and the less time required for compression recovery can directly shorten the time of the operation. The significance of this investigation can lead to realization of advanced nanocomposite scaffold for application in minimally invasive surgery and bone defect repair.

(1) Four SMPU scaffolds (SMPU-200, SMPU-200-100, SMPU-100-50, and

SMPU-50) with the three-dimensional porous structure were fabricated via a salt-leaching-phase inverse technique, a unique method to fabric porous structure. The use of different size of NaCl particles to obtain scaffolds with different apertures was investigated. With increasing of the aperture, the porosity of the scaffolds increased from 77.13% to 83.13% and their compression recovery ratio increased from 97.77% to 99.30% at room temperature, but their shape recovery ratio decreased from 95.0% to 91.1% at 55 ℃ higher than T_g. Moreover, all SMPU scaffolds promoted cell proliferation on their surface, and the ability increased with the aperture of the scaffold.

(2) nHAP particles were fabricated by the liquid phase precipitation method with a rod-like shape and their sizes were ca. 30-40 nm in length and ca. 10 nm in width. Four controllable porous SMPU/nHAP composite scaffolds (SMPU/nHAP-200, SMPU/nHAP-200-100, SMPU/nHAP-100-50 and SMPU/nHAP-50) with three-dimensional structure, which was important for cell growth, were fabricated via the salt leaching-phase inverse technique, a unique method to fabric porous structure. Their physical characteristics, mechanical properties and shape recovery behaviors were investigated. With the increase of the aperture of scaffolds, the porosity, the compression strain (at the strength of 0.12 MPa) and compression recovery ratio of the porous SMPU/nHAP composite scaffolds were increased at room temperature, but their shape recovery ratio was decreased at 55 ℃ higher than T_g. Moreover, these four porous composite scaffolds had a cell proliferation promoting ability and the ability was increased with the increase of the aperture of the scaffolds.

(3) Five-step thermo-mechanical cycle test was used to investigate the shape recovery properties and the contribution of HAP particles was clarified. The effect of

nHAP particles in porous SMPU/nHAP composite scaffold was found to enhance the compression resistance by 37%, shorten the compression recovery time by 41% and reduce the tensile resistance by 78%. From the thermo-mechanical cycle test, SMPU/nHAP composite scaffold had good shape fixity property which was more than 97% and higher shape recovery ability which reached more than 99% after 3th cycle of training. Meanwhile, the addition of nHAP particles improved the proliferation of cells by 13% after 7 days of culture which indicated that the larger the porosity of scaffold was, the easier it was for the cell to adhere to and proliferate on the scaffolds. These results revealed that in minimally invasive surgery and bone repair surgery, this porous composite scaffold could significantly reduce the operative time, promote the bone cell growth and precisely match the irregular boundaries of bone defects. Therefore, this porous SMPU/nHAP composite scaffold design has potential applications for the bone tissue engineering.

List of Figures

Chapter 1

General Introduction

1 General Introduction

1.1 Progress of bone defects repair

Bone defects come from trauma, infection, tumor, and local bone loss caused by some congenital diseases [1]. Some data shows that there are 2.5 million people need to do bone transplantation every year in the US and 3 million patients in China [2-5]. Therefore, the more and more people are interested in researching the methods of bone defects repair. Until now, the commonly clinical methods of repair include bone grafting and bone tissue engineering.

1.1.1 Bone tissue

1.1.1.1 Cell types in bone tissue

Bone tissue contains four cell types, which include osteogenic cells, osteoblasts, osteocytes and osteoclasts.

Osteogenic cells are on the surface of bone tissue. When the bone growth, reconstruction and fracture repair, it can continuously proliferate and differentiate into osteoblasts.

Osteoblasts are also on the surface of bone tissue. Its function is to synthesize, secrete the organic components of bone formation, release the organic vesicles and secrete the phosphate which is close to the inorganic substance such as calcium. These promote the deposition of calcium and other inorganic substances in osteoid-like and to complete the mineralization. That is an important part of osteoid-like mineralization. Osteoblasts derived from mesenchymal precursor cells

(It also becomes fat cells, articular cartilage cells or muscle cells.) in bone marrow [6]. The main products of osteoblast maturation are collagen type I (90% of the organic components in bone tissue), bone specific VK dependent protein, osteocalcin and matrix Gla protein, phosphorylated glycoproteins include bone sialoprotein I and II, osteopontin, bone sialoprotein, proteoglycan and alkaline phosphatase.

Osteocytes are formed by the differentiation of osteoblasts around the bone matrix.These cells play an important role in bone regeneration and maintenance. They are the markers of bone tissue survival and participate in the regulation of blood calcium balance. Cells that are called the elongated cells in the column space or the matrix of the bone, Osteocytes exchange nutrients and oxygen in the blood vessels. The distant cells can obtain nutrients and oxygen through the tubule. Osteoblasts can release calcium ions by their own osteolysis to destroy calcium balance and destroy bone matrix [7].

Osteoclasts are specialized cellS located in small recesses on the surface of the bone tissue, through integrins to adhere on the cell surface [8]. The bone resorption of osteoclasts is primarily the dissolution of minerals, followed by the degradation of organic phases. These processes occur at the fold edge, dependent on the secretion of soluble enzymes and the acidic microenvironment [9]. Osteoclasts synthesised of large amount of lysozyme, especially anti tartaric acid salt of acidic phospholipase isozyme (marker of osteoclasts) and cysteine proteases such as cathepsin, in addition, lysozyme released only in the fold edge of osteoclasts [10].

1.1.1.2 Extracellular matrix composition of bone

Type I collagen is the main organic component of mineralized extracellular matrix,

which can reach about 90% of the total organic composition, and can act as a template for mineral precipitation. There is a small amount of collagen in bone tissue, some of which are bone specific [11]. In addition to the major collagen matrix, the bone also contains a number of other non collagenous proteins. Osteocalcin, a γ-carboxy glutamate protein, is a 6 kD non-collagen protein that accounts for 15% of non-collagen in bone tissue [12]. There are three carboxylic acid residues in the osteocalcin molecule, which are located at 17, 21, and 24, respectively, and contain a disulfide bond in the interior of the molecule, which is formed by the cysteine of the 23 position and the cysteine of the 29 position. Osteocalcin is the second most abundant protein in bone matrix, which is highly conserved in vertebrates [13]. The biological activity of osteocalcin is mainly related to bone turnover and bone mineralization.

Osteopontin is a phosphorylated glycoprotein secreted by the cells, mainly composed of osteoblastic cells and activated T lymphocytes. It can be found in the peripheral blood, bone tissue and some tumors. RGD sepuence (arginine-glycine-aspartate) is present in the osteopontin, which is also the recognition sequence of the adhesion molecules on the cell membrane. Osteopontin is a multifunctional protein that promotes cell adhesion and migration, inhibits bone mineralization and Ca^{2+} binding [14]. Due to the different modifications after translation, osteopontin has variety of forms. Some studies have got a highly phosphorylated form of osteopontin from isolation of bone tissue extracellular matrix mineralization, and the protein is secreted by osteoblast synthesis.

Extracellular matrix plays an important role in the function of growth factors. This process may involve the convergence of intracellular signaling pathways triggered by

extracellular matrix proteins and growth factors. That is important in the process of tissue regeneration. In addition to serving as a scaffold for mineralization, extracellular matrix has also become the basal layer of bone cell adhesion and proliferation. Once the osteocytes interact with the matrix, they deform and experience other changes in the bone marrow (matrix-cell crosstalk) [15]. On the other hand, the cells interact with the surrounding environment by anchoring in the matrix (cell-matrix crosstalk) [16].

1.1.2 Bone defect repair

In life, bone tissues are constantly suffered damages, most of micro damages can be regenerated by autologous repair, but when there is a large bone defect, autologous regeneration has been unable to do repair. Therefore, bone transplantation is required for defect repair. At present, the commonly used methods of bone transplantation include autogenous bone graft and allograft bone transplantation.

Autogenous bone graft was transplanted into the bone defect after removal of the bone. At present, the commonly used donor bone region includes iliac crest, tibia and fibula [17, 18]. Autologous bone grafts have good biocompatibility, do not cause immune rejection, and may carry some osteocytes, can promote the formation of new bone. However this method has some defects, due to the very limited number of available autologous bone, it is unable to meet the requirements of segmental bone defect repair. It needs two times surgery in the process of bone transplantation. This process will increase the operation time, bleeding volume, individual trauma and may cause some complications such as infection [19].

Allogeneic bone transplantation is usually referred to bone allograft, which is from

the same individual as bone source. Allogeneic bone has enough resource, easy to operate and cannot be limited by size and shape. Macewen performed allogeneic bone transplantation in 1880 for the first time ever. Inclean did research for preservation methods on bone in the 1941. After being set up with the bone bank, allograft bone is increasingly used in research on bone defect repair [20, 21]. However there are also some allograft bone defects. Allogeneic bone transplantation can achieve only about 20% of the desired effect. This result may cause immune rejection, and at the same time, allograft bone can also cause the spread of blood diseases (such as hepatitis).

1.1.3 Bone tissue engineering

Tissue engineering is an interdisciplinary subject, which was named in 1987 by the National Science Foundation [22-24]. The main operation method is to prepare a scaffold with good biocompatibility, which can be biological degraded in the body and absorbed by the body. Then the scaffold was combined with the cultured cells in vitro to form the cell-material complex (Figure 1.1). Scaffold materials provide the space needed for cell growth, nutrient transport, and the removal of cellular waste. After the cell-material complex is implanted into the body, the material will gradually degrade in the body, and the cells carried will further grow, reproduce, and gradually form a defective tissue or organ [25].

Bone tissue engineering is the combination of three elements of seed cells, growth factors and scaffold materials for bone tissue construction and regeneration in vivo and in vitro. The scaffold which provides space for cell growth, proliferation and differentiation, is a key factor in bone tissue engineering [6].

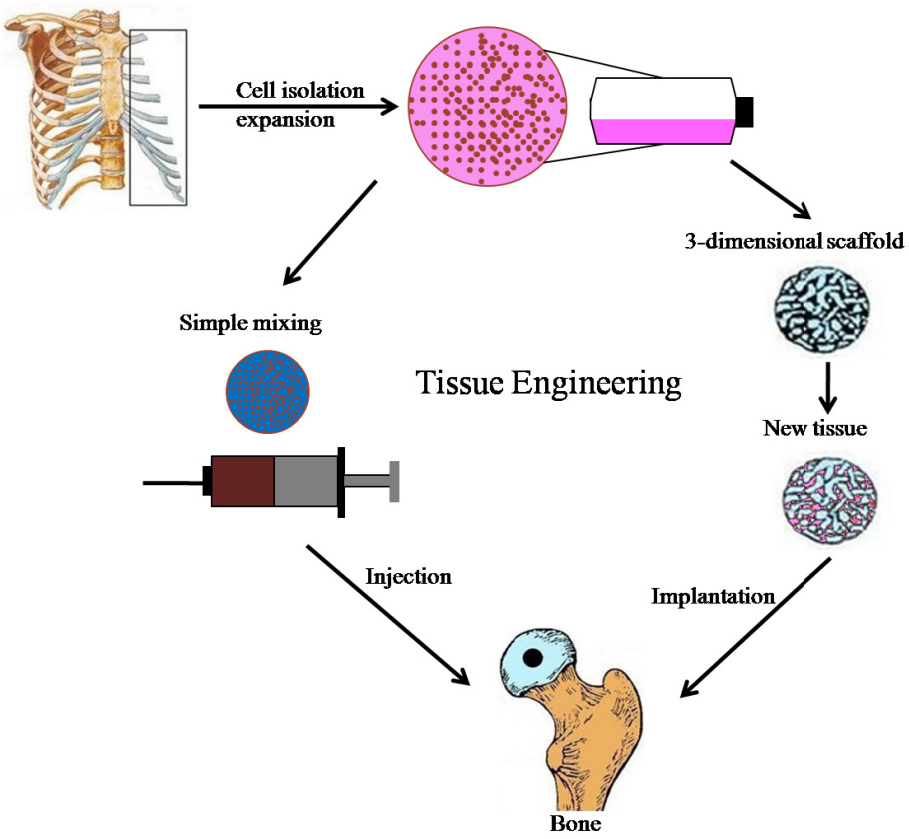

Figure 1.1 The structure of tissue engineering.

Bone repair material mainly through 3 mechanisms (bone conduction, osteogenesis and bone induction) to promote bone remodeling. Bone conduction means that the implant allow osteogenic precursor cells to grow and produce osteoblasts, and the capillaries and perivascular tissue into the body. Osteogenesis refers to the differentiation of osteoblast precursor cells, leading to the formation of new bone. The role of bone induction is that it can induce the differentiation of mesenchymal cells into osteoblasts and chondrocytes.

An ideal material for bone tissue engineering should meet the following requirements: good biocompatibility; after the implantation of material, the cells can

adhere and proliferate; material can be degraded in vivo, the degradation rate should match the regeneration speed of different tissue cell and the degradation products have no cell toxic, will not cause the body's inflammatory response; material should have a three-dimensional porous structure, plasticity and good mechanical strength [7].

1.1.3.1 Preparation of tissue engineering bone by natural polymer materials

At present, natural polymer materials such as collagen [26, 27], chitosan [28, 29], silk protein [30, 31] have been widely used in the construction of tissue engineering bone.

C.M. Murphy *et al*. [32] made a series of collagen-mucopolysaccharide scaffolds with an average aperture of 85 μm to 325 μm. The osteoblasts were seeded on the scaffold and the cell adhesion and proliferation were investigated. The results showed that after 7 days inoculation, the number of adherent cells was the highest when the aperture of scaffold was about 325 μm. However, when the time of inoculation was 2 days, the number of adherent cells was the highest on the scaffolds with aperture of 120 μm. The reason is that the surface area of the scaffold plays an important role for the initial cell adhesion. With the increase of the aperture of the scaffold, the scaffold was more favorable for cell proliferation. When the inoculation time was 7 days, the number of cells on the scaffolds with the aperture of 325 μm was the highest. In conclusion, the collagen-mucopolysaccharide scaffold with the aperture of 325μm had the best effect for bone tissue engineering.

Y. Zhang *et al*. [31] used CaP and silk fibroin to prepare the porous scaffold material. Firstly, the CaP/silk fibroin powder was prepared and dispersed in silk fibroin solution. Finally, the scaffolds were obtained by freeze-drying. The results

showed that the addition of CaP/silk fibroin powder increased the porosity of the scaffolds, and let the CaP evently distributed in the scaffolds. The human mesenchymal stem cells were cultured on the scaffolds, and the differentiation ability of the cells was enhanced. In vivo experiments also showed that the composite scaffold can promote the formation of new bone.

1.1.3.2 Preparation of tissue engineering bone by hydroxyapatite

Hydroxyapatite (HA), $Ca_{10}(PO_4)_6(OH)_2$, is the main inorganic component of natural bone. It is a kind of calcium phosphate salt containing hydroxyl, Ca/P ratio is 1.67. Calcium phosphate compounds, including a series of calcium phosphate salts with different Ca/P ratios, were used in the study of bone tissue engineering.

H. Tsurushima *et al*. [33] coated fibroblast growth factor on the surface of a hydroxyapatite ceramic material. In vitro experiments showed that growth factors could be released from the material and maintain its biological activity. The composite materials were implanted into the parietal bone defect in rats. The study found that the formation of of bone morphogenetic protein 2 can be detected at the implantation of composite materials, which can promote the formation of new bone in defect site. It is an ideal bone repair material.

G. Wang *et al*. [34] studied the effects of silk fibroin/hydroxyapatite composite on the repair of large segmental bone defects using a rabbit model. 4 kinds of silk fibroin/hydroxyapatite porous materials with different ratio of material, porosity, aperture and additives were prepared. The materials were transplanted into the rat to study its biodegradability. A kind of material with good mechanical property and degradability was selected in the 4 kinds of materials, which were cocultured with

rabbit bone marrow stromal cells. Then, a large section of bone defect was made in rabbits, and the composite material was implanted into the defect. It was found that both of the silk fibroin/hydroxyapatite material and silk fibroin/hydroxyapatite material seeded with bone marrow stromal stem cells could repair the defect site after 12 weeks, and the new bone could not be formed in the non implanted group. Among them, the bone repair effect of the group seeded with cells was more significant, which could be used as a substitute for bone transplantation.

S. Bhumiratana *et al*. [35] studied the nucleation and growth of mineralized bone matrix on silk fibroin/hydroxyapatite composite scaffold. A kind of porous silk fibroin scaffold with 3D was prepared, which has good biodegradability and biocompatibility. However, silk fibroin cannot induce bone formation, and the strength cannot meet the requirements of bone transplantation. Therefore, a new type of material which can induce the formation of new bone was prepared by silk fibroin scaffolds and hydroxyapatite particles. In addition, hydroxyapatite particles with the weight ratio of 1.6%, 3.1% and 4.6% were added to the silk fibroin scaffolds to improve the bone induction and mechanical properties. Mesenchymal stem cells were cultured on the surface of composite scaffolds, and the bone structure was found on the material and the Young's modulus of material was increased. The material is mainly through two ways to improve the formation of bone tissue engineering. The osteogenesis of the material increases the formation of bone matrix; the provision of nucleation sites for mineralization leads to the emergence of trabecular bone-like structures.

1.1.3.3 Degradation of bone tissue engineering materials

As a scaffold for bone tissue engineering, it should be able to be degraded after being implanted in the body, and absorbed or excreted by the tissue, finally replaced by the new tissue. The degradation rate of bone repair materials should be matched with the rate of new bone formation.

S. Park *et al*. [36] studied the relationship between the degradation of silk fibroin scaffold and bone formation. Two kinds of silk fibroin scaffolds with different degradation rates were prepared, and the bone formation and metabolism of bone marrow mesenchymal stem cells on 3D silk fibroin scaffold were studied. After 56 days of culture in vivo, it was found that the content of extracellular matrix was higher in the scaffolds with faster degradation. Metabolic analysis (glucose and lactate levels) showed that the scaffold with the faster degradation rate consumed more glucose, and the amount of lactic acid produced by bone marrow mesenchymal stem cells (MSCs) was higher. The results showed that the degradation rate of the scaffolds directly affected the cell metabolism, thus affected the rate of bone formation.

1.1.4 Outlook

In addition to the materials mentioned above, there are many commonly used bone tissue engineering biomaterials, such as titanium and other metal materials, bioceramic materials, polymers, etc. Different materials have different properties, the same material with different treatment methods will lead to different changes in their structure and properties. In short, with the further understanding of the structure and properties of materials, the preparation process and the gradual development of

modification technology, we believe that finally the tissue engineering bone will be prepared with the structure and performance comparable to natural bone.

1.2 Current research status of hydroxyapatite

Hydroxyapatite (HAP), $Ca_{10}(PO_4)_6(OH)_2$ with molecular weight of 1004, is belonging to the structure of the six party. It is a component of human hard tissue and has good biological activity, bone guidance and biocompatibility [37, 38].

Since Aoki and Jarcho have been synthesized HAP in 1970s, it has been widely used in basic research and clinical application. As a carrier of bone tissue drug delivery systems, HAP material has the following advantages: 1) chemical composition similar to natural bone and teeth; 2) good affinity, which can be used for long-term treatment of hard tissue; 3) strong adsorption, it can easily realize the absorption of the drugs and load. Therefore, it has become one of the hot topics of international research. For example: the application of various methods of HAP alone or with other material made the porous material, which can be used as carrier of antibiotics, anti-inflammatory drugs, growth factor and polypeptide drugs, such as α interferon [39], amino glucoside [40], gentamicin [41], methylene blue [42], ibuprofen [43], cytochrome [44], serum protein [45] and bone formation protein [46], they reached the purpose of protection and sustained release of drug. Therefore, HAP is usually used as a filling material for bone defect sites or as a surface coating to promote bone ingrowths into the implant.

1.2.1 Method for synthesizing hydroxyapatite material

At present, the mainly preparation methods of hydroxyapatite are dry synthesis

and wet synthesis.

1、Dry synthesis

C.C. Silva *et al.* [47] prepared the hydroxyapatite particles by mechanochemical method (grinding pressure method) and the diameter of particles was 22-39 nm. J. Feng *et al.* [48] obtained the hydroxyapatite particles with a size of about 40 nm which were prepared by grinding the calcium nitrate solid and sodium phosphate powder together and then microwave heating. Q.L. Liao *et al*. [49] used shock method to synthesize the hydroxyapatite particles with smaller size by the calcium carbonate and calcium hydrogen phosphate.

2、Wet synthesis

The commonly used methods include precipitation method, hydrothermal method, sol-gel method, ultrasonic synthesis method, microemulsion method and so on.

H. Zhou *et al*. [50] prepared the columnar hydroxyapatite with high crystallinity by precipitation method, which was obtained by mixing calcium salt solution and phosphate solution in a certain proportion This method is easy to operate and low cost and it is a commonly used method in laboratory.

J.S. Earl *et al*. [51] blended the calcium nitrate and ammonium hydrogen phosphate in sealed vessels under hydrothermal conditions to obtain the rod-like particles with the length of 100-500 nm and the diameter of about 40 nm. Y.J. Song *et al*. [52] let P_2O_5 and calcium nitrate dissolve in alcohol solution and then mixed to obtain the sol. The gel was formed under heating condition and hydroxyapatite particles were obtained at high temperature. L.Y. Cao *et al*. [53] obtained hydroxyapatite particles with smaller size under the conditions of ultrasound after mixture of calcium nitrate, ammonium dihydrogen phosphate and urea. The study found that the crystallinity

and particle size of particles can be controlled by adjusting the power of ultrasound.

G.K. Lim *et al*. [54] prepared the hydroxyapatite by microemulsion method. Under the condition of adding the active agent, the incompatible liquid was formed into a spherical liquid drop, and then the solid particles were obtained from the liquid drops. W. Ren *et al*. [55] also synthesized hydroxyapatite particles by this method, and found that the size of the particles can be controlled by the stirring speed and other conditions.

1.2.2 Application of hydroxyapatite in bone tissue repair

The bone tissue of human body is composed of inorganic bone salt and organic bone matrix, and the inorganic component is mainly composed of nano hydroxyapatite of which the content is as high as 50%. In bone replacement surgery, the implantation of bone matrix substitute, of which the pore morphology and structure are consistent with the natural bone and can be used as bone matrix scaffold, can enable to achieve bone tissue regeneration and repair of bone defects and replace. This is also the reason for the development of porous HAPs that are similar to human bone tissue structure [38]. At present, hydroxyapatite is often combined with other materials to make a kind of bone repair material which is similar to natural bone tissue. This is one of the hot spots in the research of bone repair [56-57].

At present, there are two main aspects in the research of HAP based composites: 1) improving the mechanical properties of materials; 2) the preparation of biocompatible and bioactive composites [58]. In order to improve the mechanical properties of the material, we can choose a kind of high strength biological material. Coating a layer of HAP on its surface will effectively improve its mechanical

compatibility. Some researchers used the characteristics of different materials to develop composite materials and coated a layer of HAP on the surface of high strength cobalt chromium alloy, titanium, stainless steel and other metal [59]. The material prepared by this method has been widely used in clinical practice. However the long-term implantation in the body will lead to the relocation of metal ions and pathological changes in the body. HAP can be combined with other polymers (such as collagen, polylactic acid, and so on) to produce biological materials with good biocompatibility and bioactivity.

T. Yoshida [60] prepared the HAP/collagen scaffold of which the porosity can be up to 95% (v/v) by freeze drying method. The collagen scaffold was used as control to evaluate the cell biology of the HAP/collagen scaffold. The results showed that the cells could better adhere and proliferate on the composite scaffolds, and that the HAP/collagen scaffold could be used as scaffold material in bone tissue engineering.

H.W. Kim [61] used a new method to make HAP/poly (lactic acid) (PLA) nanofibers. The fiber with the diameter of 1-2 μm was synthesized through the introduction of hydroxyl stearic acid surfactant by the hydrophilicity and hydrophobicity of these two materials. Through the cell experiments, it can be seen that the cells were well adhered to the surface of the fiber and had a proliferative phenomenon. These results indicate that HAP/PLA nanofibers could be used in bone tissue engineering.

1.2.3 Application of hydroxyapatite in drug delivery system

Drug delivery system has gradually developed in recent 30 years based on a series of new biological inorganic materials and organic polymer materials with good

compatibility. In order to solve current conventional medication defect, which is low efficiency and the toxicity, drug delivery system has a broad application prospect in the treatment of osteomyelitis, bone tuberculosis and infective bone defect [62-63].

Local application of drugs has the following advantages: can be accurately put the drugs in the required position, and the drug concentration can be formed in several times or even hundreds of times of systemic antibiotics; can quickly reach the peak of drug concentration in the local; although the local drug concentration is very high, but the total amount of medication and quantity entering into the blood circulation is less than systemic medication, thus it will not produce toxic to the main organs of body; it can be directly act on the lesion site without blood, which carry drugs to the region, so the local lesion of ischemia does not affect the efficacy [64-68].

At present, there are several drug carriers: cellulose, collagen, PPF-MMA, lactic acid oligomers, Biodel (dimer formed with sebacic acid and fatty acid by dehydration), calcined gypsum, poly lactic acid/glycolic acid, hydroxyapatite. Bone carrier with excellent drug delivery system should have the following conditions: 1) has good compatibility and certain mechanical strength; 2) has biological degradability with a suitable degradation rate and degradation products are harmless to the human body; 3) has osteoinduction and osteoconduction and can promote cell adhesion and proliferation and the form of organization; 4) can easy disinfect and sterilization process does not affect the biocompatibility and biodegradability; 5) has drug function and no adverse effects on drug action. From the clinical effect and practical point of view, polymer sustained release carrier (cellulose, collagen, PPF-MMA, lactic acid oligomers, Biodel, poly lactic acid/glycolic acid and calcined gypsum) are suitable for preventing the infection of bone and soft tissue. And

sustained release carrier (hydroxyapatite, tricalcium phosphate, allogeneic or xenogeneic demineralized bone and bone matrix gelatin), used as a bone graft material, are suitable for preventing infectious bone defect or deep infection of artificial joint prosthesis [69].

The research of A.M. Chen [70] using the hydroxyapatite ceramic as the carrier of rifampicin in the treatment of bone tuberculosis showed that the sustained release system can maintain at least 27 weeks of effective drug concentration in vivo after implantation. H.B. Wu [71] used tricalcium phosphate as carrier and ciprofloxacin to make tricalcium phosphate/ciprofloxacin sustained release pill and then put it into rabbits. The results showed that the bone and muscle tissue has a higher concentration of ciprofloxacin in 30 days, and the blood drug concentration is very low. F. Li [72] had developed the rifampicin bone matrix gelatin complex and the experiment showed that the drug concentration can be maintained for 3 weeks.

In drug delivery system, HAP is mainly used in bone tissue drug delivery system. C. Zhang [73] synthesized the multifunctional strontium hydroxyapatite (SrHAp) by hydrothermal method with the light and mesoporous properties. In this study, ibuprofen was used as a sustained release drug to study the drug loading and release properties of SrHAp. The results showed that this material can be loaded with drugs and controlled in vitro.

E.P. Avés [74] used Ti-6Al-4V as substrate to produce the porous hydroxyapatite membrane using sol-gel technology, and then covered it on the surface of titanium alloy. As for sustained release drug, the loading and drug release performance of gentamycin sulfate were studied. The results showed that the drug release rate within the first 3 h can be up to 30-40%, indicating that hydroxyapatite can be used as drug

carrier, prevention and treatment of bone defect or the infection of bone graft site.

1.3 Polyurethane introduction

Polyurethane refers to the high molecular compounds in a repeat of the carbamate group (-NHCOO-) in the main chain of polymer structure. The molecular chain of polyurethane is usually composed of two parts, “hard segment” and “soft segment” are often used to describe its structure. The soft segment generally is the polyether polyol and polyester polyol in the molecular structure of polyurethane. Its glass transition temperature is usually lower than normal temperature and in the high elastic state. The hard segment is composed of isocyanate and chain extender and the glass transition temperature is higher than the normal temperature. So it is in the glass state or crystalline state [75]. Due to the thermodynamic incompatibility between hard segment and soft segment, the soft and hard segments will be dispersed to form an independent micro area. The unique micro phase separation structure provide the polyurethane of good processing performance, good mechanical properties, high elasticity, lubrication, wear resistance, fatigue resistance and biocompatibility [76], it is widely used in chemical industry, light industry, textile, electronics, medical, construction, building materials, automotive, defense, aviation and aerospace [77].

Since the first application of polyurethane in the field of biomedicine in the last century in 50s, polyurethane biomedical materials have been widely and deeply developed, and still have broad application prospects. Compared with other biomedical materials, the micro phase separation structure of polyurethane is similar to biological membrane mechanism. Not only the given material with good mechanical properties and easy processing, it also improves the blood compatibility

and biocompatibility [78]. A large number of animal experiments and toxicity experiments confirmed the medical polyurethane material in the clinical application of non-toxic, non-teratogenic effect and local non-allergic reactions. On the other hand, it also has good antibacterial property, solvent resistance, water resistance, and has high toughness, abrasion resistance, controllable performance, so it is recognized as one of the most valuable biomedical materials [79].

1.3.1 Application of polyurethane in biomedical field

Polyurethane was synthesized for the first time in 1930s. Because of its excellent physical and mechanical properties, good blood compatibility and tissue compatibility; it is quickly applied in the biomedical field. Polyurethane was first used as a fracture repair material for medical purposes in 1958, and was used as a surgical suture with a supplemental coating for vascular closure soon. Then in the 1980s, the artificial heart made of polyurethane elastomer was successfully applied to heart transplantation. In recent years, the development and application of polyurethane medical materials is in full swing, the new medical polyurethane materials continue to emerge, the performance of various products have been constantly improved [80].

1.3.1.1 Application of polyurethane in artificial heart and heart auxiliary device

Artificial heart and heart auxiliary devices are mainly used in all kinds of clinical cardiac surgery. In all types of heart surgery including heart transplant surgery, there is an urgent need for a device which can replace the human heart in a short period of time to provide power for human blood circulation because patients cannot be

separated from extracorporeal circulation. Artificial heart and heart auxiliary device at this time can temporarily replace the body's natural heart, and play a role in transition. This requires that the materials used for artificial heart and heart auxiliary device must have good flexing resistance and excellent blood compatibility and biological compatibility, mainly cannot cause the thrombosis for blood contaction, cannot damage the plasma protein, enzyme and other blood cell components, cannot cause harmful immune reactions, cannot damage the related organization, no toxicity and carcinogenicity; cannot produce allergic reaction. A large number of applications and clinical trials have proved that polyurethane elastomer is superior to olefin rubber, silicone rubber and natural rubber in blood compatibility, biocompatibility and durability. Because of the existence of aromatic amines, which are harmful to human beings in the degradation products of aromatic polyurethane, aliphatic polyether polyurethane is mainly used. The main preparation method is that the hard segment of the polyether is first reacted with the soft segment of the aliphatic polyisocyanate to form a prepolymer, and then a small molecular diol or two amine used as a chain extender are added to obtain the polymer. In order to further improve the anticoagulant properties of the surface of polyurethane, a lot of researchs of modification of polyurethane have done at home and abroad. The main method of modification is grafted silicon or vitamins in the molecular chains of polymer, and also added the cell adhesion factors (collagen, fibronectin and albumin) in promoting cell adhesion or heparin and heparin like substance on the surface of polyurethane [81].

Aortech international company, the British medical equipment maker, used the method of block copolymerization of silane into segments of polyurethane to form a

block copolymer, and named polyurethane-silane copolymer as Elast-Eon. This material is used in the manufacture of artificial heart valves, and the resulting products have good durability, flexibility, blood compatibility, biological stability and inertia in the human body. It has been gradually carried out in clinical trials and commercialization [82]. The United States Kontron company synthesized a kind of silane-polyurethane block copolymer material, its chemical composition of 90% polyurethane (PU) and 10% polydimethylsiloxane (PDMS). The artificial heart and auxiliary device made of this material showed good blood compatibility and antithrombotic ability in clinical application [83].

1.3.1.2 Application of polyurethane in artificial blood vessel and blood catheter

The good elasticity of polyurethane let the polyurethane vascular match the natural vascular. In addtion of good blood compatibility, it makes the polyurethane used as artificial blood vessels can effectively reduce neointimal hyperplasia. Furthermore, the three-dimensional design of the material has appropriate aperture and suitable porosity, can enhance the adhesion, spreading and growth of the vascular endothelial cells in the polyurethane scaffold, thus speeded up the process of endothelial cells.

Covita Company synthesized polycarbonate-type polyurethane and published the first patent on biomedical polyurethane artificial vessels. This kind of polyurethane could be implanted in the human or animal body up to 3 years and completely through the performance test of artificial blood vessels [84].

Y. Iwasaki *et al.* grafted methic acid ethyl phosphocholine (MPC) onto the surface of block polyurethane by surface modification. The results showed that the introduction of MPC could help to reduce the adsorption of protein and platelet, and

had a good effect on the artificial blood vessel [85].

1.3.1.3 Application of polyurethane in medical orthopedic bandage

In the treatment of orthopedic and trauma department of orthopedics, plaster bandage external fixation is an essential treatment. At present, the commonly used plaster bandage is easy to cause the pruritus in plaster and inflammation, which brings great pain to the patients. In addition, the plaster is too bulky and airtight in the clinical application, no elasticity after curing and easy to break with activities, the poor wear-resisting, poor strength and poor X ray penetration, and the demolition will cause environmental pollution and other issues. Because of its good elasticity, biocompatibility and easy processing, polyurethane materials have been widely used in orthopedic and trauma department of orthopedics. Practice showed that the elastic bandage which composed of polyurethane material in clinical is esay to operate, can be used for sanitation. It has good water resistance, permeability and fast curing speed, through x ray. Also it was lightweight, plasticity, not easy to cause the wound inflammation. It is gradually replacing the traditional plaster bandage.

T. Ohki *et al.* prepared a kind of memory polyurethane bandage by mixing glass fiber in polyurethane. The results showed that the materials had good tensile strength, fatigue resistance, crack growth and the effect of shape memory [86].

1.3.1.4 Application of polyurethane in medical adhesive

Medical adhesive is included soft tissue adhesive and hard tissue adhesive. The following requirements should be met in clinical application: adhesive itself and the decomposition products are non-toxic; has good adhesion acted with the organism;

has a good adaptability to the organism; can bond in the presence of water; has the functions of disinfection and sterilization, and have similar mechanical properties of the adhesive bodies.

Bristol-Myers Company (United States) successfully made a new type of medical polyurethane pressure-sensitive adhesive by the reaction of polyether polyol, polyester polyol and mixture of these two polyol and aliphatic, alicyclic and aromatic diisocyanate. Then by adding some compound bactericide, conductive chemicals, compounds which has effective regeneration ability for wound tissue and super absorbent which can effectively remove the wound exudata in the pressure-sensitive adhesive, a medical adhesive was obtained with excellent application performance. It is widely used in the preparation of self adhesive film structure in medical field, such as wound dressing material, gauze bandage, wound adhesive plaster, and so on.

1.3.1.5 Application of polyurethane in drug delivery

The traditional mode of administration generally makes the drug rapidly absorbed in the body, resulting in the treatment effect is not sufficient, also can cause serious side effects to harm the body. In order to improve the clinical efficacy and safety of drug treatment, avoid the frequent phenomena of “valley” by conventional preparation traditional administration mode and increase the efficiency, safety and reliability in drug treatment, it is of great practical significance to use a good drug delivery material in clinical practice.

K. Bouchemal *et al*. used hydrophilic polyethylene glycol (PEG) and isophoronediisocyanate (IPDI) as raw materials to make polyurethane microcapsule. The results showed that the particle size of the microcapsules was controlled with

150~500 nm and good results were obtained when used as drug carriers [87].

Y. Ying *et al*. used two steps method. Polytetrahydrofuran (PTMG) was first reacted with toluene diisocyanate (TDI) to form polyurethane prepolymer. Then, acrylic acid and hydroxypropyl acrylate (HPA) were added to obtain polyacrylic acid-polyurethane (PUA). The obtained polymer can be used to obtain pH sensitive hydrogel for drug delivery by swelling [88].

J.A. Halliday *et al*. prepared a kind of hydrogel with interpenetrating network structure by combining hydrophobic polyurethane with hydrophobic hydrophilic polyvinyl alcohol (PVA). The results showed that the polymer hydrogel had good effect in drug delivery [89].

1.3.1.6 Application of polyurethane in wound dressing

Since 1962, the British Winter put forward the theory of "moist healing". The traditional wound dressings (such as medical cotton gauze, cotton, Vaseline gauze and other traditional dressings) have been unable to meet the needs of modern medical treatment technology. Although the traditional dressing has the advantages of simple production process, inexpensive and protective effect of the wound, but the shortcomings of it are more and more obvious. For example, the granulation tissue grew into the mesh of the dressing, the adhesion with the wound caused secondary damage, frequent replacement, moisture absorption ability is poor, easy to dry, cannot effectively isolate bacteria and hemostasis, coagulation effect is poor, and so on. Therefore, in order to solve the problems of traditional dressing, according to the “moist healing” theory, new wound dressing as a wound covering should have basic non-toxic, no stimulation, convenience to use and other characteristics, but also has

good absorption, liquid, gas permeability and bacterial isolation function, not only to avoid the effusion, maintain proper wound moist, prevent crusting, conducive to wound healing, but also has antibacterial effect, prevent wound infection. With the development of modern biomedical materials, a new type of dressing which can meet the above characteristics is emerging. One of the most important is polyurethane dressing [90]. A good polyurethane dressing can keep the wound moist state for a long time, maintain a certain water vapor transmission rate, and can effectively resist the intrusion of external bacteria. The texture of the dressing is soft and comfortable, easy to discharge the wound surface, and can effectively promote wound healing. At the same time, it should have good biocompatibility, non-toxic, no distortion and no allergic reaction. At present, there are three main types of polyurethane dressing: film, foam and hydrogel.

Y.H. Huang *et al*. prepared an antibacterial polyurethane hydrogel for wound dressing used isophoronediisocyanate (IPDI), polyol and poly propylene glycol as raw materials, adding with sulfadiazine (SSD) or bismuth tribromophenate (BTP) and other antimicrobial agents when mixed [91].

1.3.2 Study on modification of medical polyurethane

Polyurethane itself has a certain blood compatibility and biocompatibility. However there are still some problems in the clinical application of polyurethane materials. For example, when medical products of polyurethane directly contact with the blood, different degrees of coagulation will still be produced. Bacterial infection is easy to happen in the actual operation process or to cause damage to the body during implantation. These problems are related to the success or failure of the whole

process. To solve the above problem, the modification of medical polyurethane material is mainly manifested in three aspects: anticoagulant, antibacterial and hydrophilic modification [92].

1.3.2.1 Anticoagulant modification of medical polyurethane

In the clinical application of medical products, it is often directly contacted with blood and there will be a variety of different degrees of coagulation. When the blood clot is more serious, it can cause thrombosis, which has a great impact on the patient's tissues, and can easily lead to various complications of thrombosis, and even lead to death. Therefore, biomedical materials must have good anticoagulant and blood compatibility when they are directly contacted with blood. At present, the coagulation mechanism is not very clear, but it can be used to characterize the anticoagulant properties of the material by in vitro dynamic coagulation test, platelet adhesion test, protein adsorption test and so on [93].

The current methods for improving medical polyurethane anticoagulant properties have the following two ways. The first way is to synthesize new medical polyurethane with good anticoagulant property by using suitable polyol and isocyanate as raw material. The main methods include changing the different types of polyether or polyester polyol, studying the effects of polyol structure and molecular weight of anticoagulant activity, adopting polyol with certain molecular weight or anticoagulant activity group as prepolymer and selecting isocyanates with low toxicity and good blood compatibility and low molecular chain extender. D. Xu *et al*. [94] synthesized a series of hydrophilic polyurethane by two steps in the process of preparing medical polyurethanein and did the tests of dynamic light scattering,

surface contact angle measurement and transmission electron microscopy. The results of calcification time test showed that the anticoagulation ability of polyurethane elastomer prepared with chitosan (chain extender) was significantly improved.

The second way is to introduce anticoagulant group or graft high anticoagulant substances on the surface of medical polyurethane material. Due to the bondage of raw materials, synthesis methods and physical and mechanical properties of the requirements, it is difficult for the first way to develop new polyurethane materials. When medical materials contact with blood, the first step is to react with the material surface, so the surface properties of materials basically can determine the anticoagulant of materials. In addition, the surface modification of polyurethane material can keep the inherent excellent mechanical properties, so the second ways are likely to be used to improve the anticoagulant activity of medical polyurethane. Heparin and albumin are mainly choosed to improve the anticoagulant properties of the polyurethane material. Heparinis a kind of sulfonic acid group polysaccharide substances. In practical application, it can prevent the coagulation by inhibiting the activity of many kinds of prothrombin, delaying or preventing the formation of fibrin network. Albumin is one of the most abundant proteins in plasma, which is composed of liver parenchyma cells, which accounts for 40% to 60% of total plasma protein. Albumin is an anticoagulant protein and does not contain the sequence of lysine which can cause the cell adhesion. It can reduce the adsorption of platelets and leukocytes thereby inhibit the formation of thrombosis. Therefore, external adsorption of albumin is a kind of anticoagulant modification of polyurethane materials.

1.3.2.2 Antibacterial modification of medical polyurethane

Medical products in the practical application, with proper temperature and humidity, it is easy to grow bacterial and reproducethe surface of the product. That would be a serious threat to the health of patients and bring serious medical accidents, causing huge economic losses. Therefore, it is necessary to prepare biological materials with antibacterial activity. At present, the development of antibacterial medical polyurethane materials mainly depends on the selection of antibacterial agents and the research of antibacterial processing methods. The commonly used antibacterial agents are inorganic, organic and natural. The main natural antibacterial agents are chitin, castor oil, mustard, horseradish and so on. However, their antibacterial activity is limited, the sterilization rate is low, the heat resistance is poor, and does not have broad-spectrum antibacterial effect. Therefore it is less used in the preparation of antibacterial materials [95].

The inorganic antibacterial agents mainly include two kinds of metal ion antibacterial agents and nanometer antibacterial agents. Metal ions mainly include the silver, zinc and copper ions, especially silver ions are the most widely used. Nano antibacterial agents mainly include nano TiO_2, ZnO and so on. The organic antibacterial agents are mainly the quaternary ammonium compounds. H. Wang *et al*. prepared a kind of antibacterial polyurethane film using for the fabric by grafting the polyurethane with epichlorohydrin and then reacting with different content of quaternary ammonium salts. The results showed that the polyurethane film had good mechanical properties and good antibacterial effect on Staphylococcus aureus [96].

1.3.2.3 Hydrophilic modification of medical polyurethane

There are mainly two ways to obtain the polyurethane hydrophilic hydrophilic substances. The first way is to add a certain amount of hydrophilic substances in the polyurethane formulations, filled into polyurethane materials to improve the hydrophilicity of polyurethane. R.W. Sessions obtained the water absorbing polyurethane foam using the flexible polyurethane foams as main material, through the uniform doping some absorbent material (such as acrylic acid, pectin, cellulose, chitosan, acrylamide, starch grafted sodium and other super absorbent resin). However, due to the fact that these absorbent materials are simply dispersed in polyurethane foam and easy to dissolve in water, so the application has been limited [97]. The second method is to introduce hydrophilic groups in the molecular chain of polyurethane to improve the water absorption of polyurethane. At present, most of the polyethylene glycol is used as raw material to prepare hydrophilic polyurethane.

1.3.3 Preparation and application of medical polyurethane foam

1.3.3.1 Preparation of medical polyurethane foam

Polyurethane foam, which is often called soft polyurethane foam in industry, is a kind of flexible porous foam material, which is made of polyol, isocyanate and other additives. At present, methods mainly used in the manufacture of polyurethane foam are one step and prepolymer method. The preparation of the prepolymer method is to mix the isocyanate with small molecule chain extender, and then react to form prepolymer at certain temperature. Then, the mixed homogeneous polyol, foaming agent and other additives are added into the prepolymer, after rapid mixing evenly

into the mold foam and curing, the foam product was prepared [98]. The one step is to add all the raw materials together and mix with high speed to obtain the foam. It is widely used because of the simple process, low equipment requirement and stable product quantity.

1.3.3.2 Application of medical polyurethane foam

Medical polyurethane foam is porous with greater absorption capacity of the liquid and has good air permeability. It also has the advantages of easy processing, lightweight, non-toxic, safe use and good biocompatibility. That is why it is often used as materials of various skin dressings [99].

KCI Company of the United States used the open-cell polyurethane foam for negative pressure wound therapy. The polyurethane foam dressing is soft and can conform to the filling of deep and irregular contour of the wound. Moreover, it can promote granulation tissue regeneration, and its hydrophobic surface structure is more conducive to the removal of leachate.

1.4 Purposes and significances of research

The purposes of this study are to fabricate and characterize the nanocomposite scaffolds we prepared. The main materials we used in this study are NaCl powders, nHAP particles and SMPU. First, we undertake the challenges to overcome the problem of preparation of different sizes of NaCl powders. We fabricated the SMPU porous scaffold used NaCl powders with different sizes. The main purpose is to obtain a controllable method of preparing a porous three-dimensional structure. Then we synthesized nHAP particles and mixed with SMPU to obtain the porous SMPU/

nHAP nanocomposite scaffolds. The effect of nHAP particles on mechanical behavior and biological performance was mainly investigated. The purpose of these investigations is to design a three-dimensional porous nanocomposite scaffold which possesses high compression resistance, good shape memory recovery ratio and high biocompatibility. Good shape memory recovery ratio can lead the nanocomposite scaffold more precisely match the irregular boundaries of bone defects and the less time required for compression recovery can directly shorten the time of the operation. The significance of this investigation can lead to realization of advanced nanocomposite scaffold for application in minimally invasive surgery and bone defect repair.

1.5 Outline of dissertation

This dissertation is structured to provide a summary of "Development and properties of multifunctional biomedical composites".

In Chapter 1, an overview of bone defects repair, bone tissue engineering, preparation and application of hydroxyapatite and polyurethane has been presented.

In Chapter 2, characterization method in this dissertation has been summarized. Apparent density, porosity, shape fixity ratio and shape recovery ratio of scaffold also have been listed out.

In Chapter 3, four SMPU scaffolds (SMPU-200, SMPU-200-100, SMPU-100-50, and SMPU-50) with the three-dimensional porous structure were fabricated via a salt-leaching-phase inverse technique, a unique method to fabric porous structure. The use of different size of NaCl particles to obtain scaffolds with different apertures was investigated. The porosity, compression recovery rate, shape recovery rate, the

ability of cell proliferation of the porous scaffolds were related to the apertures of scaffolds.

In Chapter 4, nHAP particles were fabricated by the liquid phase precipitation method and four porous SMPU/nHAP composite scaffolds (SMPU/nHAP-200, SMPU/nHAP-200-100, SMPU/nHAP-100-50 and SMPU/nHAP-50) were prepared with the three-dimensional porous structure. Their physical characteristics, mechanical properties, shape recovery behaviors and biological performance related to the apertures of scaffolds had been discussed.

In Chapter 5, five-step thermo-mechanical cycle test was used to investigate the shape recovery properties. And the contribution of HAP particles on the physical characteristics, mechanical properties, shape recovery behaviors and biological performance of the scaffolds had been investigated.

In Chapter 6, summary and conclusions of this dissertation were presented.

References

[1] G.H. Altman, F. Diaz, C. Jakuba, *et al*. Silk-based biomaterials. Biomaterials, 2003, 24 (3): 401-416.

[2] M.J. Lysaght, N.A. Nguy and K. Sullivan. An economic survey of the emerging tissue engineering industry. Tissue Eng, 1998, 4 (31): 231-238.

[3] D.T. Felson, R.C. Lawrence, P.A. Dieppe, *et al*. Osteoarthritis: new insights. Part 1: the disease and its riskfactors. Ann Inten Med, 2000, 133 (8): 635-646.

[4] G.G. Niederauer, D.R. Lee and S. Sankaran. Bone grafting in arthroscopy and sports medicine. Sports Med Arthrosc, 2006, 14 (3): 163-168.

[5] J.P. Chen and F. Zhang. Advanced research on treatment for bone defect. China J Orthop & Trauma, 2004, 17 (12): 767-768.

[6] I. Bab, B.A. Ashton, D. Gazit, *et al*. Kinetics and differentiation of marrow stromal cells in diffusion chambers in vivo. J Cell Sci, 1986, 84 (1): 139-151.

[7] T.M. Skerry, L. Bitensky, J. Chayen, *et al*. Early strain-related changes in enzyme activity in osteocytes following bone loading in vivo. J Bone Miner Res, 1989, 4 (5): 783-788.

[8] G. Vaes. Cellular biology and biochemical mechanism of bone resorption: A review of recent developments on the formation, activation, and mode of action of osteoclasts. Clin Orthop Relat Res, 1998, 231 (1): 239-271.

[9] R. Baron. Molecular mechanisms of bone resorption by the osteoclast. Anat Rec, 1989, 224 (2): 317-324a.

[10] R. Baron. Polarity and membrane transport in osteoclasts. Connect Tissue Res, 1989, 20 (1-4): 109-120b.

[11] S. Shi, M. Kirk and A.J. Kahn. The role of type I collagen in the regulation of the osteoblast phenotype. J Bone Miner Res, 1996, 11 (8): 1139-1145.

[12] P.A. Price, A.A. Otsuka, J.W. Poser, *et al.* Characterization of a gamma-carboxyglutamic acid-containing protein from bone. Proc Natl Acad Sci U S A, 1976, 73 (5): 1447-1451.

[13] P.V. Hauschka, J.B. Lian, D.E. Cole, *et al*. Osteocalcin and matrix Gla protein: vitamin K-dependent proteins in bone. Physiol Rev, 1989, 69 (3): 990-1047.

[14] E.A. Wayner and N.L. Kovach. Activation-dependent recognition by hematopoietic cells of the LDV sequence in the V region of fibronectin. J Cell Biol, 1992, 116 (2): 489-497.

[15] J. Klein-Nulend, R.G. Bacabac, J.P. Veldhuijzen, *et al*. Microgravity and bone cell mechanosensitivity. Adv Space Res, 2003, 32 (8): 1551-1559.

[16] D.E. Discher, P. Janmey and Y.L. Wang. Tissue cells feel and respond to the stiffness of their substrate. Science, 2005, 310 (5751): 1139-1143.

[17] Y.G. Liu, Y.J. Yang, F.G. Kuang, *et al*. Repair of tibial defects with vascular autologous fibular graft. Medical Journal of National Defending Forces in Southwest China, 2009, 19 (8): 791-793.

[18] Z.W. Zhang, C.S. Cheng, W.L. Ma, *et al*. Clinical application study on repair of femur massive defect with fibula flap transplantation. World Journal of Integrated Traditional and Western Medicine, 2009, 4 (7): 514-515.

[19] R.C. Sasso, J.I. Williams, N. Dimasi, *et al*. Postoperative Drains at the Donor Sites of Iliac-Crest Bone Grafts. J Bone and Joint Surg, 1998, 80 (5): 631-635.

[20] W.W. Tao, J.F. Zhu, Q. Zhang, *et al*. Clinical study on treatment of limb fractures with allogeneic bone graft. Chinese Journal of Bone and Joint Injury,

2009, 24 (4): 342-343.

[21] S. Karaogh, A. Baktir, S. Kabak, *et al*. Experimental repair of segmental bone defects in rabbits by demineralized allograft covered by free autogenous periosteum. Injury, 2002, 33 (8): 679-683.

[22] C.A. Vacanti, W. Kim, J. Upton, *et a1*. Tissure-engineered growth of bone and cartilage. Transplant Proc, 1993, 25 (1): 1019-1021.

[23] K.E. Healy and R.E. Guldberg. Bone tissue engineering. J Musculoskelet Neuronal Interact, 2007, 7 (4): 328-330.

[24] R. Langer and J.P. Vacanti. Tissue engineering. Science, 1993, 260 (5110): 920-926.

[25] J.Y. Ding and A.M. Ji. Advances in biological scaffold material in bone tissue engineering. Orthopedic Journal of China, 2006, 14 (1): 56-58.

[26] C. Xu, P. Su, X. Chen, *et al*. Biocompatibility and osteogenesis of biomimetic Bioglass-Collagen-Phosphatidylserine composite scaffolds for bone tissue engineering. Biomaterials, 2011, 32 (4): 1051-1058.

[27] K. Matsui, A. Matsui, T. Handa, *et al*. Bone regeneration by octacalcium phosphate collagen composites in a dog alveolar cleft model. Int J Oral Max Surg, 2010, 39 (12): 1218-1225.

[28] J. Venkatesan, Z. Qian, B. Ryu, *et al*. Preparation and characterization of carbon nanotube-grafted-chitosan-Natural hydroxyapatite composite for bone tissue engineering. Carbohydr Polym, 2011, 83 (2): 569-577.

[29] Y.C. Kuo, C.F. Yeh and J.T. Yang. Differentiation of bone marrow stromal cells in poly (lactide-co-glycolide)/chitosan scaffolds. Biomaterials, 2009, 30 (34): 6604-6613.

[30]. D.N. Rockwood, E.S. Gil, S. Park, *et al*. Ingrowth of human mesenchymal stem cells into porous silk particle reinforced silk composite scaffolds: An in vitro study. Acta Biomaterialia, 2011, 7 (1): 144-151.

[31] Y. Zhang, C. Wu, T. Friis, *et al*. The osteogenic properties of CaP/silk composite scaffolds. Biomaterials, 2010, 31 (10): 2848-2856.

[32] C.M. Murphy, M.G. Haugh and F.J. O'Brien. The effect of mean aperture on cell attachment, proliferation and migration in collagen-glycosaminoglycan scaffolds for bone tissue engineering. Biomaterials, 2010, 31 (3): 461-466.

[33] H. Tsurushima, A. Marushima, K. Suzuki, *et al*. Enhanced bone formation using hydroxyapatite ceramic coated with fibroblast growth factor-2. Acta Biomaterialia, 2010, 6 (7): 2751-2759.

[34] G. Wang, H. Yang, M. Li, *et al*. The use of silk fibroin/hydroxyapatite composite cocultured with rabbit bone-marrow stromal cells in the healing of a segmental bone defect. J of Bone Joint Surg Br, 2010, 92 (2): 320-325.

[35] S. Bhumiratana, W.J. Grayson, A. Castaneda, *et al*. Nucleation and growth of mineralized bone matrix on silk-hydroxyapatite composite scaffolds. Biomaterials, 2011, 32 (11): 2812-2820.

[36] S. Park, E.S. Gil, H. Shi, *et al*. Relationships between degradability of silk scaffolds and osteogenesis. Biomaterials, 2010, 31 (32): 6162-6172.

[37] D.F. Williams. On the mechanisms of biocompatibility. Biomaterials, 2008, 29 (20): 2941-2953.

[38] L.L. Hench and J.M. Polak. Third-Generation Biomedical Materials. Science, 2002, 295 (5557): 1014-1017.

[39] Y. Mizushima, T. Ikoma, J. Tanaka, *et al*. Injectable porous hydroxyapatite

microparticles as a new carrier for protein and lipophilic drugs. Journal of Controlled Release, 2006, 110 (2): 260-265.

[40] M. Itokazu, W. Yang, T. Aoki, *et al*. Synthesis of antibiotic-loaded interporous hydroxyapatite blocks by vacuum method and in vitro drug release testing. Biomaterials, 1998, 19 (7-9): 817-819.

[41] I. Soriano and C. Évora. Formulation of calcium phosphates/poly (d,l-lactide) blends containing gentamicin for bone implantation. Journal of Controlled Release, 2000, 68 (1): 121-134.

[42] V.S. Komlev, S.M. Barinov and E.V. Koplik. A method to fabricate porous spherical hydroxyapatite granules intended for time-controlled drug release. Biomaterials, 2002, 23 (16): 3449-3454.

[43] P. Yang, Z. Quan, C. Li, *et al*. Bioactive, luminescent and mesoporous europium-doped hydroxyapatite as a drug carrier. Biomaterials, 2008, 29 (32): 4341-4347.

[44] T. Matsumoto, M. Okazaki, M. Inoue, *et al*. Hydroxyapatite particles as a controlled release carrier of protein. Biomaterials, 2004, 25 (17): 3807-3812.

[45] M.I. Alam, I. Asahina, K. Ohmamiuda, *et al*. Evaluation of ceramics composed of different hydroxyapatite to tricalcium phosphate ratios as carriers for rhBMP-2. Biomaterials, 2001, 22 (12): 1643-1651.

[46] T. Matsumoto, M. Okazaki, M. Inoue, *et al*. Hydroxyapatite particles as a controlled release carrier of protein. Biomaterials, 2004, 25 (17): 3807-3812.

[47] C.C. Silva, A.G. Pinheiro, M.A.R. Miranda, *et al*. Structural properties of hydroxyapatite obtained by mechanosynthesis. Solid State Sciences, 2003, 5 (4): 553-558.

[48] J. Feng, J.M. Cao, S.G. Deng, *et al*. Two novel methods of nano-hydroxyapatite synthesis. New chemical materials, 2005, 33 (1): 27-29.

[49] Q.L. Liao, G.L. Xu, G.F. Yin, *et al*. Hydrothermal synthesis of nano-hydroxyapatite crystals. Functional materials, 2002, 33 (3): 338-340.

[50] H. Zhou, Z.D. Li, D.F. Li, *et al*. Preparation and characterization of nano-sized hydroxyapatite. Nonferrous Metals: Extractive Metallurgy, 2006 (Z1): 12-14.

[51] J.S. Earl, D.J. Wood and S.J. Milne. Hydrothermal sunthesis of hydroxyapatite. J Phys, 2006, 26, 268-271.

[52] Y.J. Song, M.S. Li, S.L. Wen, *et al*. Effects of technological parameters on the forms and phase structures of hydroxyapatite. J Chin Electr Microsc Soc, 2002, 2 1(5): 695-696.

[53] L.Y. Cao, C.B. Zhang and J.F. Huang. Influence of temperature, [Ca2+], Ca/P ratio and ultrasonic power on the crystallinity and morphology of hydroxyapatite nanoparticles prepared with a novel ultrasonic precipitation method. Materials letters, 2005, 59 (14-15): 1902-1906.

[54] G.K. Lim, A.L. Khoo, L.S. Tham, *et al*. Hypoglycemia in nondiabetetic patients undergoing albumin dialysis by molecular adsorbent recirulating system. Liver transpl, 2003, 9 (9): 949-953.

[55] W. Ren, S.P. Li and Y.F. Wang. Synthetic mechanism of hydroxyapatite nanoparticles via AOT inverse microemulsions. Chinese Journal of Materials Research, 2004, 18 (3): 257-264.

[56] Y.S. Pek, S. Gao, M.S.M. Arshad, *et al*. Porous collagen-apatite nanocomposite foams as bone regeneration scaffolds. Biomaterials, 2008, 29 (32): 4300-4305.

[57] E. Landi, F. Valentini and A. Tampieri. Porous hydroxyapatite/gelatine scaffolds

with ice-designed channel-like porosity for biomedical applications. Acta Biomaterialia, 2008, 4 (6): 1620-1626.

[58] Y.H. Xu, S.Q. Li and Z.A. Li. Development of nanometer hydroxyapatite complex materials-Cytotoxicity test of nano-hydroxyapatite by MTT-assay. J Pract Stomatol, 2004, 20 (2): 147-150.

[59] E. Fidancevska, G. Ruseska, J. Bossert, *et al*. Fabrication and characterization of porous bioceramic composites based on hydroxyapatite and titania. Materials Chemical and Physics, 2007, 103 (1): 95-100.

[60] T. Yoshida, M. Kikuchi, Y. Koyama, *et al*. Osteogenic activity of MG63 cells on bone-like hydroxyapatite/collagen nanocomposite sponges. J Mater Sci: Mater Med, 2010, 21 (4): 1263-1272.

[61] H.W. Kim, H.H. Lee and J.C. Knowles. Electrospinning biomedical nanocomposite fibers of hydroxyapaite/poly (lactic acid) for bone regeneration. J Biomed Mater Res Part A, 2006, 79 (3): 643-649.

[62] T.M. Allen and P.R. Cullis. Drug delivery systems: entering the mainstream. Science, 2004, 303 (5665): 1818-1822.

[63] C. Kaparissides, S. Alexandridou, K. Kotti, *et al*. Recent advances in novel drug delivery systems. Journal of Nanotechnology, 2006, 2, 1-11.

[64] S. Aluri, S.M. Janib and J.A. Mackay. Environmentally responsive peptides as anticancer drug carriers. Advanced Drug Delivery Reviews, 2009, 61 (11): 940-952.

[65] M. Biondi, F. Ungaro, F. Quaglia, *et al*. Controlled drug delivery in tissue engineering. Advanced Drug Delivery Reviews, 2008, 60 (2): 229-242.

[66] M.C. Branco and J.P. Schneider. Self-assembling materials for therapeutic

delivery. Acta Biomaterialia, 2009, 5 (3): 817-831.

[67] J.W. Yoo and C.H. Lee. Drug delivery systems for hormone therapy. Journal of Controlled Release, 2006, 112 (1): 1-14.

[68] R. Langer. New methods of drug delivery. Science, 1990, 249 (4976): 1527-1533.

[69] L.C. Palmer, C.J. Newcomb, S.R. Kaltz, *et al*. Biomimetic systems for hydroxyapatite mineralization inspired by bone and enamel. Chemical Reviews, 2008, 108 (11): 4754-4783.

[70] A.M. Chen, T.Y. Wang, S.Z. Sun, *et al*. Experimental study and clinical application of ceramic artificial bone (R-PHA) in the treatment of bone tuberculosis. Zhonghua Journal of Orthopedics, 1992. 12 (1): 18-20.

[71] H.B. Wu, Q.X. Zheng, F.R. Xu, *et al*. Experimental study on local drug delivery system for treatment of open fractures. Chin J Traumatol, 1998, 14 (4): 226-229.

[72] F. Li, Z.F. Li, T.Y. Wang, *et al*. Study on repairing bone defect with rifampicin bone matrix gelatin complex. Chinese Journal of Experimental Surgery, 1995, 12 (3): 165-166.

[73] C. Zhang, C. Li, S. Huang, *et al*. Self-activated luminescent and mesoporous strontium hydroxyapatite nanorods for drug delivery. Biomaterials, 2010, 31 (12): 3374-3383.

[74] E.P. Avés, G.F. Estévez, M.S. Sader, *et al*. Hydroxyapatite coating by sol-gel on Ti-6Al-4V alloy as drug carrier. J Mater Sci: Mater Med, 2009, 20 (2): 543-547.

[75] X.B. Zhao, L. Du and X.P. Zhang. Brief review of relations of structure and microphase separation of polyurethane. Polyurethane industry, 2001, 16 (1): 4-8.

[76] C.C. Zhu, H.Y. Weng, G.H. Lyu, *et al*. The latest development of polyurethane industry at home and abroad. Chemical propellants & polymeric materials, 2012, 10 (5): 1-20.

[77] H.Y. Weng. Development of polyurethane industry and technical progress. Chemical propellants & polymeric materials, 2008, 6 (1): 1-6.

[78] B. Li, H.L. Zhang, Z.H. Li, *et al*. Research progress and application of polyurethane materials in biological field. Polyurethane, 2008, 8 (4): 96-100.

[79] W.J. Lin, K.L. Huang, X.Y. Peng, *et al*. Progress of medical polyurethane application. Enterprise science and technology & development, 2010 (12): 20-23.

[80] C.Y. Zhang. Talking about medical polyurethane. World rubber industry, 2003, 31 (5): 45-48.

[81] L. Luo and H.Y. Dou. Development of antithrombogenic biomedical polyurethanes. Thermosetting resin, 2005, 20 (3): 42-45.

[82] Y.J. Liu. Polyurethane anchor agent for mine. Polyurethane Industry, 2000, 15 (4): 30.

[83] W.Z. Wang, C. Zhang and J.H. Chen. Research progress of silicone modified polyurethane. Silicone Material, 2001, 15 (5): 33-37.

[84] C.Y. Zhang. Application and development of medical polymeric materials (2). China Academic Journal Electronic Publishing House, 2005, 11 (6): 17-22.

[85] Y. Iwasaki, Y. Aiba, N. Morimoto, *et al*. Semi-interpenetrating polymer networks composed of biocompatible phospholipid polymer and segmented polyurethane. Journal of biomedical materials research, 2000, 52 (4): 701-708.

[86] T. Ohki, Q.Q. Ni, N. Ohsako, *et al*. Mechanical and shape memory behavior of

composites with shape memory polymer. Composites Part A: applied science and manufacturing, 2004, 35 (9): 1065-1073.

[87] K. Bouchemal, S. Briancon, E. Perrier, *et al*. Synthesis and characterization of polyurethane and poly (ether urethane) nanocapsules using a new technique of interfacial polycondensation combined to spontaneous emulsification. International journal of pharmaceutics, 2004, 269 (1): 89-100.

[88] Y. Ying, X. Gu and C. Yang. Abnormal pH sensitivity of polyacrylate-polyurethane hydrogels. Journal of applied polymer science, 1998, 70 (6): 1047-1052.

[89] J.A. Halliday, S. Robertson. Oral transmucosal delivery: U.S. Patent 6, 488, 953 [P]. 2002-12-3.

[90] Y.K. Jin and H.L. Yin. Research progress of polyurethane wound dressing. Prac J Med & Phan, 2010, 27 (11): 1040-1041.

[91] Y.H. Huang. Hydrogel wound dressing and the method of making and using the same: CA2241188 [P]. 1998-4-30.

[92] Q. Wang, R.X. Li, Y. Feng, *et al*. Research progress on modification and its application of medical polyurethane in biomedicine. Plastic technology, 2010, 38 (9): 91-96.

[93] J. Ji, Y.X. Qiu, X.J. Yu, *et al*. Research progress of anticoagulant polyurethane materials. Journal of Functional Polymers, 1995, 8 (2): 225-235.

[94] D. Xu, Z. Meng, M. Han, *et al*. Novel blood-compatible waterborne polyurethane using chitosan as an extender. Journal of Applied Polymer Science, 2008, 109 (1): 240-246.

[95] Z.G. Wen, S.X. Dong and C.Y. Li. Research progress of antibaterial

polyurethane biomaterials. New chemical materials, 2010, 38 (11): 24-26.

[96] H.H. Wang and M.S. Lin. Biocidal polyurethane and its antibacterial properties. Journal of Ploymer Research, 1998, 5 (3): 177-186.

[97] R.W. Sessions. Wound dressing suitable for insertion in nasal passages: U.S. Patent 6, 022, 890 [P]. 2006-4-4.

[98] L. Piszczyk, M. Strankowski, M. Danowska, *et al*. Preparation and characterization of rigid polyurethane-polyglycerol nanocomposite foams. European Polymer Journal, 2012, 48 (10): 1726-1733.

[99] V.S. Dagostin, D.L. Golcalves, C.B. Pacheco, *et al*. Bactericidal polyurethane foam mattresses: Microbiological characterization and effectiveness. Materials Science and Engineering: C, 2010, 30 (5): 705-708.

Chapter 2

Characterization methods

2 Characterization methods

2.1 Preparation of reagents

Phosphate buffer (PBS, pH 7.4):

0.8 g NaCl, 0.2 g KCl, 3.58 g $Na_2HPO_4 \cdot 12H_2O$ and 0.24 g KH_2PO_4 were weighed and dissolved in 700 mL ddH_2O with adjusting the solution to pH 7.4. Then the solution was adjusted to 1 L with ddH_2O with adjusting the solution to pH 7.4, high pressure steam Sterilized for 30 minutes and stored at 4 ℃.

Cell culture medium of Dulbecco's modified Eagle's medium (DMEM):

13.5 g DMEM dry powder and 3.7 g $NaHCO_3$ were dissolved in 1000 mL ddH_2O, with magnetic stirring. After a period of time, the solution was added with 5.94 g HELPS and 0.11 g sodium pyruvate and adjusted to the pH 7.1-7.2 ℃. After standing 4 hours, the solution was sterilized with 0.22 μm filter and sub-installed in the sterile reagent bottle and then stored at 4 ℃.

DMEM cell complete medium:

Penicillin/Streptomycin double solution and L-glutamine were added to DMEM cell culture medium at a ratio of 1: 100. After mixing, the appropriate amount of fetal bovine serum (FBS) was added to the solution to obtain DMEM cells complete culture medium and store at 4 ℃.

MTT solution:

0.05 g 3-(4, 5-dimethylthiazole-2)-2, 5-diphenyltetrazole bromide (MTT) was dissolved in 10 mL sterile PBS. Until it was fully dissolved, the solution was sterilized by the disposable sterile filter with the aperture of 0.22 μm, sealed away

from light and stored at -20 ℃.

2.2 Characterization methods

2.2.1 X-ray photoelectron spectroscopy

SMPU and SMPU/nHAP scaffolds were made into the specimens with the size of $0.7 \times 0.7 \times 0.2$ cm^3 and dried in vacuum. The complete removal of NaCl of scaffolds and the existence of calcium in scaffolds were determined using X-ray photoelectron spectroscopy (XPS; AXIS-Ultra DLD, Kratos, Japan).

2.2.2 Chemical method of determining the removal of NaCl of the scaffold

Since chloride ions can react with silver ions to form the white precipitates, so whether the sodium chloride (NaCl) in the leaching liquid of scaffolds has been completely removed can be determined by detecting the presence or absence of chloride ions in the leaching liquid. Firstly, $AgNO_3$ solution (0.1 M) was prepared. Secondly, SMPU-NaCl and SMPU/nHAP-NaCl scaffolds were soaked in distilled water (dH_2O) at 40 ℃ and refreshed every 4 hours.Then the leaching liquid obtained every 4 hours was determined by reacting with the $AgNO_3$ solution.

2.2.3 Scanning electron microscopy

Scanning electron microscopy (SEM; S-3000N, Hitachi, Japan) was selected to observe the morphology of SMPU and SMPU/nHAP scaffolds and the morphology of cells cultured in the scaffolds at 20 kV. Prior to testing, the specimens were sputter-coated with platinum to impart electrical conductivity and reduce charging artifacts. High vacuum conditions were applied and a secondary electron detector

was used for image acquisition.

Specimens cultured with cells: the size of specimens was controlled of Φ 6 mm × 2 mm. Firstly, after the removal of culture medium, specimens were cleaned with PBS for 2-3 times and added with 100 μL glutaraldehyde (GA) solution, then saved at 4 ℃ for one night. Secondly, specimens were cleaned with PBS for 2-3 times after the removal of GA solution and gradiently dehydrated by ethanol with concentration from 50% to 90%. Then the specimens were added with 100 μL t-butyl alcohol and saved at room temperature for 30 minutes. Finally, the specimens were added with new t-butyl alcohol and frozen at -20 ℃ for one hour and then dried under reduced pressure.

2.2.4 X-ray micro-computed tomography

X-ray micro-computed tomography (μ-CT; Skyscan 1272 Micro-CT, Bruker, Germany) was used for determing the three-dimensional structure of the scaffolds. The size of specimens was controlled of Φ 6 mm × 2 mm.

2.2.5 Tensile test

The tensile test was carried out with a tensile tester (RTC1250A, A&D Co., Ltd, Japan) using a speed of 1 mm/min at room temperature. The Young's modulus (E) of tensile of scaffolds was calculated from Eqns. (2-1).

$$E = (\sigma_{0.04} - \sigma_{0.02})/(\varepsilon_{0.04} - \varepsilon_{0.02}) \quad (2\text{-}1)$$

Where E is the Young's modulus of samples, σ is the stress of the sample, ε is the strain of the sample.

2.2.6 Compression behavior test

The compression behavior test was conducted with an automatic compression tester (KES-FB3-AUTO-A, Kato Tech Co., Ltd) at room temperature, and the compression speed and the pressure are 0.06 mm/s and 2 cm^2, respectively. And the sample is a cylinder with a cross-sectional area greater than 2 cm^2 and a height greater than 5 mm. The modulus of compression of scaffolds at the stress of 0.00215 MPa (E_0) and 0.12065 MPa (E_1) were calculated from Eqns. (2-2) and (2-3). The compression shape recovery ratios of SMPU and SMPU/nHAP scaffolds were determined using Eqn. (2-4).

$$E_0 = \left(\sigma_{0.00215} - \sigma_{0.00126}\right) / \left(\varepsilon_{0.00215} - \varepsilon_{0.00126}\right) \quad (2\text{-}2)$$

$$E_1 = \left(\sigma_{0.12065} - \sigma_{0.11006}\right) / \left(\varepsilon_{0.12065} - \varepsilon_{0.11006}\right) \quad (2\text{-}3)$$

$$R_c = \left(S_1 - S_2\right) / S_1 \times 100\% \quad (2\text{-}4)$$

Where E_0 and E_1 are the modulus of compression of samples at the stress of 0.00215 MPa and 0.12065 MPa, respectively, σ is the stress of the sample, ε is the strain of the sample, R_c is the compression shape recovery rate of the sample, S_1 is the biggest strain with the stress of 0.125 MPa of the sample and S_2 is the residual strain of the sample after the recovery.

2.2.7 Dynamic mechanical analysis

The specimens were determined using a DVA-200 instrument (Keisoku Seigyo Co., Ltd., Japan) at a frequency of 10 Hz from 30 ℃ to 100 ℃ at a rate of 5 ℃ /min.

2.2.8 Thermo-mechanical test

A thermo-mechanical test was conducted to investigate the shape recovery properties of the scaffolds, using a thermal mechanical analyzer (SS6100, Hitachi High-Tech Science Corporation, Japan). The shape fixity ratio and shape recovery ratio were derived from the Eqns. (2-5) and (2-6).

$$R_f = \varepsilon_u / \varepsilon_m \times 100\% \tag{2-5}$$

$$R_r = \left(\varepsilon_u - \varepsilon_p\right) / \varepsilon_u \times 100\% \tag{2-6}$$

Where R_f is the shape fixity ratio of the sample, R_r is the shape recovery ratio of the sample, ε_u is the unloading strain strain at the end of step 4, ε_m is the pre-deformation strain at the end of step 3 and ε_p is the permanent strain at the end of step 5.

2.2.9 The apparent density and porosity of the scaffolds

The quantity of the specimen in air and the quantity of the water saturated specimen in air were weighed in this research. The apparent density and porosity of scaffolds were derived from the Eqns. (2-7), (2-8) and (2-9).

$$\begin{aligned}\rho_{PS} &= m_2 / V = m_2 / \left(V_P + V_H\right) = m_2 / \left[m_2 / \rho_P + \left(m_1 - m_2\right) / \rho_H\right] \\ &= m_2 \rho_P \rho_H / \left[m_2 \rho_H + (m_1 - m_2)\rho_P\right]\end{aligned} \tag{2-7}$$

$$\begin{aligned}\rho_{PAS} &= m_2 / V = m_2 / \left(V_P + V_A + V_H\right) = m_2 / \left[m_P / \rho_P + m_A / \rho_A + \left(m_1 - m_2\right) / \rho_H\right] \\ &= \left(t+1\right)\rho_P \rho_A \rho_H m_2 / \left[\left(\rho_A + t\rho_H\right)\rho_H m_2 + \left(t+1\right)\rho_P \rho_A (m_1 - m_2)\right]\end{aligned} \tag{2-8}$$

$$P = V_H / V \times 100\% = \rho\left(m_1 - m_2\right) / \left(\rho_H m_2\right) \times 100\% \tag{2-9}$$

Where ρ_{PS} and ρ_{PAS} are the apparent densities of the SMPU and SMPU/nHAP scaffolds (g/cm^3), respectively, m_1 is the quantity of the water saturated specimen in air (g), m_2 is the quantity of the specimen in air (g), V is the volume of the specimen

(cm^3), V_P is the volume of the SMPU (cm^3), V_H is the volume of the water (cm^3), V_A is the volume of the nHAP particles (cm^3), ρ_P is the density of the SMPU (1.22 g/cm^3), ρ_H is the density of the water (0.99705 g/cm^3, 25 ℃), ρ_A is the density of the nHAP particles (3.16 g/cm^3), t is the ratio of nHAP particles to SMPU, ρ is the apparent density of the specimen, P is the porosity of specimen.

2.2.10 X-ray power diffraction

The chemical composition and crystallinity of nHAP were analyzed with an X-ray power diffraction (XRD) (ARL X'TRA, Thermo Electron, USA) using a monochromatic CuKα radiation (λ=1.54056 nm) in a range of 2θ=10 °-70 ° with a speed, tube current and voltage of 5 °/min, 35 mA and 40 kV, respectively.

2.2.11 Transmission electron microscope

nHAP particles were dispersed in the absolute ethyl alcohol and then dropped onto carbon-coated copper grids for investigating the morphology of nHAP using a TEM (JEM-2100, JEOL, Japan) at 200 Kv.

2.2.12 Evaluation of biocompatibility scaffolds in vitro

Cell counting: hemocytometer counting method:

Firstly, hemocytometer counting plate and coverslip are washed with absolute ethanol and dried at room temperature. Secondly, the cells are digested with 0.25% trypsin to prepare a single cell suspension. About 10 μL of cell suspension was drawn with a pipette between hemocytometer counting plate and coverslip. Then cells are counted with an inverted microscope to calculate the total number of cells in the four

squares. If cells are clustered together, it will be counted as a cell. If the cells are pressed against the grid, it will be counted following the principle of "Count on the next, the left and does not count the right". Cell density calculation method is calculated from Eqn. (2-10).

$$\rho_C = \frac{N_C}{4} \times 10^4 (cell / \mathrm{m}L) \tag{2-10}$$

Where ρ_C is the cell density (cell/cm^3), N_C is the total number of cells.

Cell proliferation experiments

MTT can be reduced by succinate dehydrogenase in the mitochondrial of living cells into water-insoluble blue-violet crystal forma (Formazan) and deposited in the cells. But the dead cells do not have this function. The blue-violet crystal can be dissolved by a specific solvent, such as dimethylsulfoxide (DMSO). And its absorbance can be measured at 595 nm using a spectrophotometric microplate reader (Model 680, Bio-Rad, USA), which can indirectly reflect the amount of viable cells.

In vitro cell proliferation experiments were used to evaluate the SMPU and SMPU/nHAP scaffolds. Firstly, the sterilized scaffolds (Φ 6 mm × 2 mm) were added to 96-well plates. MG-63 cells were seeded into the 96-well plates at a density of 1 × 10^4 cells/well and maintained in DMEM containing 5% fetal bovine serum (FBS) (Gibco, USA). After 1 d, 3 d, 5 d, and 7 d of culture, the cell growth was determined by MTT assay. The absorbance was measured at 595 nm using a spectrophotometric microplate reader. For comparison, a blank was also used for the cell culture. All operations were carried out under aseptic conditions.

Preparation of SEM samples of porous scaffolds with cells

After 1 d, 3 d, 5 d, and 7 d of culture with cells, the scaffolds were washed with phosphate buffered solution (PBS) for 2-3 times, and then 100 μL glutaric dialdehyde

solution (GA, 2.5%) was added to every well and the samples were stored at 4 ℃ for one night. After one night, the samples were washed with PBS for 2-3 times and dehydrated with ethanol from low concentration to high concentration (50%, 60%, 70%, 80%, 90%, 99%, 99%) for 10 minutes at each ethanol concentration. Then, 100 μL t-butyl alcohol was added to every well and the samples were maintained for 30 minutes at room temperature. Lastly, replacement of 100 μL new t-butyl alcohol, the samples were stored at -20 ℃ for 1 hour and then dried under reduced pressure.

Chapter 3

Fabrication and characterization of shape memory polyurethane porous scaffold

3 Fabrication and characterization of shape memory polyurethane porous scaffold

3.1 Introduction

Tissue engineering is a promising alternative for treating bone defects caused by trauma, tumors, congenital malformations, degeneration, aging, or bone diseases [1, 2]. Treatment options are mainly centered on remodeling the damaged bone. One of the most commonly employed strategies for bone remodeling is surgical intervention to implant a suitable bone substitute in the damaged area, or bone grafting using natural and synthetic materials [3, 4]. Therefore, the development of synthetic materials for bone tissue engineering is paramount to satisfy the booming demand for orthopedic implantations. Artificial bone implants made of metals, ceramic, polymers, and composites are synthesized and widely used for bone reconstruction and regeneration [5-11]. These scaffolds play a crucial role in tissue engineering because they represent an alternative to the conventional implantation of organs and tissues. The main goal of scaffolds is to provide an appropriate base for tissue growth and cell proliferation [12]. However, the design of scaffolds should be improved so that they can precisely match the irregular boundaries of bone defects as well as facilitate their clinical application. Shape memory polymers (SMP) are a well-known class of stimuli-responsive materials [13]. They can be controlled to hold a secondary shape but recover their permanent shape under an external stimulus. This property can be designed and altered by changing the structure, morphology, and various processing parameters of the polymer during fabrication [14]. The fabrication of

three-dimensional porous SMP structures can be designed following the methods below: (1) Solvent casting/particle leaching (SC/PL) [15], (2) thermally-induced phase separation (TIPS) [16], (3) melt molding [17], (4) gas foaming [18], and (5) emulsion freeze-drying [19].

In this chapter, Shape memory polyurethane (SMPU) which is synthesized with diphenylmethane-4, 4,-diisocyanate (MDI), adipic acid, ethylene glycol, ethylene oxide (EO), polypropylene oxide (PO), 1, 4-butanediol, bisphenol A and ε-caprolactone is purchased from SMP Technologies Inc. A SMPU scaffold with the three-dimensional porous structure was fabricated using a salt-leaching-phase inverse technique, a unique method to fabric porous structure. The use of different size of NaCl particles to obtain scaffolds with different apertures was investigated. The porosity, compression recovery rate, shape recovery rate of the porous scaffolds were related to the apertures of scaffolds. In the research, the present scaffold design was revealed to have good potential for application in the field of bone tissue engineering.

3.2 Experimental

3.2.1 Materials

SMPU solution (MS5520, SMP Technologies Inc, Japan), composed of hard segment (diisocyanate and chain extender) and soft segment (polyol) with glass transition temperature (T_g) of 50 ℃, was used as a base material. NaCl and distilled water (dH_2O) were obtained from Wako Pure Chemical Industries, Ltd. (Nagano, Japan).

3.2.2 Fabrication of different sizes of NaCl particles

NaCl was ground in a ball mill (Pulverisette 6, Fritsch Janpan Co., Ltd) at 300 rpm for 5 min. Four sizes of NaCl powders were filtered using sieves with different mesh sizes (200 mesh, 100 mesh, 50 mesh and 10 mesh). The flowchart was shown in Figure 3.1. Theoretically, these four sizes of NaCl powders were <50 μm (>200 mesh), 50-100 μm (200-100 mesh), 100-160 μm (100-50 mesh) and 160-450μm (50-10 mesh).

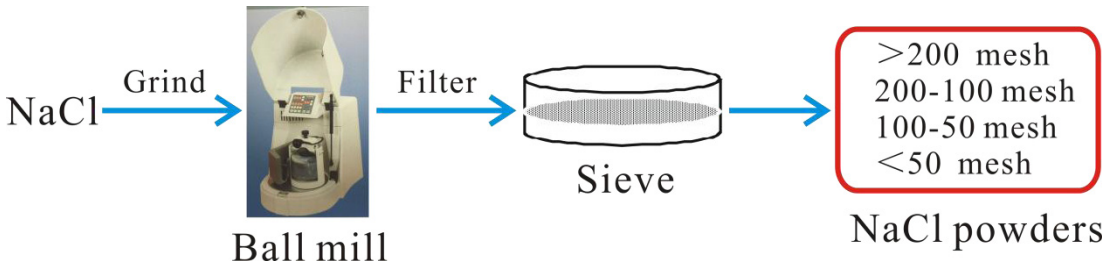

Figure 3.1 Flowchart of the preparation of NaCl powders with different sizes.

3.2.3 Fabrication of SMPU scaffolds

Firstly, 6.7 mL of SMPU solution was completely dissolved in 3.3 mL dimethylformamide (DMF), followed by the addition of 15.0 g NaCl (one of the four sizes) with stirring for 24 hours. Then the solution was poured into a Teflon plate, and ultrasonicated for 10 mintues and placed under vacuum for 12 hours to remove bubbles. The degassed plate was dried at 60 ℃ for 2 hours and then at 80 ℃ for 5 days to obtain composites containing SMPU and different sizes of NaCl powder. The composites were soaked in dH_2O at 40 ℃ refreshed every 4 hours to remove the NaCl. Finally, the composites were dried at 40 ℃ for one day to obtain the SMPU

sponge scaffolds, denoted SMPU-200, SMPU-200-100, SMPU-100-50 and SMPU-50 based on the size of the NaCl powder used. The flowchart was shown in Figure. 3.2.

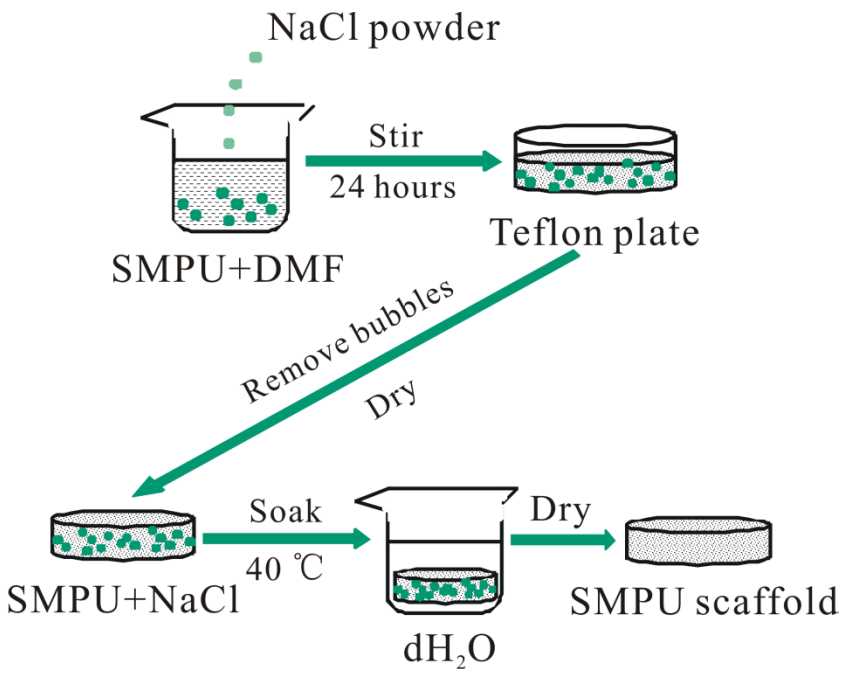

Figure 3.2 Flowchart of the preparation of SMPU porous scaffold.

3.2.4 Characterization of SMPU scaffolds

The complete removal of NaCl was determined using the chemical method and XPS of the SMPU scaffold. The morphology of the SMPU scaffold was analyzed with SEM and μ-CT. Compression tests were conducted with KES. DMA of the SMPU and SMPU scaffold specimens was carried out a thermo-mechanical cycle test was conducted to investigate the shape recovery properties of the SMPU scaffolds. The density and porosity of the SMPU scaffolds was analyzed using Eqns. (2-7) and (2-9).

3.2.5 Evaluation of SMPU scaffold in vitro

In vitro cell proliferation experiments were used to evaluate the four synthesized scaffolds (SMPU-200, SMPU-200-100, SMPU-100-50, and SMPU-50). Firstly, the sterilized scaffolds (Φ 6 mm × 2 mm) were added to 96-well plates. MG-63 cells were seeded into the 96-well plates at a density of 1×10^4 cells/well and maintained in DMEM containing 5% FBS. After 1 d, 3 d, 5 d, and 7 d of culture, the cell growth was determined by MTT assay. The absorbance was measured at 595 nm using a spectrophotometric microplate reader. For comparison, a blank was also used for the cell culture. All operations were carried out under aseptic conditions.

3.3 Results and discussion

3.3.1 The removel of NaCl of SMPU scaffold

In this chapter, SMPU-200 and SMPU-200-NaCl were selected for the determination of NaCl removal. Figure 3.3A showed photographic images of the reaction between silver ions and chloride ions in the leaching liquid of SMPU-200-NaCl. After 5 days of leaching treatment, no white precipitate was observed in the solution, which meant that all NaCl had been removed from the scaffold. XPS analysis was performed to further confirm the complete removal of NaCl from the scaffold. Figure 3.3B showed that unlike the spectrum of SMPU-200-NaCl, that of SMPU-200 contained no peaks from Na and Cl, which meant that no NaCl remained inside SMPU-200 scaffold.

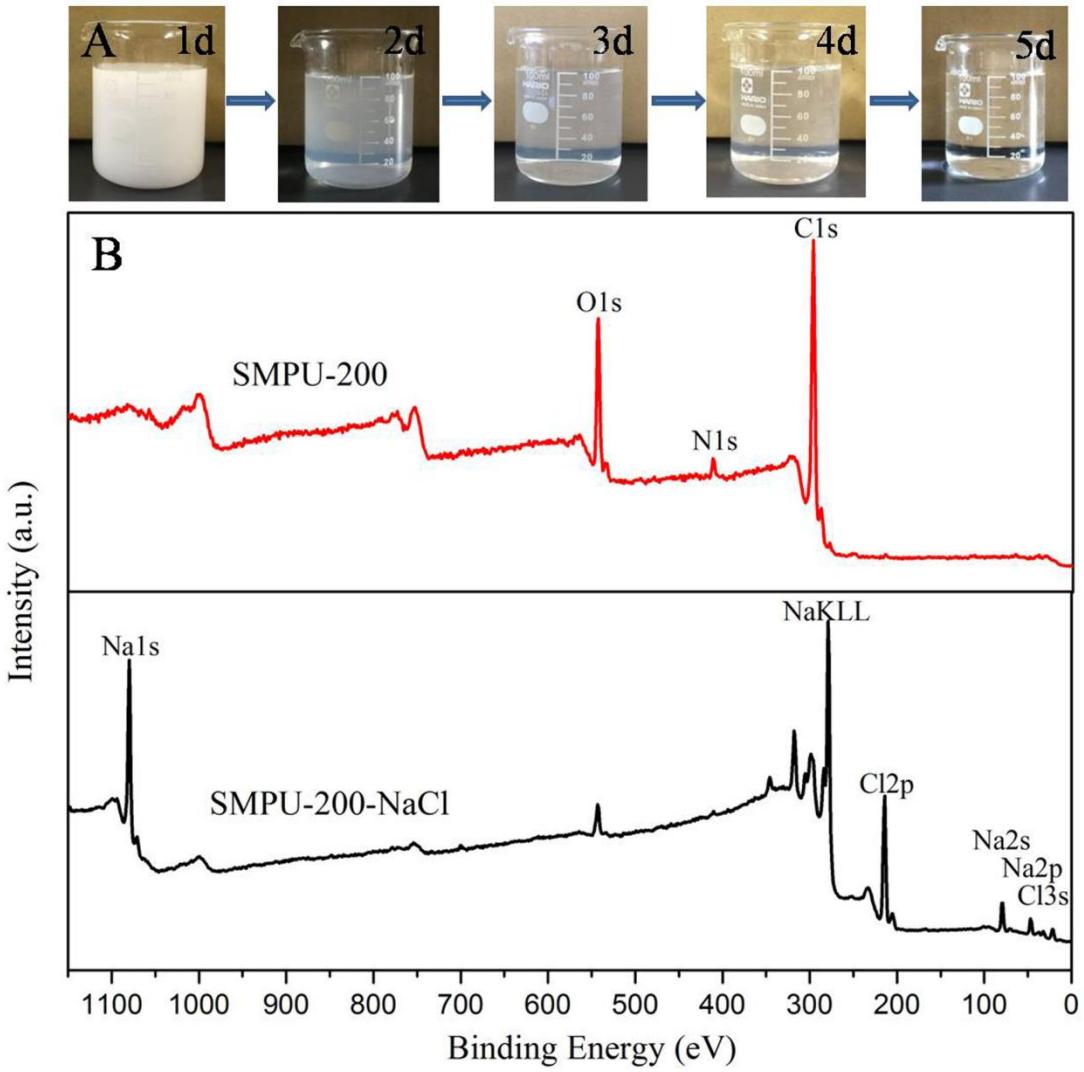

Figure 3.3 (A) Photographs of the evaluation of the removal of NaCl using the chemical method (reaction of silver ions with chloride ions in the leaching liquid); (B) XPS spectra of SMPU-200 and SMPU-200-NaCl.

3.3.2 The morphology and physical characteristics of SMPU scaffolds

The morphology of the four scaffolds was shown in Figure 3.4 and 3.5, and their physical properties were summarized in Table 3-1. The apertures of the scaffolds were found to be irregular owing to the irregularity of NaCl particles. Theoretically,

the apertures of SMPU-200, SMPU-200-100, SMPU-100-50, and SMPU-50 scaffolds should have been 0-50 μm, 50-110 μm, 110-160 μm, and 160-450 μm, respectively. Using the software Nano Measurer 1.2 (Jie Xu, Department of Chemical, Fudan University), the mean apertures of the four scaffolds were found to be 36.47 μm, 82.73 μm, 123.00 μm, and 243.47 μm, respectively (Table 3-1). According to Eqns. (2-7) and (2-9), the porosity of the four SMPU scaffolds were calculated to be 77.13%, 79.50%, 80.85%, and 83.13%, respectively. In other words, the porosity of the scaffolds increased with their apertures. The three-dimensional structure of the four SMPU scaffolds was shown in Figure 3.5. The obtained μ-CT images confirmed that all of the scaffolds had a three-dimensional structure with a different aperture, and the size of pores increased with the NaCl particle sizes.

Table 3-1

Porosity and apertures of the four SMPU scaffolds

Sample	ρ (g/cm^3)	Porosity (%)	Theoretical aperture (μm)	Mean aperture (μm)
SMPU-200	0.2790	77.13	0-50	36.47
SMPU-200-100	0.2501	79.50	50-110	82.73
SMPU-100-50	0.2336	80.85	110-160	123.00
SMPU-50	0.2059	83.13	160-450	243.47

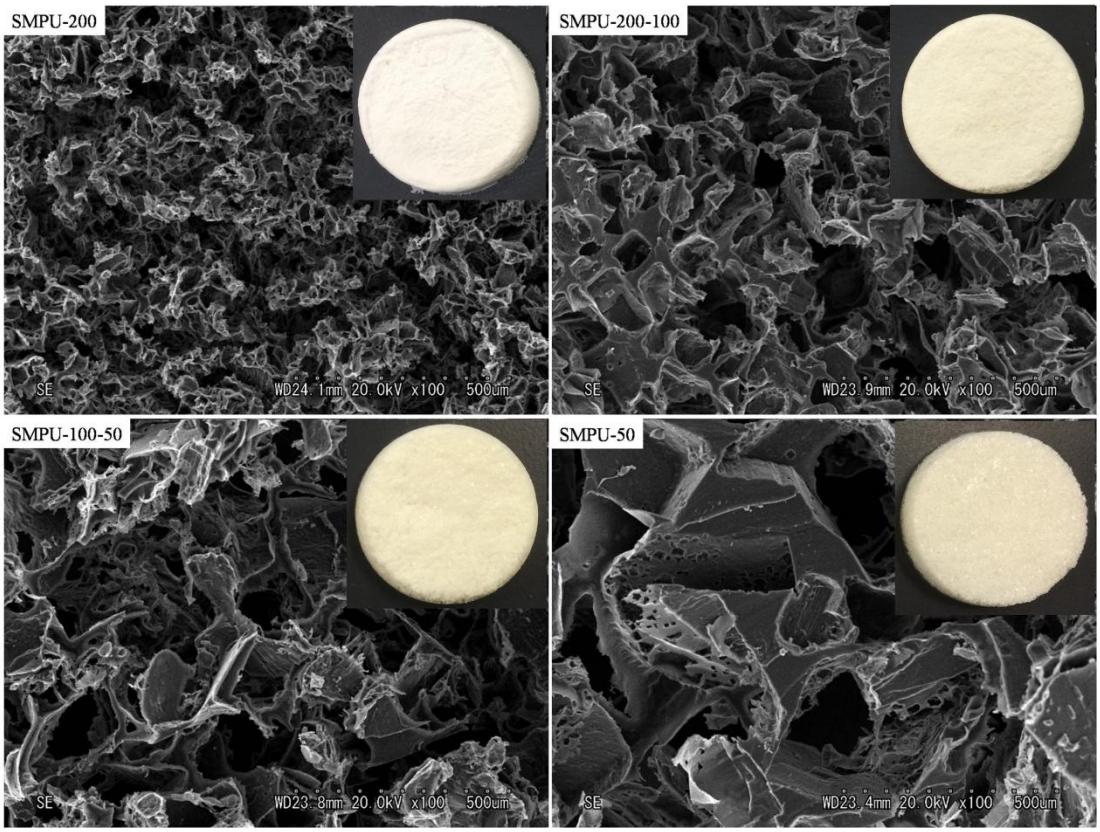

Figure 3.4 SEM images of the four SMPU scaffolds (SMPU-200, SMPU-200-100, SMPU-100-50, and SMPU-50).

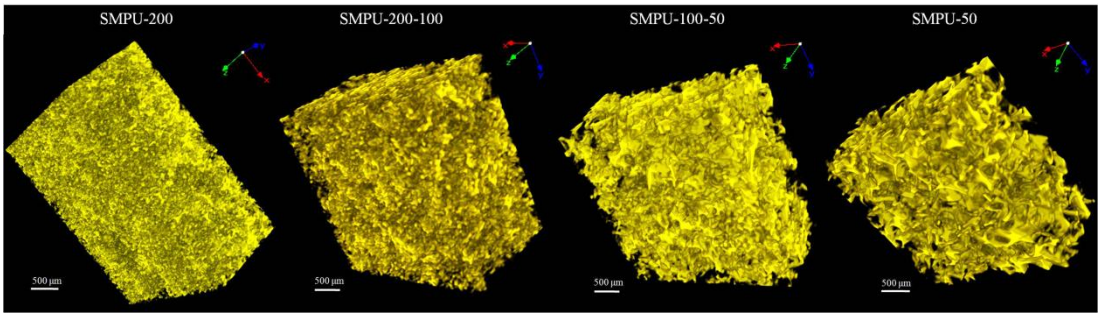

Figure 3.5 μ-CT images of the four SMPU scaffolds (SMPU-200, SMPU-200-100, SMPU-100-50, and SMPU-50).

3.3.3 Compression behavior

The compressive stress-strain curves of the four SMPU scaffolds were shown in Figure 3.6. Under the maximum load, the strains of the four scaffolds (SMPU-200, SMPU-200-100, SMPU-100-50 and SMPU-50) which increased with their apertures were 16.83%, 26.51%, 29.44%, and 42.88%, respectively. This meant that the smaller the pores of the scaffolds were, the less deformation they experienced and the greater their compression resistanced. From the Eqns. (2-2) and (2-3), the modulus of compression of four scaffolds at the stress of 0.00215 MPa (E_0) and 0.12065 MPa (E_1) were calculated in Table 3-2. According to the data, with the increase of the apertures of these four scaffolds, the values of E_0 and E_1 were increased and decreased, respectively. It meant that, at the beginning of the compression test, the bigger the pores of scaffolds were, the more difficult for scaffolds compressed and the higher the carrying capacity of scaffolds had. And at the end of the test, the smaller the pores of the scaffold were, the less deformation they experienced and the greater their compression resistance was. Furthermore, using Eqn. (2-4), at an applied stress of 0.125 MPa, the compression shape recovery ratios of SMPU-200, SMPU-200-100, SMPU-100-50, and SMPU-50 were determined to be 97.77%, 98.53%, 99.13% and 99.30%, respectively. Therefore, these results demonstrated that the compression shape recovery of the SMPU scaffolds increased with their apertures.

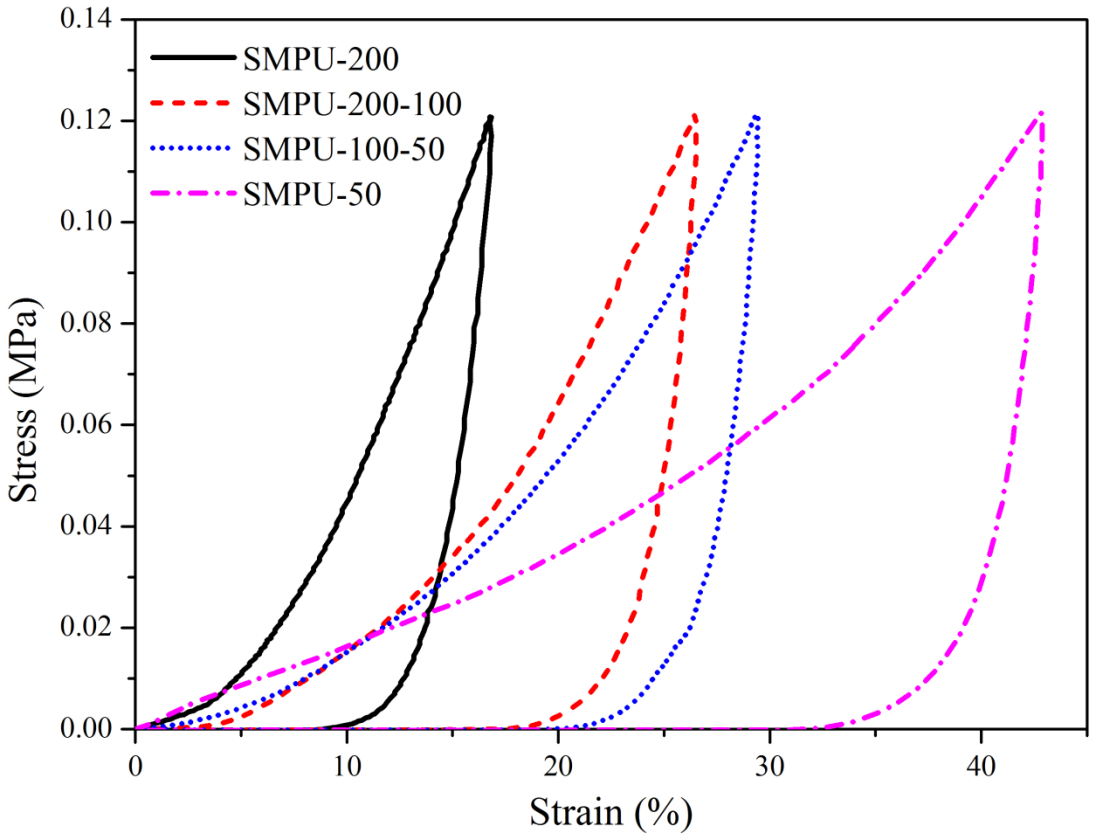

Figure 3.6 Compressive stress-strain curves of the four SMPU scaffolds (SMPU-200, SMPU-200-100, SMPU-100-50, and SMPU-50) at room temperature.

Table 3-2

The data of four scaffolds with compressive test

Sample	Strain (at 0.12 MPa)	R_c (at 0.12 MPa)	E_0	E_1
SMPU-200	16.83%	97.77%	0.1218	1.1780
SMPU-200-100	26.51%	98.53%	0.1618	0.8862
SMPU-100-50	29.44%	99.13%	0.1703	0.6736
SMPU-50	42.88%	99.30%	0.1740	0.5814

3.3.4 DMA analysis

The storage modulus and tan delta of the four SMPU scaffolds from the DMA test were shown in Figure. 3.7. The glass-transition temperatures (T_g) of SMPU scaffods were the same, 50 ℃, using the tan delta peak, indicating that the aperture of the SMPU scaffolds had no significant effect on its T_g.

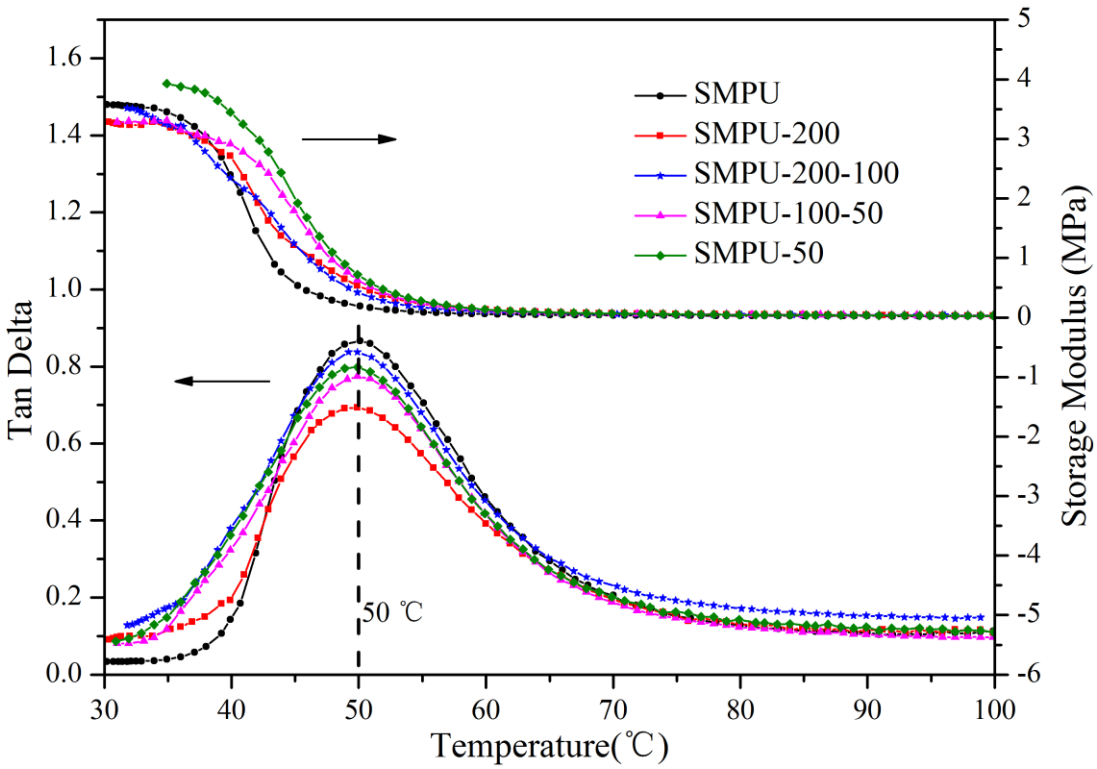

Figure 3.7 Storage modulus and tan delta of SMPU, SMPU-200, SMPU-200-100, SMPU-100-50 and SMPU-50 from DMA tests.

3.3.5 Thermo-mechanical properties

The stress-strain-temperature curves of SMPU-200, SMPU-200-100, SMPU-100-50, and SMPU-50 scaffolds which were obtained using the five-step

thermo-mechanical test were shown in Figure 3.8. Step 1: samples were tensiled to a maximum force of 100 mN at 55 ℃; step 2: samples were holded at 100 mN for 5 minutes at 55 ℃; step 3: samples were cooled to about 20 ℃ under 100 mN load; step 4: samples were holded for 5 minutes at about 20 ℃ under no load; step 5: samples were heated to 55 ℃ under no load. These five steps which associated with the shape fixity and recovery of the samples were highlighted. The shape fixity and recovery ratios were the important parameters for determining and evaluating the characteristics of SMPU scaffolds. From the Eqn. (2-4), the shape recovery ratio of SMPU-200, SMPU-200-100, SMPU-100-50, and SMPU-50 was determined to be 97.46%, 93.04%, 92.28% and 90.86%, respectively, indicating that the shape recovery ratio of the SMPU scaffolds was decreased with the increase of aperture.

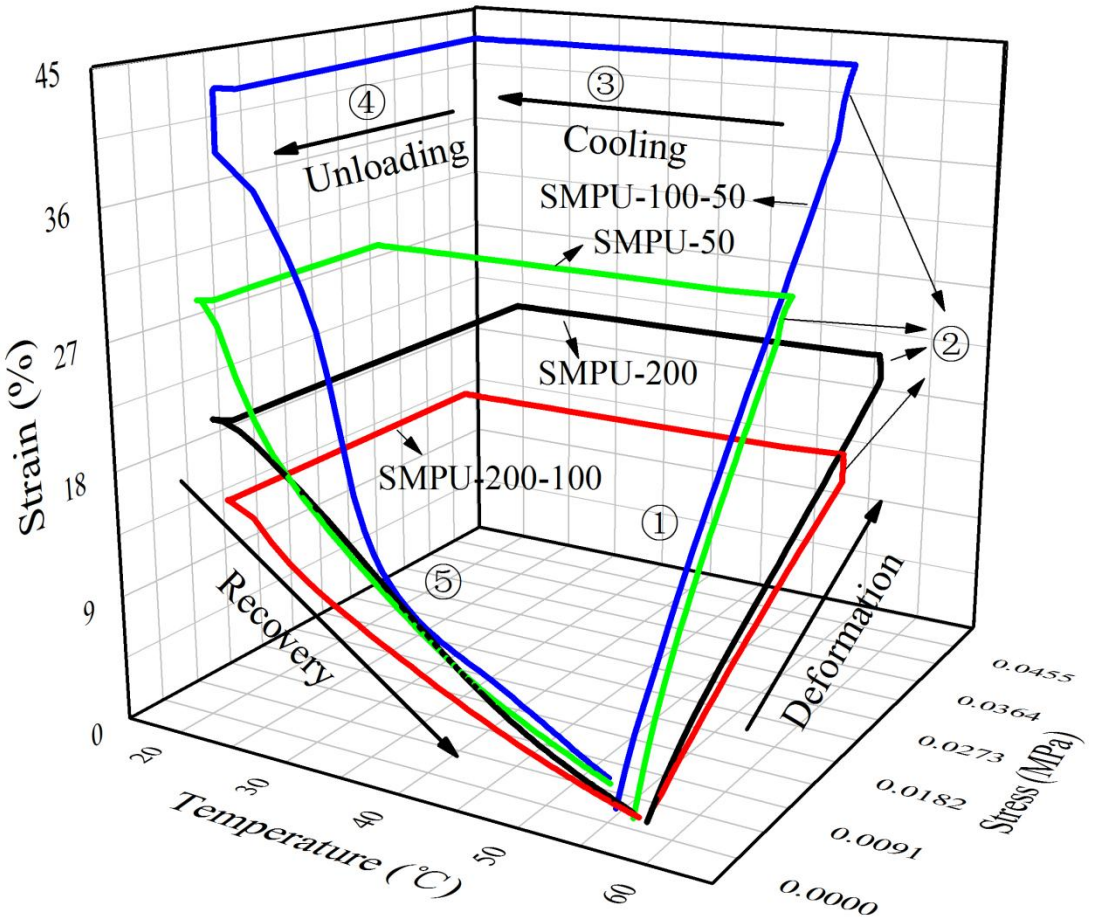

Figure 3.8 Five-step thermo-mechanical test: ① tensiled to a maximum force of 100 mN at 55 ℃, ② holded at 100 mN for 5 minutes, ③ cooled to about 20 ℃ under 100 mN load, ④ holded for 5 minutes at about 20 ℃ under no load, and ⑤ heated to 55 ℃ under no load. The black, red, blue, and green lines are the stress-strain-temperature curves of SMPU-200, SMPU-200-100, SMPU-100-50, and SMPU-50, respectively.

3.3.6 Properties of SMPU scaffolds in vitro

The proliferation of MG-63 cells on the SMPU scaffolds after 1 d, 3 d, 5 d, and 7 d

of culture were shown in Figure. 3.9. Compared with that of the blank control, the $OD_{595\ nm}$, which represented the number of living cells, of the samples which were cultured with MG-63 cells for 1 d, 3 d, 5 d, and 7 d were slightly higher. At the same day number, the cell number slightly increased with the aperture of the scaffolds. This indicated that the larger the aperture was, the easier it was for the cell to adhere to and proliferate on the scaffolds.

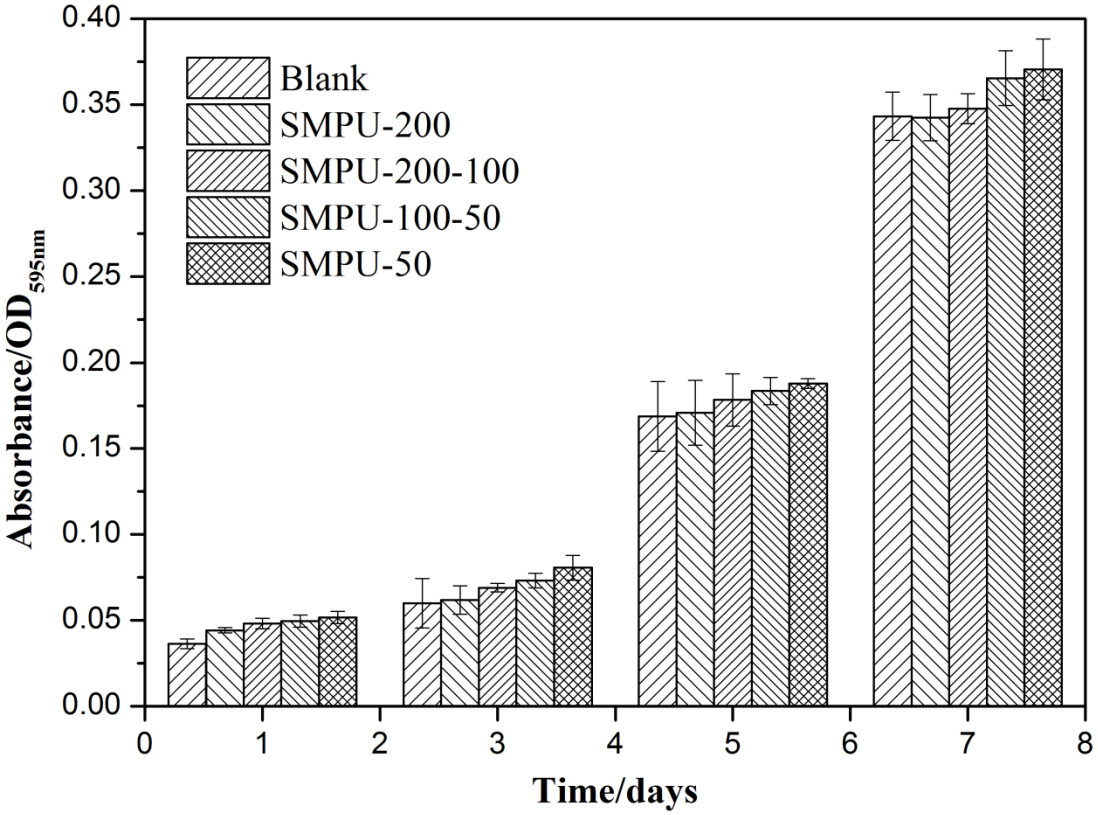

Figure 3.9 Proliferation of MG-63 cells on the four SMPU scaffolds (SMPU-200, SMPU-200-100, SMPU-100-50, and SMPU-50) after 1 d, 3 d, 5 d, and 7 d of culture.

Meanwhile, the morphology of the MG-63 cells on the SMPU scaffolds was observed to be fusiform-like with pseudopodia (Figure 3.10). The SEM images of scaffolds cultured with MG-63 cells for 1 d, 3 d, 5 d, and 7 d are shown in Figure

3.11. The images showed that the number of living cells in all samples increased with the culture day. On the same day of culture, the number cells on the scaffolds slightly increased with the aperture, consistent with the results in Figure. 3.9. In other words, the four SMPU scaffolds (SMPU-200, SMPU-200-100, SMPU-100-50 and SMPU-50) had a cell proliferation promoting ability that increased with the aperture of the scaffold.

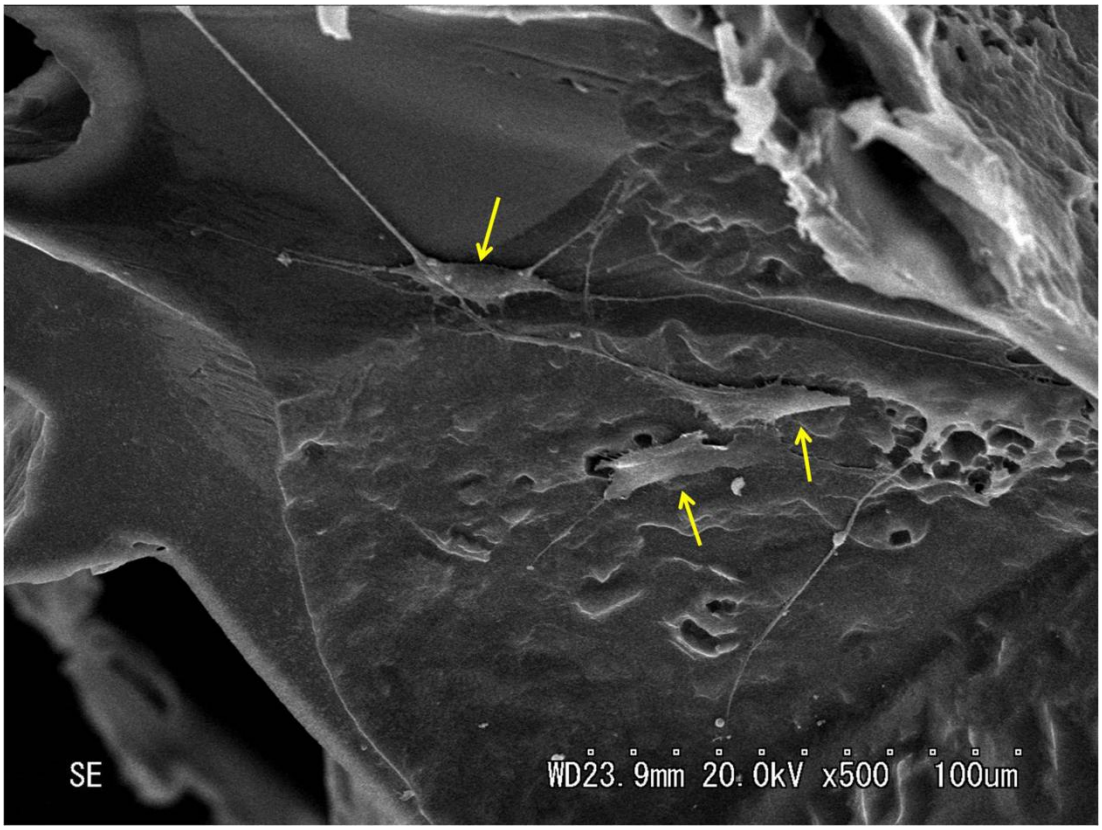

Figure 3.10 Morphology of MG-63 cells on the SMPU scaffolds (×500). Yellow arrows indicate MG-63 cells.

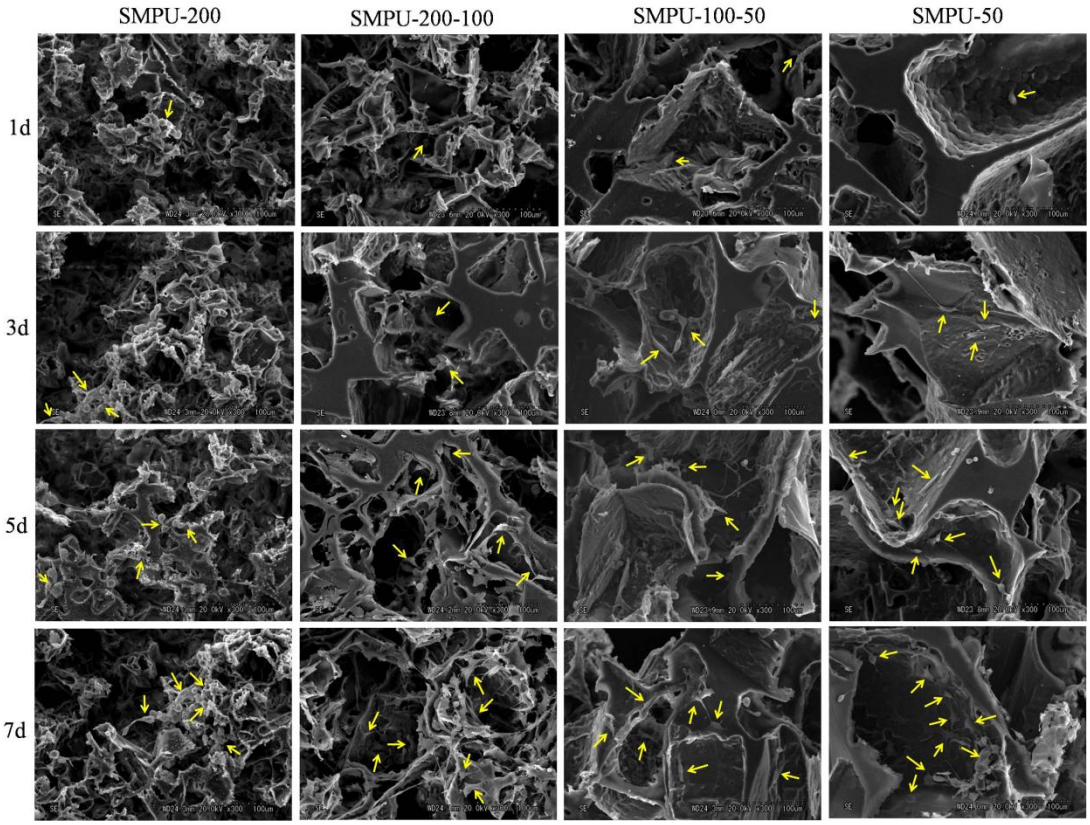

Figure 3.11 SEM images of MG-63 cultured on the four SMPU scaffolds (SMPU-200, SMPU-200-100, SMPU-100-50, and SMPU-50) after 1 d, 3 d, 5 d, and 7 d (×300). Yellow arrows indicate MG-63 cells.

3.4 Conclusions

Four scaffolds (SMPU-200, SMPU-200-100, SMPU-100-50, and SMPU-50) were fabricated via a salt-leaching-phase inverse technique, a unique method to fabric porous structure. Their mechanical properties and shape recovery behaviors were investigated. Aperture had no significant effect on the T_g (50 ℃) of the SMPU scaffolds. However, with increasing of the aperture, the porosity of the scaffolds increased from 77.13% to 83.13% and their compression recovery ratio increased from 97.77% to 99.30% at room temperature, but their shape recovery ratio

decreased from 95.0% to 91.1% at 55 ℃ higher than T_g. Moreover, all SMPU scaffolds promoted cell proliferation on their surface, and the ability increased with the aperture of the scaffold. Thus, the present scaffolds have good prospects for application in bone tissue engineering.

References

[1] S.L. Wu, X.M. Liu, K.W.K. Yeung, *et al*. Biomimetic porous scaffolds for bone tissue engineering. Mater. Sci. Eng. R., 2014, 80: 1-36.

[2] N. Shadjou and M. Hasanzadeh. Bone tissue engineering using silica-based mesoporous nanobiomaterials: Recent progress. Mater. Sci. Eng. C., 2015, 55: 401-409.

[3] S. Sethuraman, L.S. Nair, S. El. Amin, *et al*. Mechanical properties and osteocompatibility of novel biodegradable alanine based polyphosphazenes: Side group effects. Acta Biomater., 2010, 6 (6): 1931-1937.

[4] S. Sethuraman, L.S. Nair, S. El. Amin, *et al*. Development and Characterization of Biodegradable Nanocomposite Injectables for Orthopaedic Applications Based on Polyphosphazenes. J. Biomater. Sci. Polym. Ed., 2011, 22 (4-6): 733-752.

[5] K. Alvarez and H. Nakajima. Metallic Scaffolds for Bone Regeneration. Materials, 2009, 2 (3): 790-832.

[6] Z.J. Li, X.N. Gu, S.Q. Lou, *et al*. The development of binary Mg-Ca alloys for use as biodegradable materials within bone. Biomaterials, 2008, 29 (10): 1329-1344.

[7] R. Rai, T. Keshavarz, J.A. Roether, *et al*. Medium chain length polyhydroxyalkanoates, promising new biomedical materials for the future. Mater. Sci. Eng. R., 2011, 72 (3): 29-47.

[8] J. He, T. Huang, L. Gan, *et al*. Collagen-infiltrated porous hydroxyapatite coating and its osteogenic properties: In vitro and in vivo study. J. Biomed. Mater. Res. A., 2012, 100A (7): 1706-1715.

[9] X.P. Fan, B. Feng, Z.Y. Liu, *et al*. Fabrication of TiO_2 nanotubes on porous titanium scaffold and biocompatibility evaluation in vitro and in vivo. J. Biomed. Mater. Res. A., 2012, 100A (12): 3422-3427.

[10] M.L. Xie, M.O. Olderoy, Z.B. Zhang, *et al*. Biocomposites prepared by alkaline phosphatase mediated mineralization of alginate microbeads. RSC Adv., 2012, 2: 1457-1465.

[11] S.L. Wu, X.M. Liu, K.W.K. Yeung, *et al*. Hydrogen release from titanium hydride in foaming of orthopedic NiTi scaffolds. Acta Biomater., 2011, 7 (3): 1387-1397.

[12] P.X. Ma. Scaffolds for tissue fabrication. Mater. Today, 2004,7 (5): 30-40.

[13] C. Liu, H. Qin and P.T. Mather. Review of progress in shape-memory polymers. J. Mater. Chem., 2007, 17: 1543-1558.

[14] T. Xie. Recent advances in polymer shape memory. Polymer, 2011, 52 (22): 4985-5000.

[15] D.C. Sin, X.G. Miao, G. Liu, *et al*. Polyurethane (PU) scaffolds prepared by solvent casting/particulate leaching (SCPL) combined with centrifugation. Mater. Sci. Eng. C., 2010, 30 (1): 78-85.

[16] A.S. Rowlands, S.A. Lim, D. Martin, *et al*. Polyurethane/poly (lactic-co-glycolic) acid composite scaffolds fabricated by thermally induced phase separation. Biomaterials, 2007, 28 (12): 2109-2121.

[17] K. Ishizaki, S. Komarneni and M. Nanko. Porous Materials, Processing Technology and Applications. 1998.

[18] H.J. Kim, K. Park, J.H. Kim, *et al*. Gas foaming fabrication of porous biphasic calcium phosphate for bone regeneration. Tissue Eng. Regen. Med., 2012, 9 (2):

63-68.

[19] A.M. Clyne. Thermal processing of tissue engineering scaffolds. J. Heat Transf., 2011, 133 (3): DOI: 10.1115/1.4002464.

Chapter 4

Preparation and characterization of porous shape memory polyurethan nano-hydroxyapatite composite scaffold

4 Preparation and characterization of porous shape memory polyurethan nano-hydroxyapatite composite scaffold

4.1 Introduction

Tissue engineering is a promising alternative for treating bone defects, which come from trauma, infection, tumor, and local bone loss caused by some congenital diseases [1]. Bone tissue engineering is the combination of three elements of seed cells, growth factors and scaffold materials for bone tissue construction and regeneration in vivo and in vitro [2, 3]. The scaffold which provides space for cell growth, proliferation and differentiation, is a key factor in bone tissue engineering [4-8]. And also scaffolds with interconnected pores and a large surface area tend to promote cell attachment, growth, and tissue regeneration in three dimensions [9-11].

Shape memory materials are defined by their capacity to recover a predetermined shape after significant mechanical deformation and the shape memory effect is typically initiated by a change in temperature [12]. The widespread applications of the shape memory effect in polymers were heat-shrink tubing [13], shape memory polymer-based medical devices [14-16] and microsystem components [17, 18]. Shape memory polymers have the potential to significantly impact minimally invasive surgery and implants because simple and reliable actuation is often needed in the restricted and highly variable bodily environment. For example, a “smart” suture that automatically closes wounds to a tailored force level with minimal intervention has

been developed [19]. A shape memory polymer foam has been studied for filling aneurisms via endovascular intervention [15].

Polyurethane refers to the high molecular compounds in a repeat of the carbamate group (-NHCOO-) in the main chain of polymer structure. The molecular chain of polyurethane is usually composed of two parts, “hard segment” and “soft segment” are often used to describe its structure [20]. Due to the thermodynamic incompatibility between hard segment and soft segment, the soft and hard segments will be dispersed to form an independent micro area. The unique micro phase separation structure provide the polyurethane of good processing performance, good mechanical properties, high elasticity, lubrication, wear resistance, fatigue resistance and biocompatibility [21]. Compared with other biomedical materials, the micro phase separation structure of polyurethane is similar to biological membrane mechanism. Not only the given material with good mechanical properties and easy processing, it also improves the blood compatibility and biocompatibility [22].

Hydroxyapatite (HAP), $Ca_{10}(PO_4)_6(OH)_2$, is belonging to the structure of the six party. It is a component of human hard tissue and has good biological activity, bone guidance and biocompatibility [23, 24]. The application of various methods of HAP alone or with other material made the porous material, which can be used as carrier of antibiotics, anti-inflammatory drugs, growth factor and polypeptide drugs, such as α interferon [25], amino glucoside [26], gentamicin [27], methylene blue [28], ibuprofen [29], cytochrome [30], serum protein [31] and bone formation protein [32]. Therefore, HAP is usually used as a filling material for bone defect sites or as a surface coating to promote bone ingrowths into the implant.

In this chapter, we have successfully fabricated nHAP particles which were used

as the main inorganic component of bone to promote cell ingrowths into the scaffold. Before being used, the nHAP particles had been mixed with SMPU by the method of size controllable design to obtain the three-dimensional (3D) porous SMPU/nHAP composite scaffolds with different apertures. Using the shape memory property of SMPU in order to let the scaffold can better match the boundaries of bone defects. And their physical characteristics, mechanical properties, shape recovery behaviors and biological performance related to the aperture of the scaffolds were investigated. In this research, it is found that the porous SMPU/nHAP composite scaffolds with interconnected pores have good potential for application in the field of minimally invasive surgery and bone tissue engineering.

4.2 Materials and methods

4.2.1 Materials

SMPU solution (MS5520, SMP Technologies Inc, Japan), composed of hard segment (diisocyanate and chain extender) and soft segment (polyol) with glass transition temperature (*Tg*) of 50 ℃, was used as a base material. Sodium chloride (NaCl), calcium chloride ($CaCl_2$), disodium phosphate (Na_2HPO_4), sodium hydroxide (NaOH), N,N-dimethylformamide (DMF), absolute ethanol, distilled water (dH_2O), 96-well plates, phosphate buffered solution (PBS), glutaric dialdehyde (GA) and t-butyl alcohol were obtained from Wako Pure Chemical Industries, Ltd. (JAPAN). Dulbecco's modified Eagle's medium (DMEM) and fetal bovine serum (FBS) were obtained from Gibco company (USA). MG-63 cells were obtained from Riken BioResource Center (Japan).

4.2.2 Preparation of rod-like nHAP particles

Firstly, 5.78 g $CaCl_2$ and 10.853 g Na_2HPO_4 were dissolved in 500 mL dH_2O, separately. Then, 500 mL Na_2HPO_4 (0.06 M) was added dropwisely into the 500 mL $CaCl_2$ (0.1 M) solution, while keeping the pH value of the reaction system at 9 by adding NaOH aqueous solution (1 M) with stirring for 6 hours. After the reaction, the solution was placed in an incubator at 37 ℃ for 4 days. Lastly, the precipitate was collected by centrifugation and rinsed with dH_2O and absolute ethyl alcohol for 3 times alternatively to obtain the nHAP particles.

4.2.3 Fabrication of SMPU/nHAP scaffolds

Firstly, 6.7 mL of SMPU solution was completely dissolved in 3.3 mL dimethylformamide (DMF), followed by adding 0.15 g nHAP particles with stirring for 2 hours and 15.0 g NaCl (four sizes: >200 mesh, 200-100 mesh, 100-50 mesh and 50-10 mesh) with stirring for 24 hours. Then the solution was poured into a Teflon plate, and ultrasonicated for 10 minutes and placed under vacuum for 12 hours to remove bubbles. The degassed plate was dried at 60 ℃ for 2 hours and then at 80 ℃ for 5 days to obtain composites containing SMPU, nHAP and different sizes of NaCl powders. The composites were soaked in dH_2O at 40 ℃ to remove the NaCl and refreshed with dH_2O every 4 hours. Finally, the composites were dried at 40 ℃ for one day to obtain the SMPU/nHAP sponge scaffolds, denoted SMPU/nHAP-200, SMPU/nHAP-200-100, SMPU/nHAP-100-50 and SMPU/nHAP-50 based on the size of the NaCl powders used (Figure 4.1).

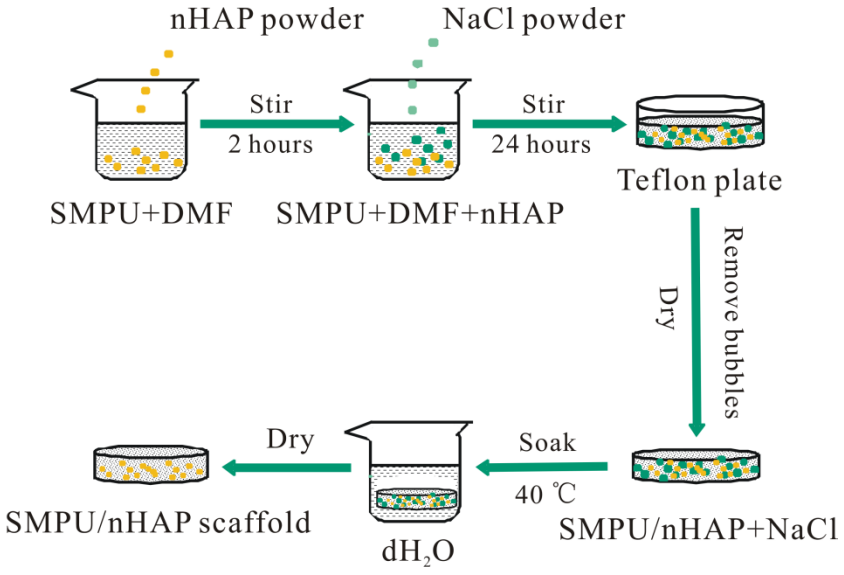

Figure 4.1 Flowchart of the preparation of SMPU/nHAP porous scaffold.

4.2.4 Characterization

The chemical composition and crystallinity of nHAP particles were analyzed with an XRD and the morphology of nHAP particles were investigated using a TEM.

The removal of NaCl of SMPU/nHAP scaffolds was determined by using the chemical method and XPS. The morphology of SMPU/nHAP scaffolds was analyzed with SEM and μ-CT. The density and porosity of SMPU/nHAP scaffolds was analyzed by the Eqns. (2-8) and (2-9). Compression test was conducted with KES. Thermo-mechanical test was conducted to investigate the shape recovery property of SMPU/nHAP scaffolds using TMA.

4.3 Results and discussion

4.3.1 Characterization of nHAP

First, chemical composition of nanoparticles had been characterized using XRD

and the predominant HAP crystal phase had been confirmed according to the standard card of HAP (JCPDS 09-432) (as shown in Figure 4.2a). Generally, the narrower band gap and higher intensity of the diffraction peak indicate the better crystallinity of the particle. From Figure 4.2a, the diffraction peak in the pattern was narrow and intensity was relatively high, which implied that the nanoparticles had higher crystallinity. The morphology of nHAP was shown in Figure 4.2b, in which the nanoparticles had a rod-like shape and were uniformly distributed. The sizes of nHAP particles were ca. 32 nm in length and ca. 10 nm in diameter using the software of Nano Measurer 1.2 (Jie Xu, Department of Chemistry, Fudan University).

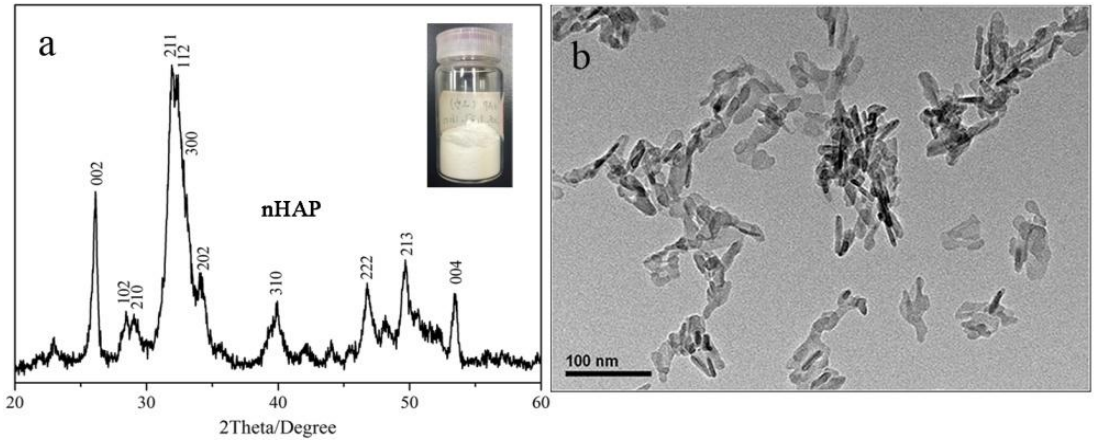

Figure 4.2 XRD pattern (a) and TEM image (b) of nano hydroxyapatite (nHAP) particles.

4.3.2 SMPU/nHAP scaffolds

In this research, SMPU/nHAP-200-100 and SMPU/nHAP-200-100-NaCl had been selected to determine the removal of NaCl. Figure 4.3A showed the reaction of silver ions and chloride ions in the leaching liquid of SMPU/nHAP-200-100-NaCl. After 5

days, it had been seen that there was no white precipitate in the solution, which meant that all NaCl had been removed from the scaffolds. To further determine the removal of NaCl from the scaffolds, XPS analysis was performed. The patterns in Figure 4.3B confirmed that compared with the SMPU/nHAP-200-100-NaCl, SMPU/nHAP-200-100 had no peaks of Na and Cl, which meant that there was no NaCl inside of SMPU/nHAP-200-100 scaffold. In addition, SMPU/nHAP-200-100 scaffold had a peak of Ca, which verified the existence of nHAP particles. According to the mass ratio of nHAP particles to SMPU was 0.075 which indicated that in contrast to the SMPU, the amount of nHAP particles was small, so the intensity of Ca was weak showed in the XPS pattern. Also according to the EDX spectra, the presence of calcium (Ca) and phosphorus (P) was detected which confirmed the existence of nHAP particles.

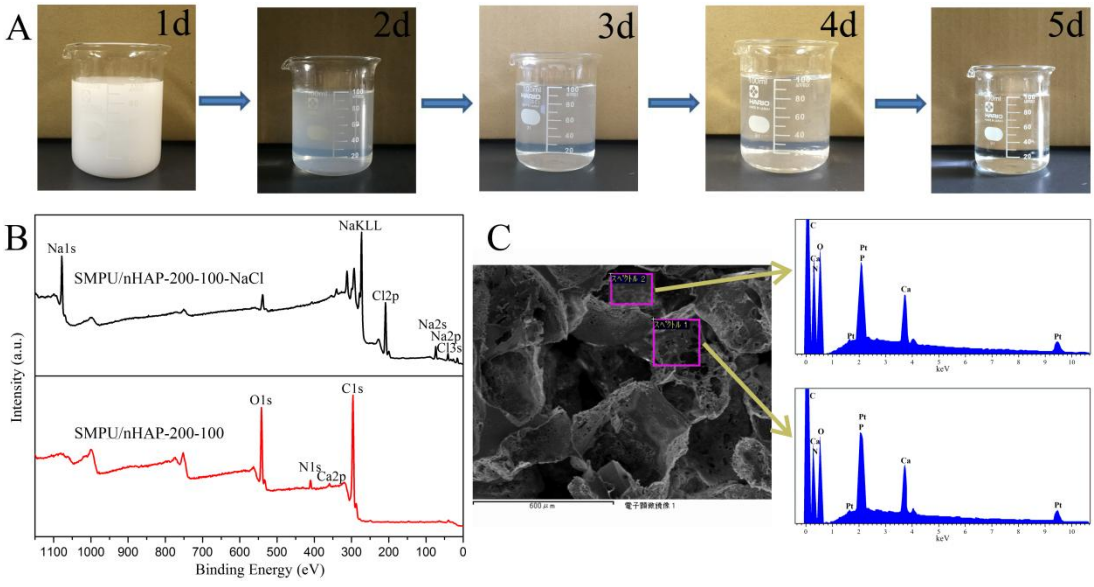

Figure 4.3 (A) Images of the removal of NaCl by using the chemistry method of SMPU/nHAP-200-100-NaCl; (B) XPS patterns of SMPU/nHAP-200-100 and SMPU/nHAP-200-100-NaCl; (C) EDX spectra of SMPU/nHAP-200-100.

The morphology and the distribution of nHAP particles of four scaffolds was shown in Figure 4.4 and 4.5, and their physical properties are summarized in Table 4-1. From Figure 4.4, it was shown that the apertures of scaffolds were irregular due to the irregularity of NaCl particles. Theoretically, the apertures of SMPU/nHAP-200, SMPU/nHAP-200-100, SMPaU/nHAP-100-50, and SMPU/nHAP-50 should have been 0-50 μm, 50-110 μm, 110-160 μm, and 160-450 μm, respectively. Using the software Nano Measurer 1.2, the mean apertures of SMPU/nHAP composite scaffolds were 30.54 μm, 84.38 μm, 126.37μm and 196.97μm, respectively (Table 4-1). It meant that the aperture of scaffolds was controlled by the sizes of NaCl particles. According to Eqns. (2-8) and (2-9), the apparent density and porosity of four scaffolds (SMPU/nHAP-200, SMPU/nHAP-200-100, SMPU/nHAP-100-50, and SMPU/nHAP-50), were found to be 0.2064±0.0008 g/cm^3, 0.1984±0.0033 g/cm^3, 0.1924±0.0026 g/cm^3, 0.1799±0.0090 g/cm^3 and 83.81±0.06%, 84.43±0.26%, 84.91±0.20%, 85.89±0.70%, respectively, and the results were shown in the Table 4-1 and Figure 4.6. According the data, there was a true difference between four scaffolds. In other words, the porosity of the composite scaffolds increased with their increase of apertures. The higher the porosity of scaffold was, the larger the surface area of it. And scaffolds with interconnected pores and a large surface area tend to promote cell attachment, growth, and tissue regeneration in three dimensions.

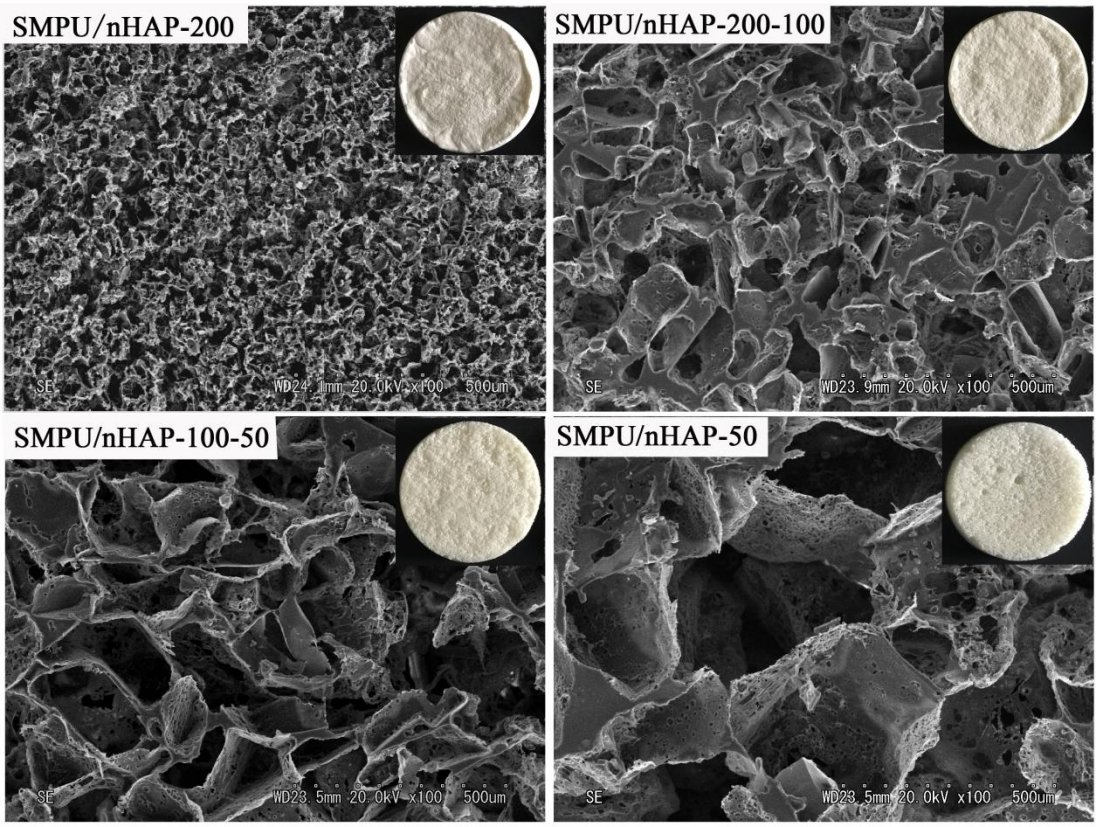

Figure 4.4 SEM images of four SMPU/nHAP scaffolds (SMPU/nHAP-200, SMPU/nHAP-200-100, SMPU/nHAP-100-50, and SMPU/nHAP-50).

Table 4-1

The apparent density, porosity and apertures of four scaffolds

Sample	Apparent density (g/cm^3)	Porosity (%)	Theoretical aperture (μm)	Mean aperture (μm)
SMPU/nHAP-200	0.2064±0.0008	83.81±0.06	0-50	30.54
SMPU/nHAP-200-100	0.1984±0.0033	84.43±0.26	50-110	84.38
SMPU/nHAP-100-50	0.1924±0.0026	84.91±0.20	110-160	126.37
SMPU/nHAP-50	0.1799±0.0090	85.89±0.70	160-450	196.97

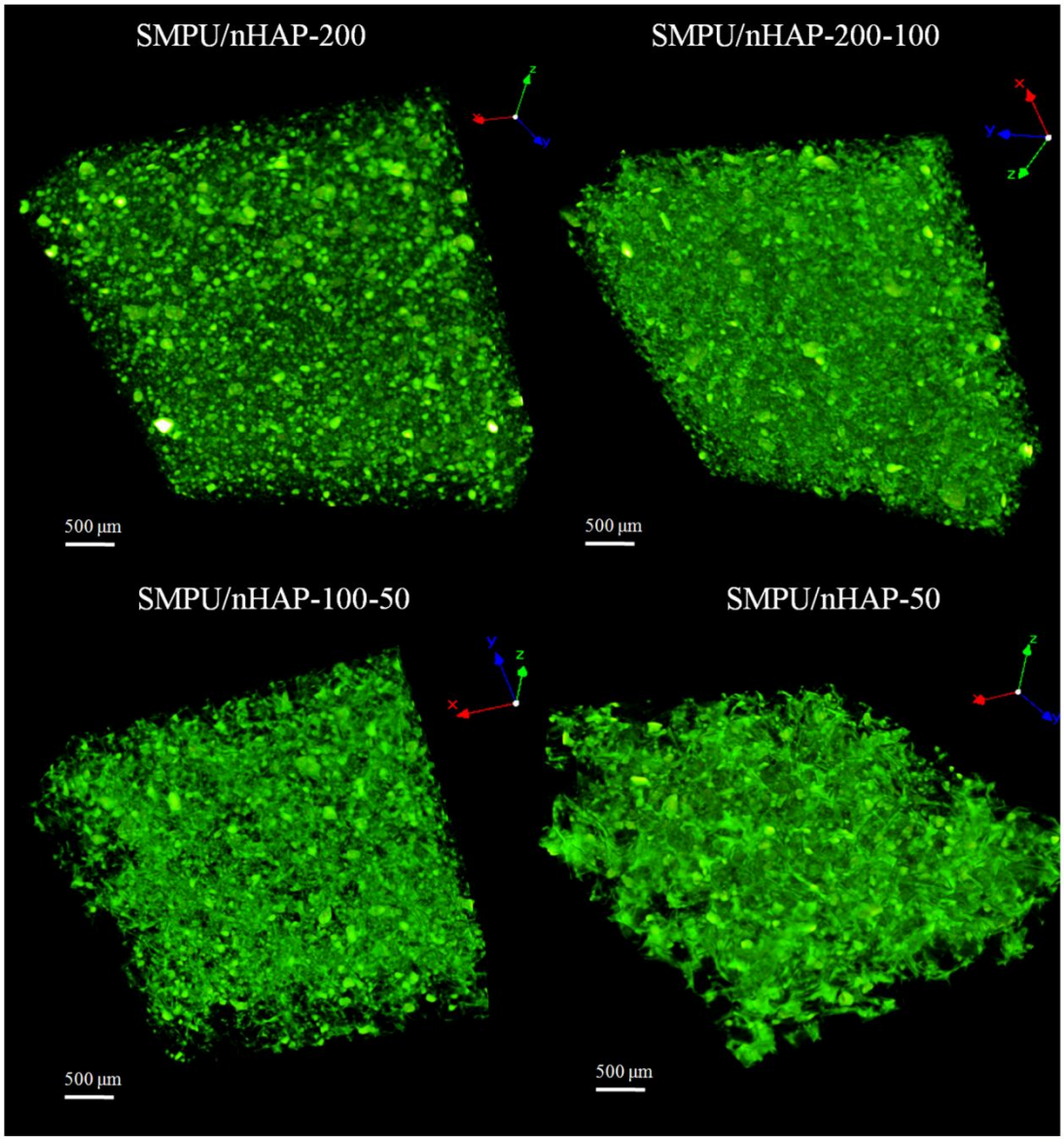

Figure 4.5 μ-CT images of four SMPU/nHAP scaffolds (SMPU/nHAP-200, SMPU/nHAP-200-100, SMPU/nHAP-100-50, and SMPU/nHAP-50).

Meanwhile, three-dimensional structure of these four composite scaffolds was shown in Figure 4.5. From μ-CT images, all SMPU/nHAP composite scaffolds had a three-dimensional structure which was important for cell growth. In these images, it had been seen that the green part represented the SMPU which constituted the skeleton of the scaffold and the yellowish, shiny part represented the nHAP particles

which were uniformly dispersed even if part of them were agglomerated.

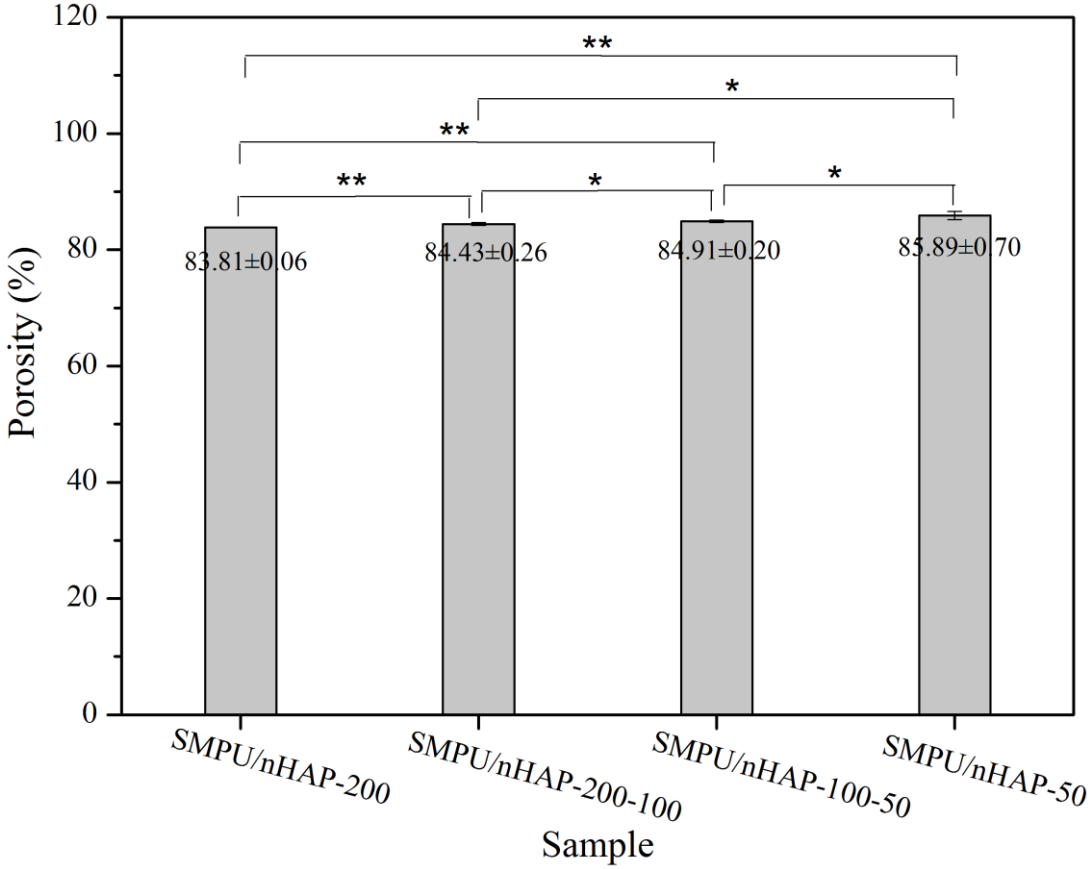

Figure 4.6 The porosity of four SMPU/nHAP composite scaffolds (SMPU/nHAP-200, SMPU/nHAP-200-100, SMPU/nHAP-100-50 and SMPU/nHAP-50). *p＜0.05, **p＜0.01.

4.3.3 Compression behavior

From Figure 4.7, under the maximum strength of 0.12 MPa, the strains of SMPU/nHAP composite scaffolds (SMPU/nHAP-200, SMPU/nHAP-200-100, SMPU/nHAP-100-50, and SMPU/nHAP-50) which increased with their apertures were 15.40%, 16.77%, 20.70% and 23.78%, respectively. From the Eqns. (2-2) and

(2-3), the modulus of compression of four scaffolds at two different stress of 0.00215 MPa (E_0) and 0.12065 MPa (E_1) were calculated and the results were given in Table 4-2. According to the data, with the increase of the apertures of these four composite scaffolds, the values of E_0 and E_1 were increased and decreased, respectively. It meant that, at the beginning of the compression test, the bigger the apertures of scaffolds were, the more difficult for scaffolds compressed and the higher the carrying capacity of scaffolds had. And at the end of the test, the smaller the apertures of the scaffold were, the less deformation they experienced and the greater their compression resistance was. Furthermore, using Eqn. (2-4), at an applied stress of 0.12 MPa, the compression shape recovery ratios of four SMPU/nHAP composite scaffolds were determined with 99.40%, 99.46%, 99.62% and 99.65%, respectively. The results demonstrated that the compression shape recovery ratio of scaffolds was increased with the increase of porosity of these four scaffolds.

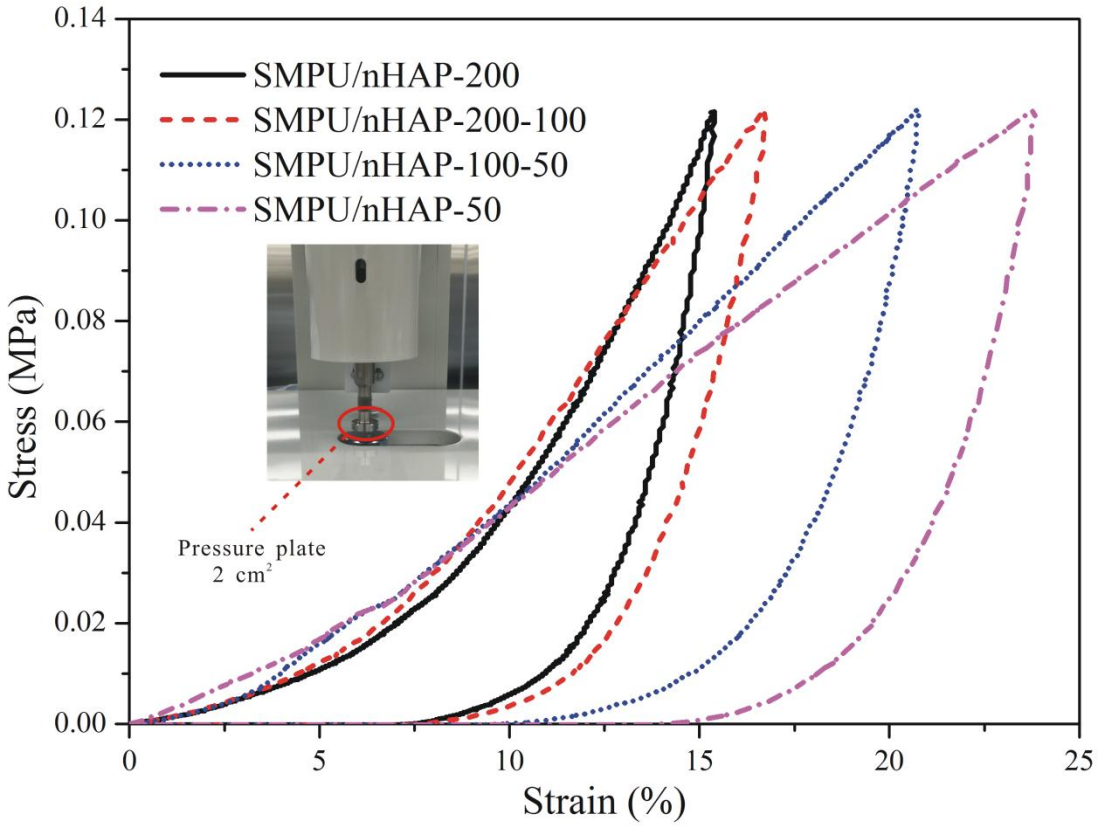

Figure 4.7 Stress-strain curves of compressive test of SMPU/nHAP composite scaffolds at room temperature.

Table 4-2

The data of the four composite scaffolds with compression test

Sample	Strain[a)]	R_c	E_0	E_1
SMPU/nHAP-200	15.40%	99.40%	0.1413	1.8903
SMPU/nHAP-200-100	16.77%	99.46%	0.1823	0.9981
SMPU/nHAP-100-50	20.70%	99.62%	0.2075	0.7479
SMPU/nHAP-50	23.78%	99.65%	0.2515	0.5285

[a)] The strains of scaffold under the maximum strength of 0.12 MPa

4.3.4 Dynamic mechanical test

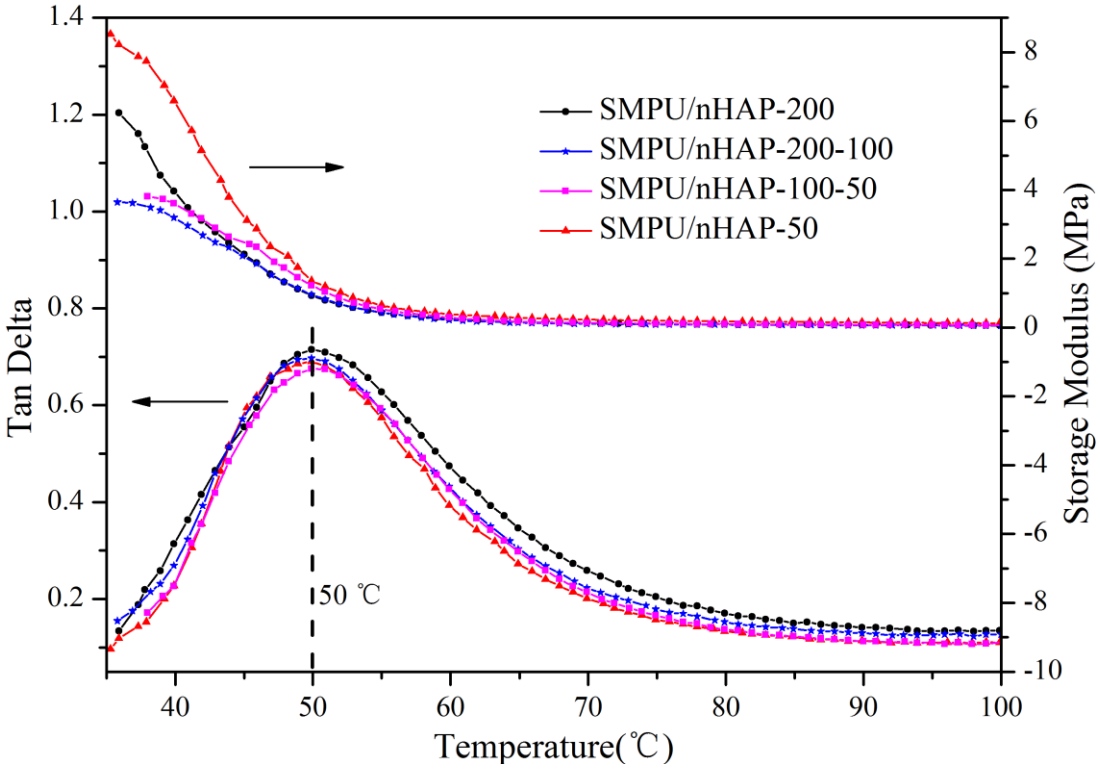

Figure 4.8 Storage modulus and tan delta of SMPU/nHAP composite scaffolds from DMA tests.

From the storage modulus and tan delta of four SMPU/nHAP composite scaffolds by the DMA test (Figure 4.8), the glass-transition temperature (T_g) of these four samples was the same at 50 ℃ using the tan delta peak. It meant that the addition of nHAP particles had no significant effect on T_g because of the small amount of particles. Storage modulus represents the ability of the material to store elastic deformation energy. The larger the storage modulus is, the more difficult for deformation. From the image, around 50 ℃, the storage modulus of SMPU/nHAP scaffolds were increased with the increase of the porosity of scaffolds, which meant that the greater the porosity was, the higher the storage modulus was and the better

the compression resistance was. Tan delta represents the viscoelastic properties of the material, the larger the tan delta, the greater the viscosity of the material, the lower the tan delta, the greater the elasticity of the material. From the picture, tan deltas of SMPU/nHAP scaffolds were all around 0.7, which could be applied to bone tissue engineering well.

4.3.5 Thermo-mechanical analysis

The stress-strain-temperature curves of four scaffolds which were obtained using the five-step thermo-mechanical test were shown in Figure 4.9. Samples were tensiled to a maximum force of 100 mN at 55 ℃ above T_g (at the rubbery state) (step 1). Maintaining the force at 100 mN for 5 minutes at 55 ℃ (step 2), the samples were cooled to about 20 ℃ below T_g (at the glass state) (step 3). The samples were unloaded at about 20 ℃ and kept for 5 minutes (step 4), where small unloading strain occurred. Then the samples were heated to 55 ℃ under no load (step 5), where the strain of the samples was recovered. This is one complete thermo-mechanical cycle. These five steps which associated with the shape fixity and recovery of the samples are highlighted. Shape fixity and recovery ratios, which were determined in terms of the strain [33, 34], were two important parameters for determining and evaluating characteristics of SMPU/nHAP composite scaffolds. The shape fixity ratio and shape recovery ratio were derived from the Eqns. (2-5) and (2-6). These four composite scaffolds had good shape fixity property since the shape fixity ratios of all scaffolds were above 97%. The shape recovery ratios of SMPU/nHAP-200, SMPU/nHAP-200-100, SMPU/nHAP-100-50, and SMPU/nHAP-50 were determined to be 97.6%, 93.12%, 92.53% and 91.26%,

respectively, indicating that the shape recovery ratios of the SMPU/nHAP scaffolds decreased with the increasing of apertures.

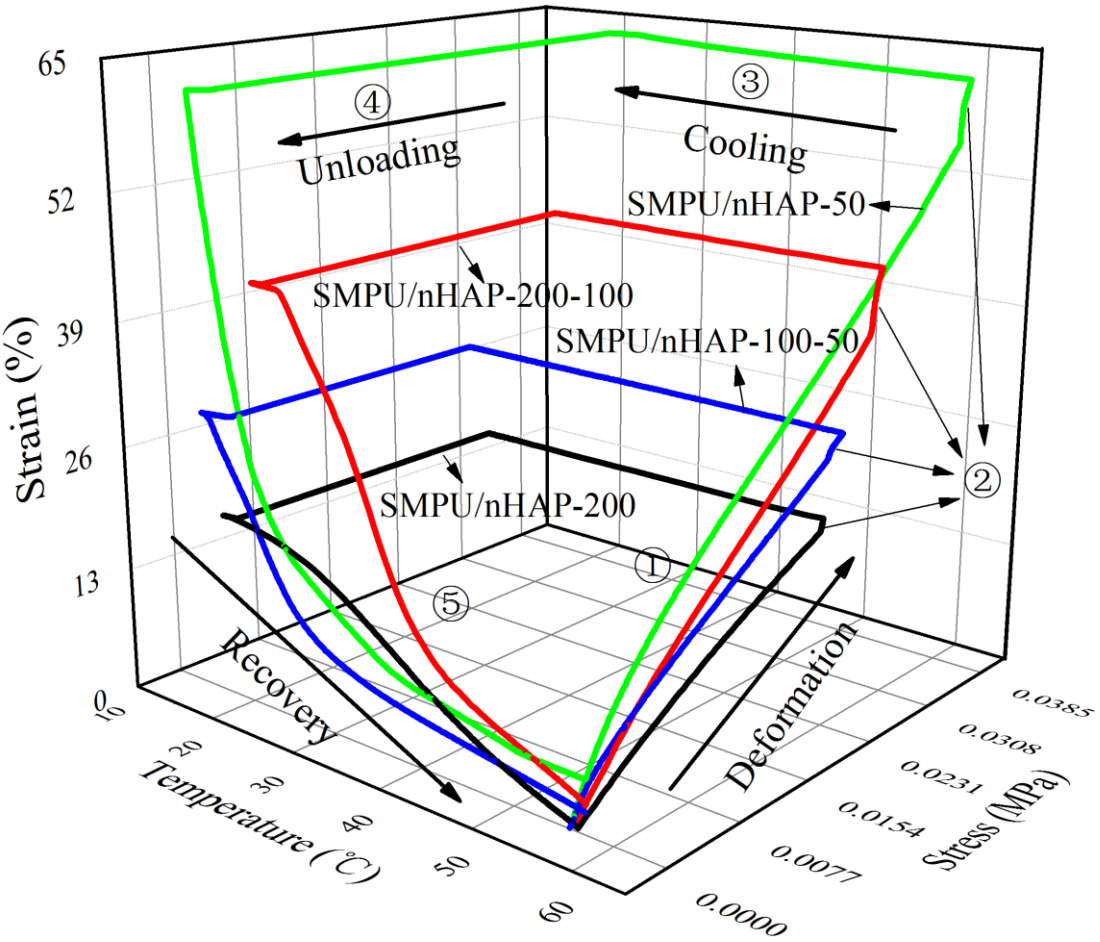

Figure 4.9 Five-step thermo-mechanical test: ① tensiled to a maximum force of 100 mN at 55 ℃, ② maintained at 100 mN for 5 minutes, ③ cooled to about 20 ℃ with force kept 100 mN, ④ holded for 5 minutes at about 20 ℃ under no load, and ⑤ heated to 55 ℃ under no load. The black, red, blue and green lines are the stress-strain-temperature curves of SMPU/nHAP-200, SMPU/nHAP-200-100, SMPU/nHAP-100-50 and SMPU/nHAP-50, respectively.

4.3.6 Properties of SMPU/nHAP composite scaffolds in vitro

The proliferation of MG-63 cells on the SMPU/nHAP composite scaffolds after 1 d, 3 d, 5 d, and 7 d of culture were shown in Figure 4.10. Compared with that of the blank control, the $OD_{595\ nm}$, which represented the number of living cells, of the samples which were cultured with MG-63 cells for 1 d, 3 d, 5 d, and 7 d were higher. At the same culture day, the cell number increased with the increase of the aperture of the scaffolds. This indicated that the larger the aperture was, the easier it was for the cell to adhere to and proliferate on the scaffolds.

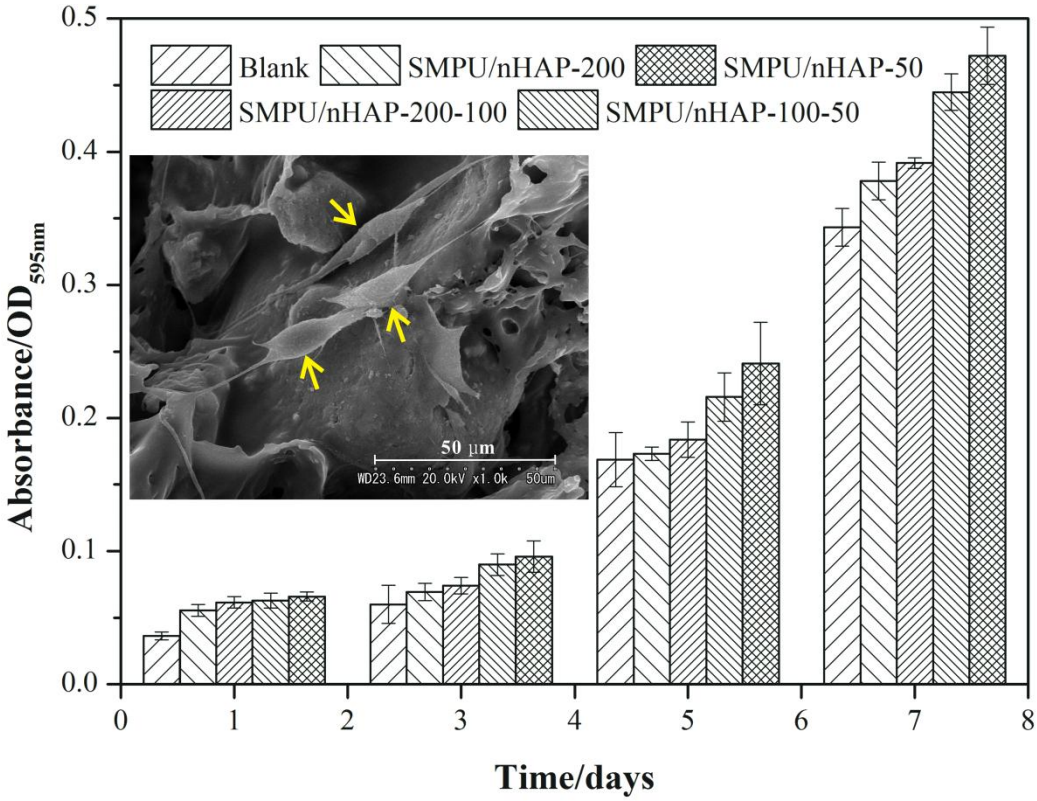

Figure 4.10 Proliferation of MG-63 cells on four SMPU/nHAP composite scaffolds (SMPU/nHAP-200, SMPU/nHAP-200-100, SMPU/nHAP-100-50 and SMPU/nHAP-50) after 1 d, 3 d, 5 d, and 7 d of culture. Yellow arrows indicate MG-63 cells on SEM image.

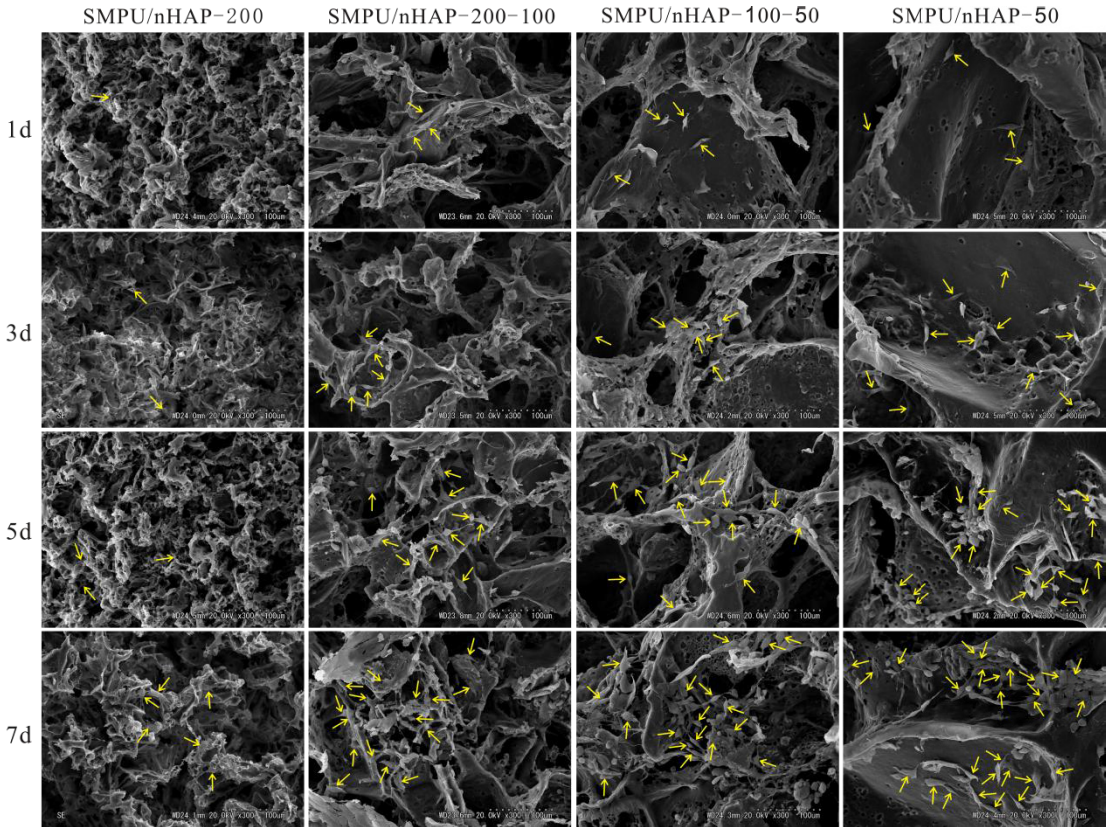

Figure 4.11 SEM images of MG-63 cultured on the four SMPU/nHAP scaffolds (SMPU/nHAP-200, SMPU/nHAP-200-100, SMPU/nHAP-100-50, and SMPU/nHAP-50) after 1 d, 3 d, 5 d, and 7 d (×300). Yellow arrows indicate MG-63 cells.

Meanwhile, the morphology of the MG-63 cells on the SMPU/nHAP scaffolds was observed to be fusiform-like with pseudopodia (Figure 4.10). The SEM images of scaffolds cultured with MG-63 cells for 1 d, 3 d, 5 d, and 7 d were shown in Figure 4.11. The images showed that the number of living cells in all samples increased with the culture day. On the same day of culture, the number cells on the scaffolds increased with the apertures, consistent with the results in Figure 4.10. In other words, these four porous SMPU/nHAP composite scaffolds (SMPU/nHAP-200,

SMPU/nHAP-200-100, SMPU/nHAP-100-50 and SMPU/nHAP-50) had a cell proliferation promoting ability that increased with the increase of the aperture of the scaffolds.

4.4 Conclusions

Four 3D porous nanocomposite scaffolds were successfully manufactured by using the method of size controllable design. The results showed these 3D porous SMPU/nHAP composite scaffolds had good shape memory recovery behaviors to let them can accurately match the irregular boundaries of bone defects. The high compression recovery property of scaffold can make it effectively recover when it is subjected to external shocks. Moreover, these porous nanocomposite scaffolds had a cell proliferation promoting ability to reach self-healing function and the ability was increased with the increase of the apertures of the scaffolds. This size controllable design from this study contributes to improving the scaffold design for bone tissue engineering and porous SMPU/nHAP composite scaffolds with interconnected pores have good potential for application in the field of minimally invasive surgery and bone defect repair.

References

[1] G.H. Altman, F. Diaz, C. Jakuba, *et al*. Silk-based biomaterials. Biomaterials, 2003, 24 (3): 401-416.

[2] S.P. Nukavarapu, S.G. Kumbar, J.L. Brown, *et al*. Polyphosphazene/Nano-Hydroxyapatite Composite Microsphere Scaffolds for Bone Tissue Engineering. Biomacromolecules, 2008, 9 (7): 1818-1825.

[3] N.L. Morozowich, J.L. Nichol and H.R. Allcock. Investigation of Apatite Mineralization on Antioxidant Polyphosphazenes for Bone Tissue Engineering. Chem Mater, 2012, 24 (17): 3500-3509.

[4] P.X. Ma. Scaffolds for tissue fabrication. Mater. Today, 2004, 7 (5): 30-40.

[5] I. Bab, B.A. Ashton, D. Gazit, *et al*. Kinetics and differentiation of marrow stromal cells in diffusion chambers in vivo. J Cell Sci, 1986, 84 (1): 139-151.

[6] S. Hofmann, H. Hagenmüller, A.M. Koch, *et al*. Control of in vitro tissue-engineered bone-like structures using human mesenchymal stem cells and porous silk scaffolds. Biomaterials, 2007, 28 (6): 1152-1162.

[7] Y. Zhang, C. Wu, T. Friis, *et al*. The osteogenic properties of CaP/silk composite scaffolds. Biomaterials, 2010, 31 (10): 2848-2856.

[8] S. Bhumiratana, W.L. Grayson, A. Castaneda, *et al*. Nucleation and growth of mineralized bone matrix on silk-hydroxyapatite composite scaffolds. Biomaterials, 2011, 32 (11): 2812-2820.

[9] T. Kasuga, H. Fujikawa and Y. Abe. Preparation of polylactic acid composites containing β-$Ca(PO_3)_2$ fibers. J Mater Res, 1999, 14 (2): 418-424.

[10] Y. Shikinami and M. Okuno. Bioresorbable devices made of forged composites

of hydroxyapatite (HA) particles and poly-L-lactide (PLLA): Part I. Basic characteristics. Biomaterials, 1999, 20 (9): 859-877.

[11] T. Kasuga, Y. Ota, M. Nogami, *et al*. Preparation and mechanical properties of polylactic acid composites containing hydroxyapatite fibers. Biomaterials, 2000, 22 (1): 19-23.

[12] K. Otsuka and C.M. Wayman. Shape memory materials. Cambridge University Press, New York, 1998.

[13] S. Ota. Current status of irradiated heat-shrinkable tubing in Japan. Rad Phys Chem, 1981, 18 (1-2): 81-87.

[14] F.El. Feninat, G. Laroche, M. Fiset, *et al*. Shape memory materials for biomedical applications. Adv Eng Mater, 2002, 4 (3): 91-104.

[15] A. Metcalfe, A.C. Desfaits, I. Salazkin, *et al*. Cold hibernated elastic memory foams for endovascular interventions. Biomaterials, 2003, 24 (3): 491-497.

[16] M.F. Metzger, T.S. Wilson, D. Schumann, *et al*. Mechanical properties of mechanical actuator for treating ischemic stroke. Biomed Microdevices, 2002, 4 (2): 89-96.

[17] K. Gall, P. Kreiner, D. Turner, *et al*. Shape memory polymers for microelectromechanical systems. J MEMS, 2004, 13 (3): 472-483.

[18] K. Gall, M.L. Dunn, Y. Liu, *et al*. Shape memory polymer nano composites. Acta Mater, 2002, 50 (20): 5115-5126.

[19] A. Lendlein and R. Langer. Biodegradable, elastic shape-memory polymers for potential biomedical applications. Science, 2002, 296 (5573): 1673-1676.

[20] X.B. Zhao, L. Du, X.P. Zhang. Brief review of relations of structure and microphase separation of polyurethane. Polyurethane industry, 2001, 16 (1):

4-8.

[21] C.C. Zhu, H.Y. Weng, G.H. Lyu, *et al*. The latest development of polyurethane industry at home and abroad. Chemical propellants & polymeric materials, 2012, 10 (5): 1-20.

[22] B. Li, H.L. Zhang, Z.H. Li, *et al*. Research progress and application of polyurethane materials in biological field. Polyurethane, 2008, 8 (4): 96-100.

[23] D.F. Williams. On the mechanisms of biocompatibility. Biomaterials, 2008, 29 (20): 2941-2953.

[24] L.L Hench and J.M. Polak. Third-Generation Biomedical Materials. Science, 2002, 295 (5557): 1014-1017.

[25] Y. Mizushima, T. Ikoma, J. Tanaka, *et al*. Injectable porous hydroxyapatite microparticles as a new carrier for protein and lipophilic drugs. Journal of Controlled Release, 2006, 110 (2): 260-265.

[26] M. Itokazu, W. Yang, T. Aoki, *et al*. Synthesis of antibiotic-loaded interporous hydroxyapatite blocks by vacuum method and in vitro drug release testing. Biomaterials, 1998, 19 (7-9): 817-819.

[27] I. Soriano, C. Évora. Formulation of calcium phosphates/poly (d,l-lactide) blends containing gentamicin for bone implantation. Journal of Controlled Release, 2000, 68 (1): 121-134.

[28] V.S. Komlev, S.M. Barinov, E.V. Koplik. A method to fabricate porous spherical hydroxyapatite granules intended for time-controlled drug release. Biomaterials, 2002, 23 (16): 3449-3454.

[29] P.P. Yang, Z.W. Quan, C.X. Li, *et al*. Bioactive, luminescent and mesoporous europium-doped hydroxyapatite as a drug carrier. Biomaterials, 2008, 29 (32):

4341-4347.

[30] T. Matsumoto, M. Okazaki, M. Inoue, *et al*. Hydroxyapatite particles as a controlled release carrier of protein. Biomaterials, 2004, 25 (17): 3807-3812.

[31] M.I. Alam, I. Asahina, K. Ohmamiuda, *et al*. Evaluation of ceramics composed of different hydroxyapatite to tricalcium phosphate ratios as carriers for rhBMP-2. Biomaterials, 2001, 22 (12): 1643-1651.

[32] J.H. Yu, X.B. Chu, Y.R. Cai, *et al*. Preparation and characterization of antimicrobial nano-hydroxyapatite composites. Mat Sci Eng C, 2014, 37: 54-59.

[33] G.Q. Li, M. John. A self-healing smart syntactic foam under multiple impacts. Composites Science and Technology, 2008, 68 (15-16): 3337-3343.

[34] Q.Q. Ni, C.S. Zhang, Y.Q. Fu, *et al*. Shape memory effect and mechanical properties of carbon nanotube/shape memory polymer nanocomposites. Composite Structures, 2007, 81 (2): 176-184.

Chapter 5

The effect of hydroxyapatite nanoparticles on mechanical behavior and biological performance of porous shape memory polyurethane scaffolds

5 The effect of hydroxyapatite nanoparticles on mechanical behavior and biological performance of porous shape memory polyurethane scaffolds

5.1 Introduction

Tissue engineering is a promising alternative for treating bone defects. The main operation method is to prepare a scaffold with good biocompatibility, which plays a crucial role in tissue engineering, because they represent an alternative to the conventional implantation of organs and tissues. The main goal of scaffolds is to provide appropriate base for tissue growth and cell proliferation [1, 2]. In order to precisely match the irregular boundaries of bone defects as well as facilitate clinical application, scaffold design should be improved.

Polyurethane refers to the high molecular compounds in a repeat of the carbamate group (-NHCOO-) in the main chain of polymer structure. Because of polyurethane's excellent physical and mechanical properties, good blood compatibility and tissue compatibility; it is quickly applied in the biomedical field. Shape memory polymers (SMP) are a well-known class of stimuli-responsive materials [3]. They can be controlled to remember a secondary shape and recover to their permanent shape under an external stimulus. This property can be designed and altered by changing a polymer's structure, morphology, and various processing parameters during fabrication [4].

Hydroxyapatite (HAP, Ca_{10} $(PO_4)_6(OH)_2$), the main inorganic component of the vertebrate animals' teeth and bones (as high as 50%), has been widely used as teeth

and bone repairing/replacement materials due to its properties of endophilicity, non-toxic, non-stimulating, non-allergenic, non-mutagenic and osteoconductive, etc [5-7]. Also, nano-hydroxyapatite (nHAP) particles are used as carriers of growth factor [8], antibiotics [9], anticancer drugs [10], and enzymes [11] for its notorious adsorption ability. At present, hydroxyapatite is often combined with other materials to make a kind of bone repair material which is similar to natural bone tissue. This is one of the hot spots in the research of bone repair [12, 13].

In this chapter, porous shape memory polyurethane/nano-hydroxyapatite (SMPU/nHAP) composite scaffold was prepared with the three-dimensional (3D) porous structure by a salt leaching-phase inverse technique, a unique method to fabric controllable porous structure. This controllable porous structure was confirmed by Scanning electron microscope (SEM), X-ray photoelectron spectroscopy (XPS), and X-ray micro-computed tomography analysis (μ-CT). The mechanical properties were investigated by tensile test, compression analysis and thermo-mechanical test. Specially, we highlighted the shape recovery behaviors and biological performance in vitro of porous SMPU/nHAP composite scaffold, which aimed at providing a substantial contribution towards the application of SMPU/nHAP composite scaffold in minimally invasive surgery and bone repair surgery.

5.2 Results and discussion

5.2.1 Characterization of nHAP

First, chemical composition of nanoparticles had been characterized using XRD and the predominant HAP crystal phase had been confirmed according to the

standard card of HAP (JCPDS 09-432) (as shown in Figure 5.1a). Generally, the narrower band gap and higher intensity of the diffraction peak indicate the better crystallinity of the particle. From Figure 5.1a, the diffraction peak in the pattern was narrow and intensity was relatively high, which implied that the nanoparticles had higher crystallinity. The morphology of nHAP was shown in Figure 5.1b, in which the nanoparticles had a rod-like shape and were uniformly distributed. The sizes of nHAP particles, which were showed in Figure 5.1c and 5.1d, were ca. 32 nm in length and ca. 10 nm in diameter using the software of Nano Measurer 1.2 (Jie Xu, Department of Chemical, Fudan University).

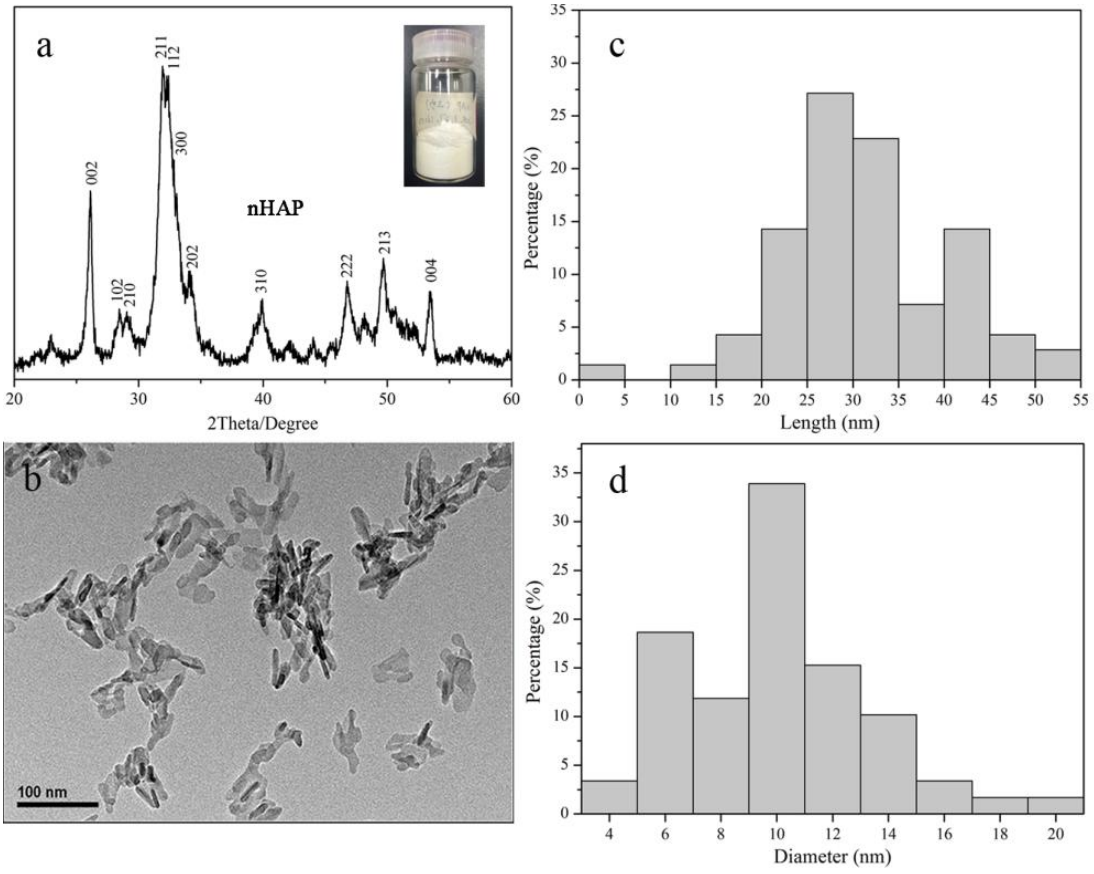

Figure 5.1 XRD pattern (a), TEM image (b), Length chart (c) and Diameter chart (d) of nano hydroxyapatite (nHAP) particles

5.2.2 SMPU/nHAP scaffold

In this research, SMPU, SMPU-NaCl, SMPU/nHAP and SMPU/nHAP-NaCl had been selected to determine the removal of NaCl. Figure 5.2A showed the reaction of silver ions and chloride ions in the leaching liquid of SMPU/nHAP-NaCl. After 5 days, it had been seen that there was no white precipitate in the solution, which meant that all NaCl had been removed from the scaffolds. To further determine the removal of NaCl from the scaffolds, XPS analysis was performed. The patterns in Figure 5.2B_1 and B_2 confirmed that compared with the SMPU-NaCl and SMPU/nHAP-NaCl, SMPU and SMPU/nHAP had no peaks of Na and Cl, which meant that there was no NaCl inside of SMPU and SMPU/nHAP scaffolds. In addition, contrasted with SMPU scaffold, SMPU/nHAP scaffold had a peak of Ca, which verified the existence of nHAP particles. From Figure 5.2C, the peaks of Ca 2p 1/2, Ca 2p 3/2, N 1s and C 1s were appeared at the binding energy of 350.8 eV, 347.4 eV, 398.1 eV and 284.3 eV, respectively. In this research, the mass ratio of nHAP particles to SMPU was 0.075 which indicated that in contrast to the SMPU, the amount of nHAP particles was small. Through the comparison of the intensity of Ca 2p, N 1s and C 1s, it also showed that the intensity of Ca 2p was relatively weak since the amount of particles was less.

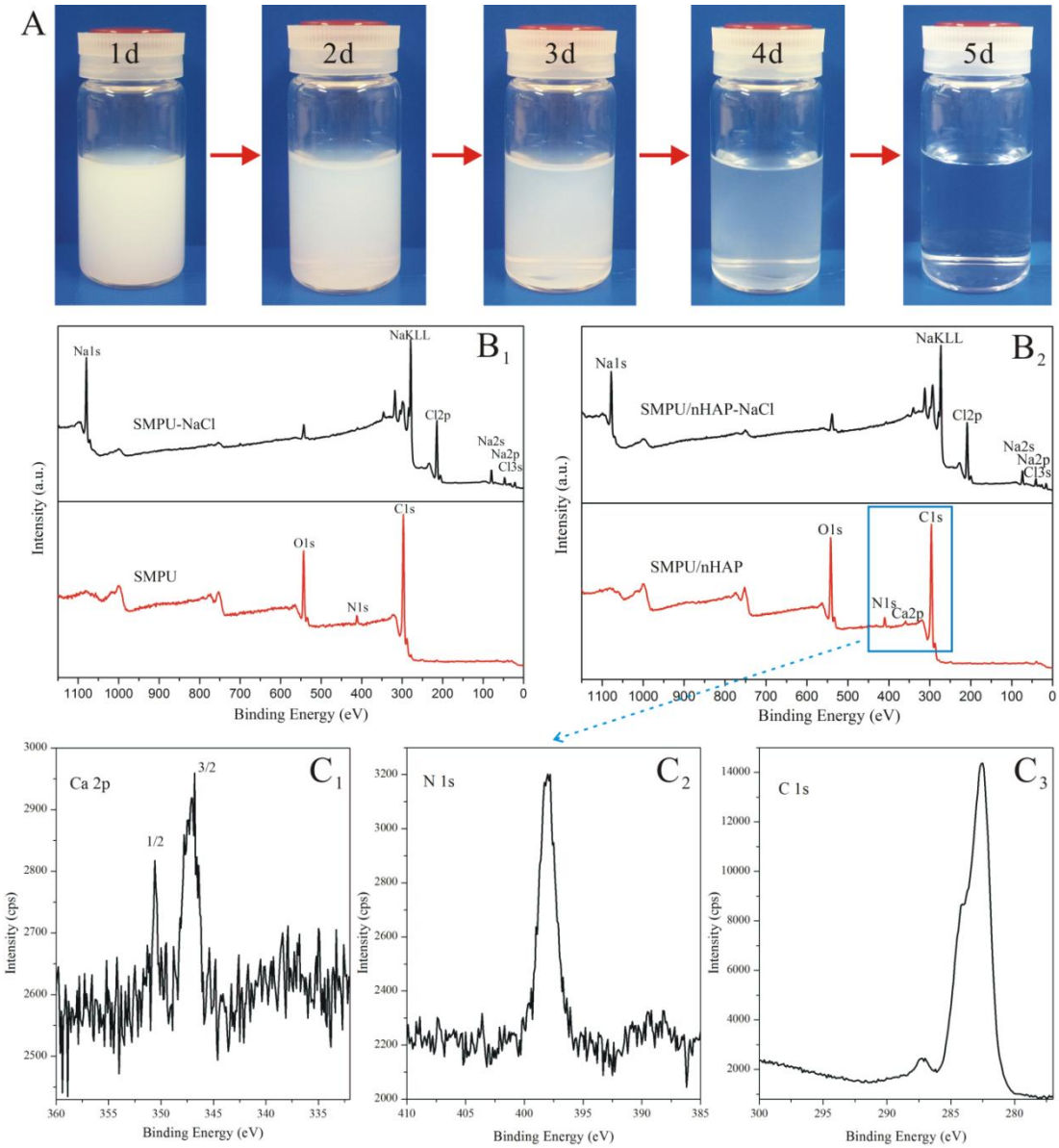

Figure 5.2 (A) Images of the removal of NaCl from SMPU/nHAP-NaCl by using the chemical method for five days; XPS spectra: wide scan of SMPU and SMPU-NaCl (B_1), SMPU/nHAP and SMPU/nHAP-NaCl (B_2), narrow scan of Ca 2p (C_1), N 1s (C_2) and C 1s (C_3) of SMPU/nHAP scaffold.

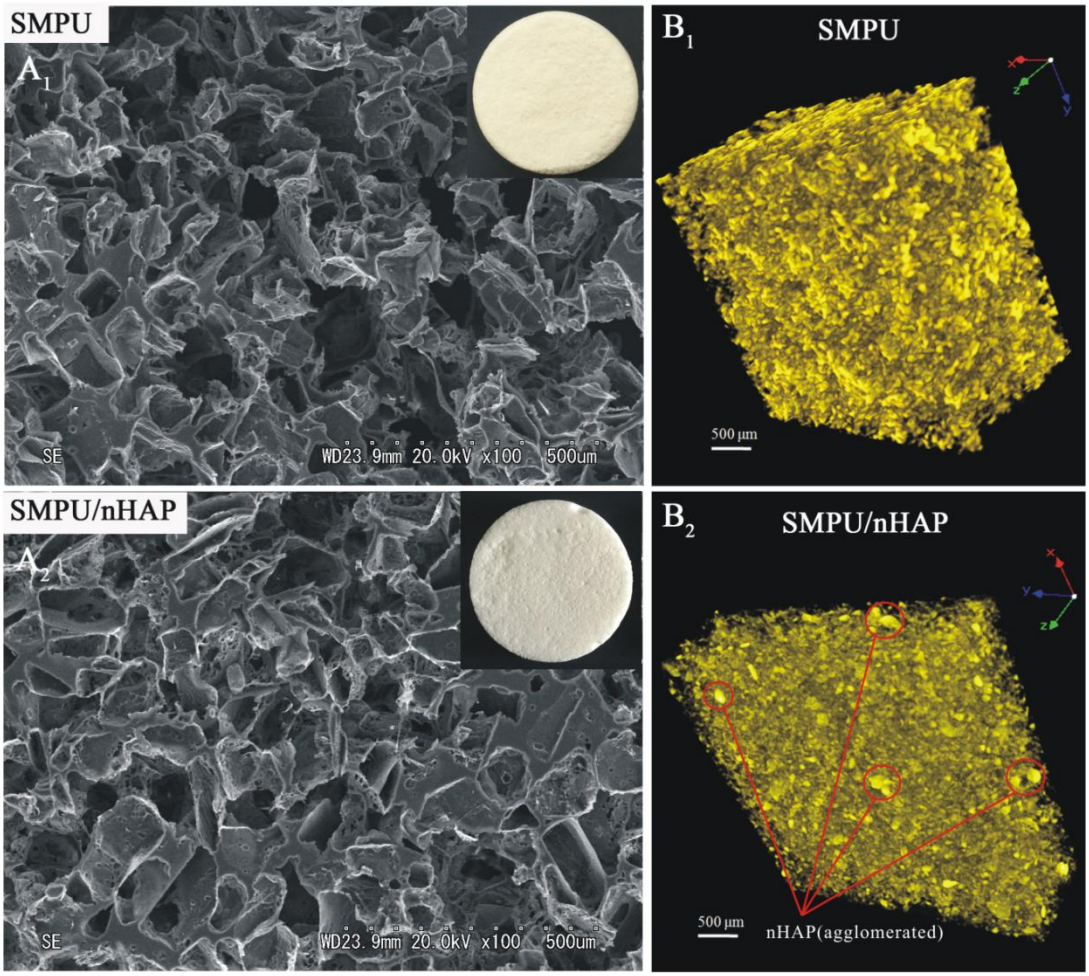

Figure 5.3 (A) SEM images and (B) μ-CT images of SMPU and SMPU/nHAP scaffolds.

The morphology of two scaffolds was shown in Figure 5.3. From Figure 5.3, it is shown that the apertures of scaffolds were irregular which was due to the irregularity of NaCl particles. Theoretically, the apertures of SMPU and SMPU/nHAP scaffolds were the same, lied between 50 μm and 110 μm. Using the software Nano Measurer 1.2, the mean apertures of SMPU and SMPU/nHAP scaffolds were found to be 82.73 μm and 84.38 μm, respectively (Table 5-1). It meant that the aperture of scaffolds was controlled by the sizes of NaCl particles. According to the Eqns. (2-7), (2-8) and (2-9), the apparent density and porosity of two scaffolds (SMPU and SMPU/nHAP)

were found to be 0.2501 g/cm^3, 0.1984 g/cm^3 and 79.50%, 83.85%, respectively, and the results were shown in the Table 5-1. It meant that the apparent density of SMPU/nHAP scaffold was decreased due to the addition of nHAP particles. Theoretically, when SMPU was replaced by the nHAP particles of higher density, the apparent density of SMPU/nHAP scaffold would be higher. But actually it was decreased. The reason for that was, although the nHAP particles were combined with SMPU, the interface between these two materials was not good and some of them also left the pores. The result of the porosity of these two scaffolds confirmed this reason well. Three-dimensional structure of these two scaffolds was shown in Figure 5.3B. From μ-CT images, all scaffolds had a three-dimensional structure which was important for cell growth. From Figure 5.3B$_2$, nHAP particles in the SMPU/nHAP scaffold were uniformly distributed in addition to some agglomeration of particles. But it did not affect subsequent experiments because even if there was the agglomeration of nHAP particles, it was uniformly dispersed.

Table 5-1

The apparent density, porosity and apertures of two scaffolds

Sample	Apparent density (g/cm^3)	Porosity (%)	Theoretical aperture (μm)	Mean aperture (μm)
SMPU	0.2501	79.50	50-110	82.73
SMPU/nHAP	0.1984	84.43	50-110	84.38

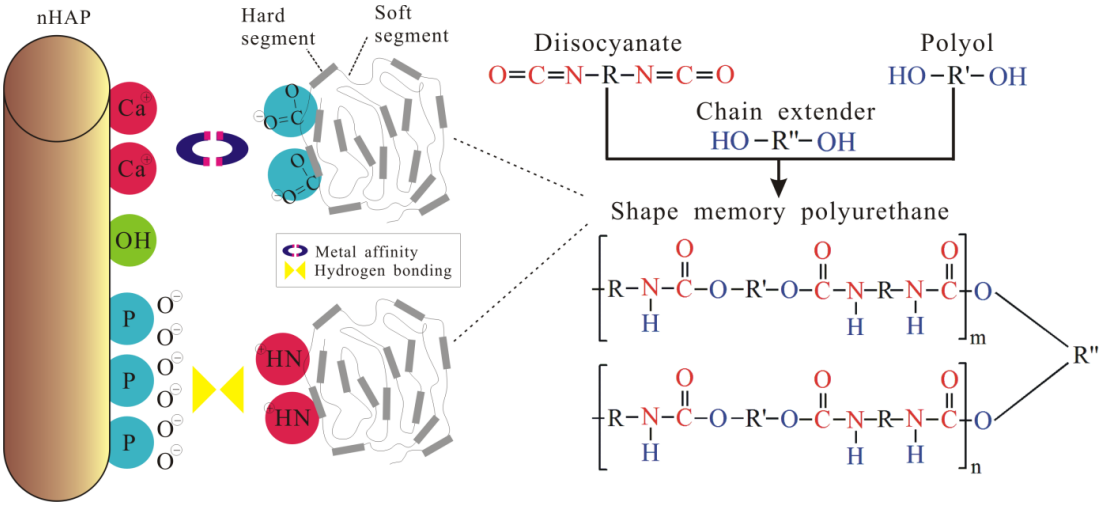

Figure 5.4 Schematic illustration for the interaction of nHAP particles and SMPU.

Hydroxyapatite, $Ca_{10}(PO_4)_6(OH)_2$, is a mixed-mode support with functional groups consisting of pairs of positively charged crystal calcium ions (C-sites) and clusters of six negatively charged oxygen atoms associated with triplets of crystal phosphates (P-sites). The C-sites, P-sites, and hydroxyl groups are distributed in a fixed pattern on the nHAP crystal structure, as presented in classic studies by T. Kawasaki [14, 15] and T. Kawasaki et al [16]. In theory, nHAP can retain solutes by weak anion exchange or calcium metal affinity with C-sites, by cation exchange with P-sites, and by hydrogen bonding with hydroxyl groups. In this research, SMPU were formed by reacting a diisocyanate with a polyol. The positively charged crystal calcium ions of nHAP particles may interact with negatively charged oxygen atoms of urethane bond of SMPU by the metal affinity. And negatively charged oxygen atoms associated with triplets of crystal phosphates of nHAP particles may interact with the positively charged nitrogen atoms of urethane bond of SMPU by the hydrogen bonding. The interaction of nHAP particles and SMPU and was shown in Figure 5.4. Schematic illustration for the existence of nHAP particles in

SMPU/nHAP scaffold was shown in Figure 5.5. According to the Figure 5.5A, nHAP particles were dispersed in the SMPU/nHAP scaffold, in addition to some agglomeration, which was consistent with the results of the Figure 5.3B_2. This image showed there were two ways of the existence of nHAP particles. One was embedding in the SMPU and the other was existing on the interface of the NaCl and SMPU. But the main mode of existence was nHAP particles embedded in SMPU.

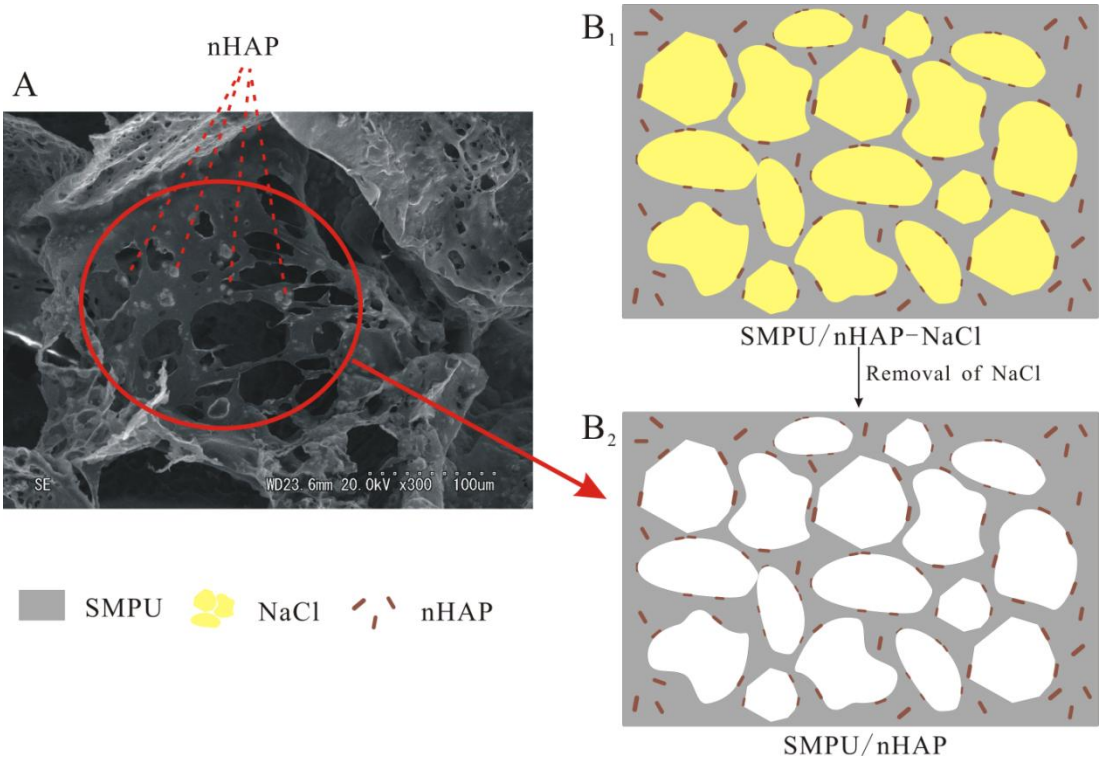

Figure 5.5 Schematic illustration for the existence of nHAP particles in SMPU/nHAP scaffold. A: SEM images; B_1: schematic illustration for SMPU/nHAP-NaCl; B_2: schematic illustration for SMPU/nHAP.

5.2.3 Tensile test

The effect of nHAP particles on the mechanical behavior of SMPU and

SMPU/nHAP scaffolds was shown in Figure 5.6. From Figure 5.6, the maximum tensile stress of these two scaffolds (SMPU and SMPU/nHAP) was 0.12676 MPa and 0.11201 MPa, respectively. Compared with SMPU scaffold, the maximum tensile stress of SMPU/nHAP scaffold was lower with the addition of nHAP particles. According to the Eqn. (2-1), Young's modulus of SMPU and SMPU/nHAP scaffolds were 0.9539 MPa and 0.8256 MPa, respectively. It meant that compared with SMPU scaffold, SMPU/nHAP scaffold could be easier to tensile. Because the addition of nHAP particles improved the porosity of scaffold and also weakened the strength of wall between the neighboring pores.

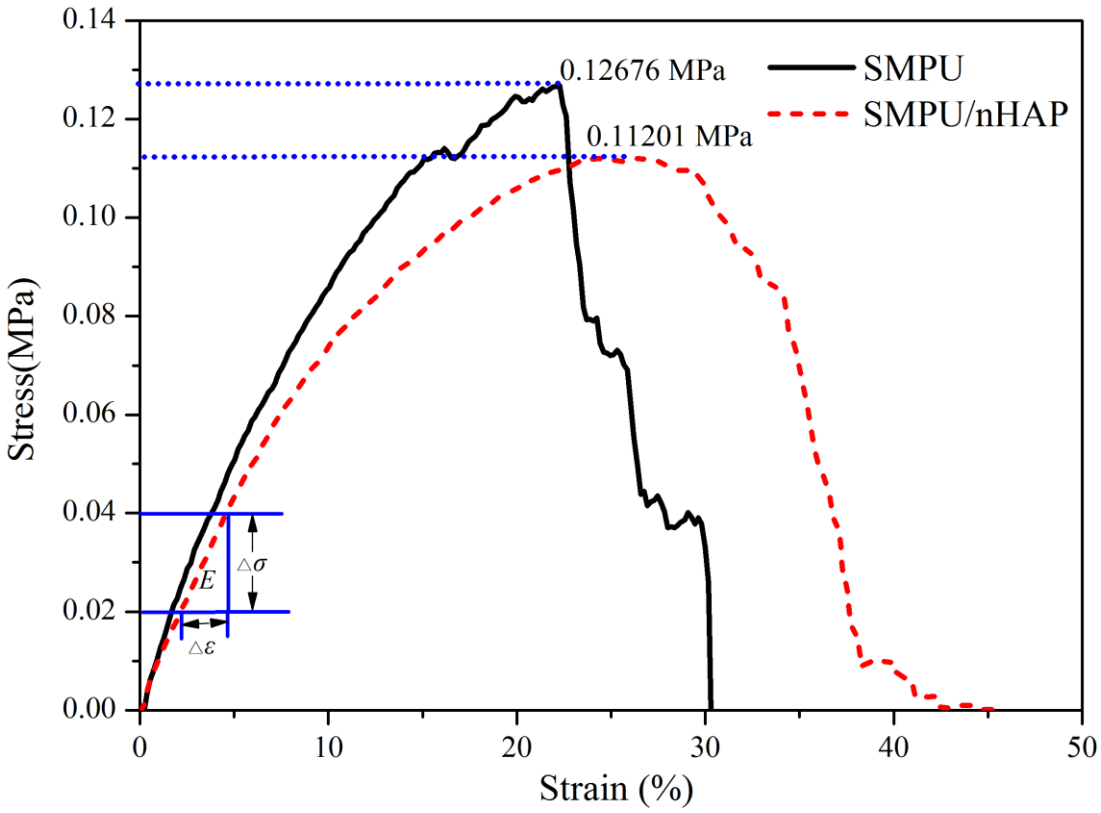

Figure 5.6 Stress-strain curves of tensile test of SMPU and SMPU/nHAP scaffolds at room remperature.

5.2.4 Compression behavior

The effect of nHAP particles on the compression behavior of SMPU and SMPU/nHAP scaffolds was shown in Figure 5.7. From Figure 5.7, under the maximum strength of 0.12 MPa, the strains of SMPU and SMPU/nHAP scaffolds were 26.51% and 16.77%, respectively, which indicated that the compression resistance of SMPU/nHAP scaffold was improved 37% contrasted with SMPU scaffold. The strain of SMPU/nHAP scaffold was lower than the strain of SMPU because of the addition of nHAP particles. From the Eqns. (2-2) and (2-3), the modulus of compression of two scaffolds at two different stresses of 0.00215 MPa and 0.12065 MPa were calculated in Table 5-2. According to the data, the modulus of compression of SMPU/nHAP scaffold was higher than SMPU scaffold in both cases, which meant that it was more difficult to compress the SMPU/nHAP scaffold than the SMPU scaffold due to the addition of nHAP particles improved the compression resistance. Furthermore, using Eqn. (2-4), at an applied stress of 0.125 MPa, the compression shape recovery ratios of SMPU and SMPU/nHAP scaffolds were determined with 98.54% and 99.46%, respectively. The results demonstrated that the compression shape recovery ratio of scaffolds was increased with the increase of porosity of these two scaffolds.

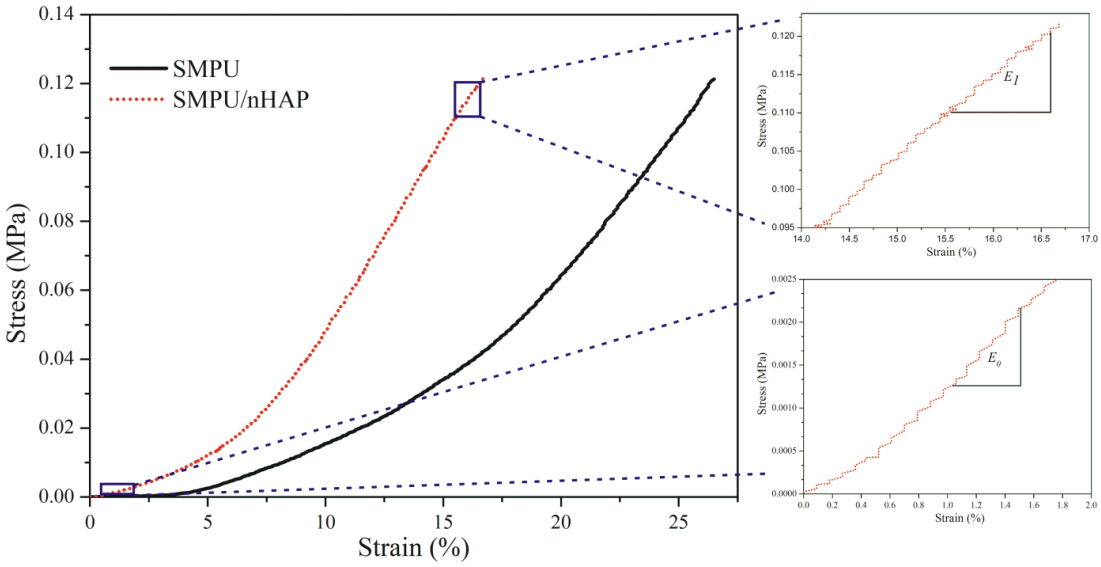

Figure 5.7 Stress-strain curves of compressive test of SMPU and SMPU/nHAP scaffolds at room temperature.

Table 5-2

The data of two scaffolds with compressive test

Sample	Strain (at 0.12 MPa)	R_c (at 0.12 MPa)	E_0	E_1
SMPU	26.51%	98.54%	0.1618	0.8862
SMPU/nHAP	16.77%	99.46%	0.1823	0.9981

The compression recovery behavior of SMPU and SMPU/nHAP scaffolds at room temperature were shown in Figure 5.8. The test was conducted with 50% of the amount of compression. And the sample was a cuboid with a cross-sectional area of 7 × 7 mm^2 and height of 8 mm. From Figure 5.8, 25%, 50%, 75% and 100% represented the recovery ratios of two scaffolds at each time. Also to achieve the same recovery ratio, the time required for SMPU/nHAP scaffold was reduced about 41% contrasted with SMPU scaffold. Considering both great compression recovery

property and rapid recovery performance, SMPU/nHAP scaffold is more conducive to minimally invasive surgery and bone tissue application.

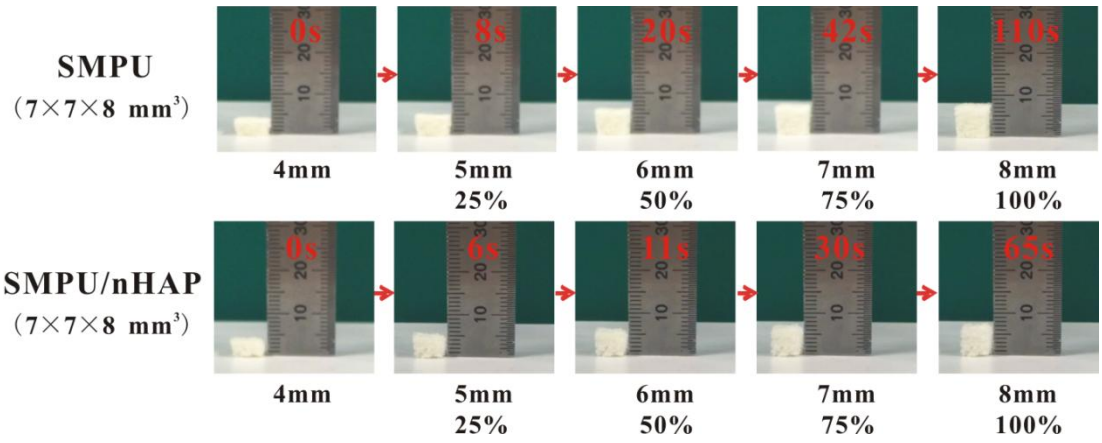

Figure 5.8 Digital photos of compression recovery of SMPU and SMPU/nHAP scaffolds at room temperature.

5.2.5 Thermo-mechanical analysis

In order to investigate the shape recovery property of the developed nanocomposite, the thermo-mechanical cycle test was conducted. The cross-sectional areas of SMPU and SMPU/nHAP scaffolds were 1.665 mm^2 and 3.315 mm^2, respectively. Figure 5.9 showed the stress-strain-temperature-time curves of two scaffolds which were obtained using five-step thermo-mechanical test. Samples were tensiled to a maximum force of 100 mN at 55 ℃ above T_g (at the rubbery state) (step 1). Maintaining the force at 100 mN for 5 minutes at 55 ℃ (step 2), the samples were cooled to about 20 ℃ below T_g (at the glass state) (step 3). The samples were unloaded at about 20 ℃ and kept for 5 minutes (step 4), where small unloading strain occurred. Then the samples were heated to 55 ℃ under no load

(step 5), where the strain of the samples was recovered. This is one complete thermo-mechanical cycle. When this one cycle is finished a residual strain, ε_p, is remained. The test was repeated for three cycles.

Observing the first cycle, when samples were tensiled to a maximum force of 100 mN at 55 ℃, the strain of samples was increased. From the curves, in order to achieve the same strain, the stress required for SMPU/nHAP scaffold was reduced about 78% contrasted with SMPU scaffold. This is due to the addition of nHAP particles improved the porosity of the scaffold. When samples were cooled at step 3, the strain of both scaffolds was slightly decreased due to the phenomenon of thermal expansion and contraction of scaffolds. There occurred a small reduction of strain at step 4 when the force was withdrawn, where the shape fixity ratio could be calculated. These five steps associated with the shape fixity and recovery was highlighted. Shape fixity and recovery ratio, which were determined in terms of the strain [18, 19], were the two important parameters for determining and evaluating SMPU characteristics. The shape fixity ratio and shape recovery ratio were derived from the Eqns. (2-5) and (2-6).

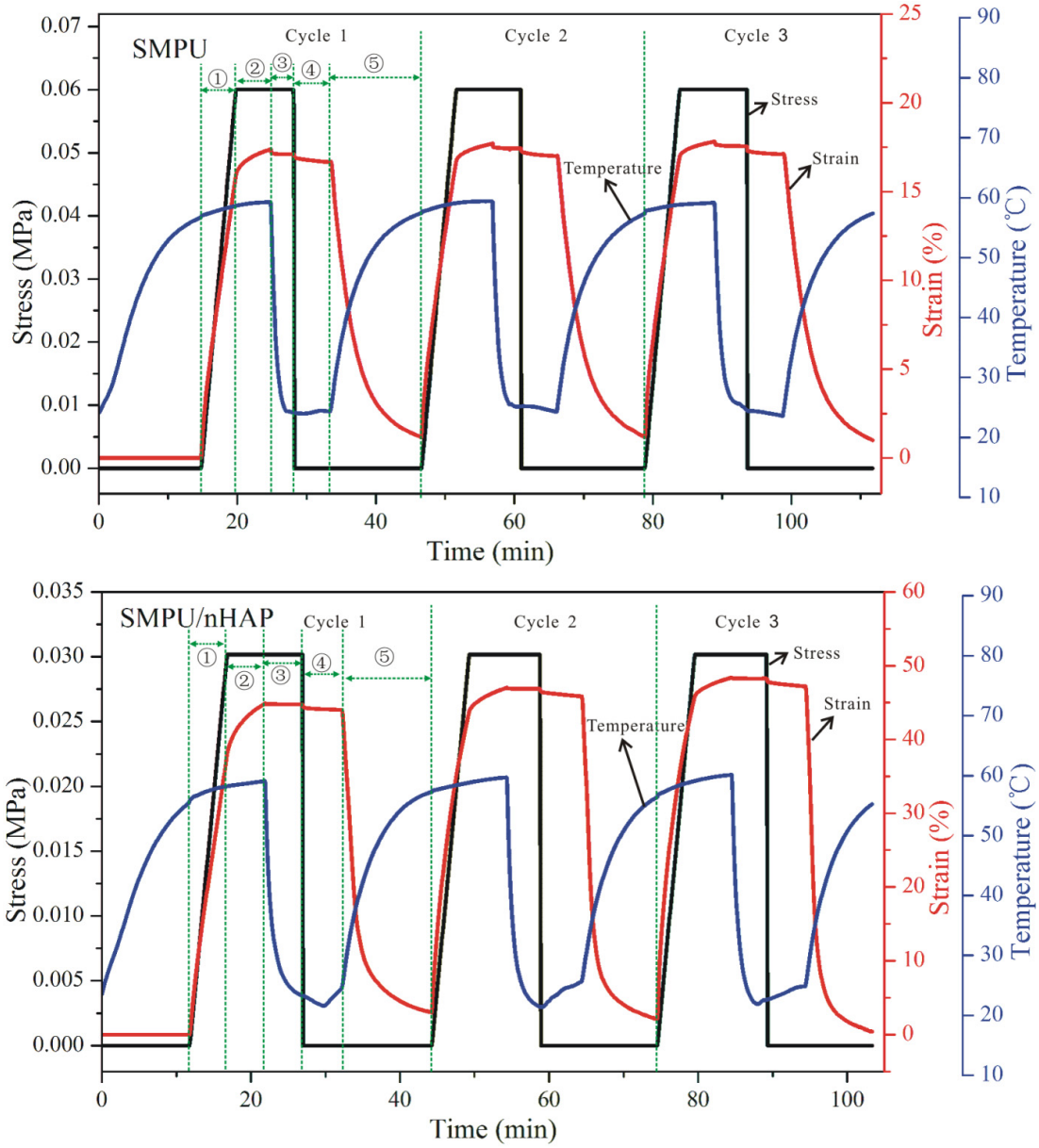

Figure 5.9 Stress-strain-temperature-time curves of the relationship of shape fixity ratio and recovery ratio to the cycle number of SMPU and SMPU/nHAP scaffolds. ① Samples were tensiled to a maximum force of 100 mN at 55 ℃, ② maintained at 100 mN for 5 minutes, ③ cooled to about 20 ℃ with force kept 100 mN, ④ holded for 5 minutes at about 20 ℃ under no load, and ⑤ heated to 55 ℃ under no load.

The relationship of the shape fixity ratio and recovery ratio to the cycle number was shown in Figure 5.10, and also the data were shown in Table 5-3. The shape fixity ratio for each sample was above 97%. It was clear that the SMPU/nHAP composites scaffold had good shape fixity property. In the first cycle, the shape recovery ratios of SMPU and SMPU/nHAP scaffolds were determined as 93.04% and 93.12%, respectively. The results demonstrated that the addition of nHAP particles enhanced the shape recovery ratio of SMPU scaffold. The shape recovery ratios of both scaffolds were increased with the cycle number. Moreover, SMPU/nHAP scaffold had a shape recovery ratio of more than 95% after the second cycle and more than 99% after the third cycle. Hence, for the developed nanocomposite with nHAP particles, it was found that higher strain recovery ability could be obtained after several cycles of training.

Table 5-3

Relationship between cycle number and shape memory property of two scaffolds

Cycle number	Shape fixity ratio (R_f, %)		Shape recovery ratio (R_r, %)	
	SMPU	SMPU/nHAP	SMPU	SMPU/nHAP
1	97.43	98.32	93.04	93.12
2	97.53	97.97	93.06	95.36
3	97.49	97.85	94.10	99.15

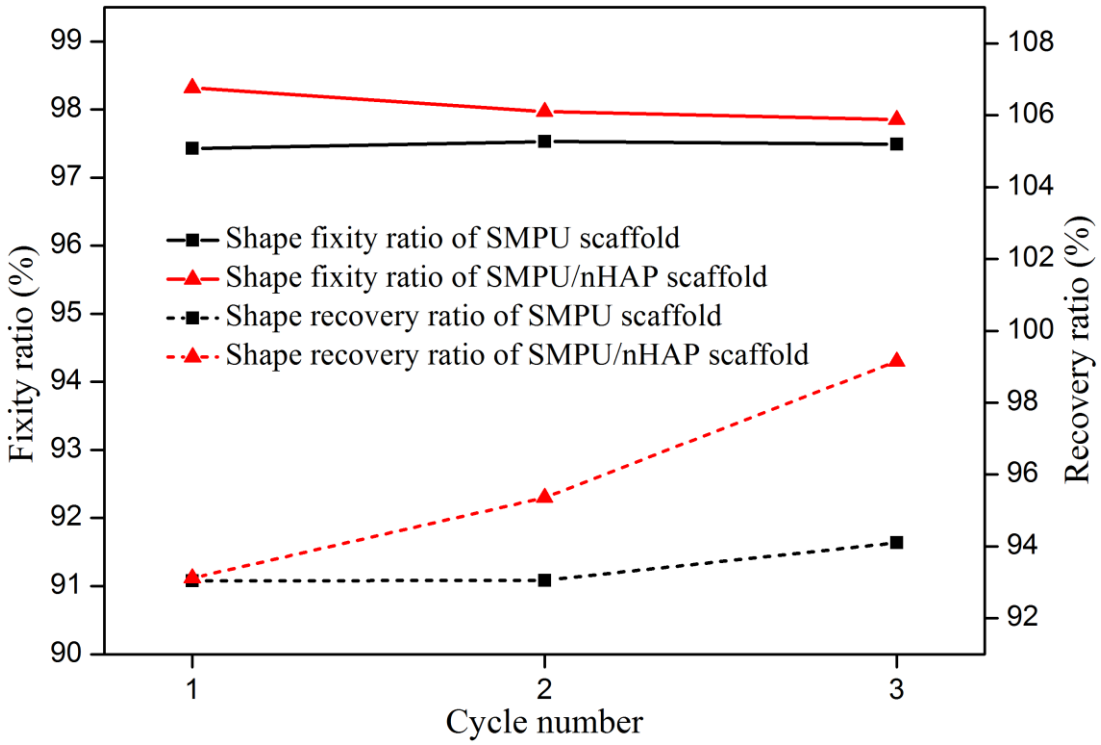

Figure 5.10 Relationship of the shape fixity ratio and recovery ratio to the cycle number of SMPU and SMPU/nHAP scaffolds.

5.2.6 Properties of SMPU/nHAP composite scaffolds in vitro

The proliferation of MG-63 cells on the SMPU scaffold and SMPU/nHAP composite scaffold after 1 d, 3 d, 5 d, and 7 d of culture were shown in Figure 5.11. Compared with that of the blank control, the $OD_{595\ nm}$, which represented the number of living cells, of the samples which were cultured with MG-63 cells for 1 d, 3 d, 5 d, and 7 d were higher. At the same culture day, the cell number of the SMPU/nHAP composite scaffold was higher than that of the SMPU scaffold because of that the addition of nHAP particles improved the proliferation of cells and increased the porosity of scaffold which could provide the space for cell adhesion. This indicated that the larger the porosity of scaffold was, the easier it was for the cell to adhere to

and proliferate on the scaffolds. On the 7th day of culture, the cell number of SMPU/nHAP scaffold was increased by 13% compared with SMPU scaffold. Meanwhile, the SEM images of scaffolds cultured with MG-63 cells for 1 d, 3 d, 5 d, and 7 d were shown in Figure 5.12. The morphology of the MG-63 cells on two scaffolds was observed to be fusiform-like with pseudopodia. And the images also showed that the number of living cells in all samples increased with the culture day. At the same day of culture, the cell number of the SMPU/nHAP composite scaffold was higher than that of the SMPU scaffold, consistent with the results in Figure 5.11. In other words, SMPU scaffold and SMPU/nHAP composite scaffold had a cell proliferation promoting ability that increased with the increase of the porosity of the scaffold.

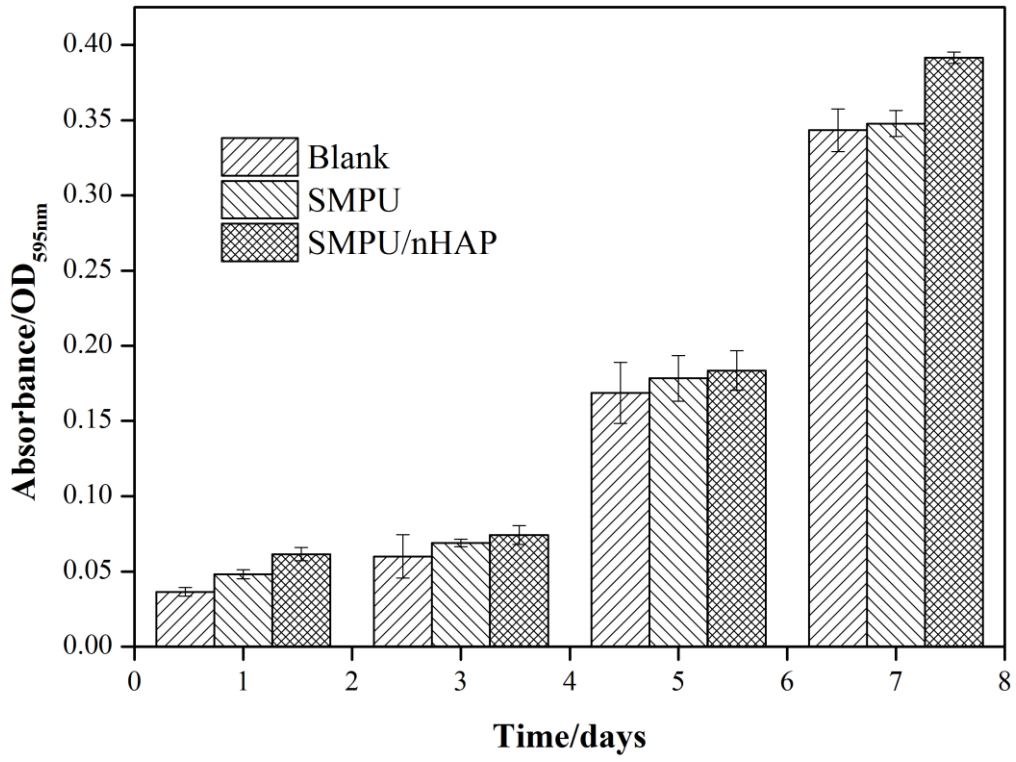

Figure 5.11 Proliferation of MG-63 cells on SMPU scaffold and SMPU/nHAPcomposite scaffold after 1 d, 3 d, 5 d, and 7 d of culture.

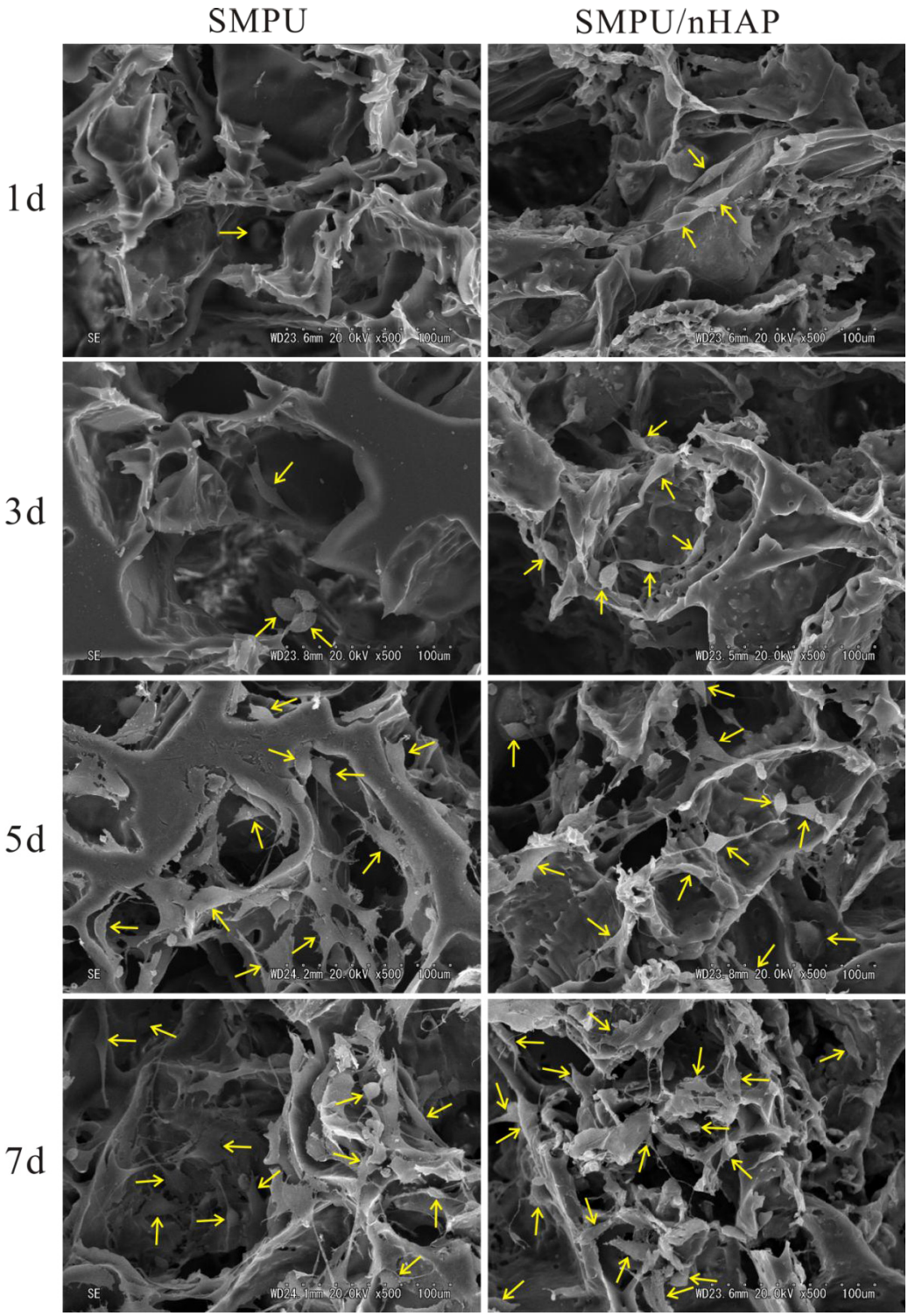

Figure 5.12 SEM images of MG-63 cultured on SMPU scaffold and SMPU/nHAP composite scaffold after 1 d, 3 d, 5 d, and 7 d (×500). Yellow arrows indicate MG-63 cells.

5.3 Conclusions

Two scaffolds (SMPU and SMPU/nHAP) with controllable three-dimensional structure, which was important for cell growth, were fabricated via the salt leaching-phase inverse technique, a unique method to fabric porous structure. The effect of nHAP particles in porous SMPU/nHAP composite scaffold was found to enhance the compression resistance by 37%, shorten the compression recovery time by 41% and reduce the tensile resistance by 78%. From the thermo-mechanical cycle test, SMPU/nHAP composite scaffold had good shape fixity property which was more than 97% and higher shape recovery ability which reached more than 99% after 3^{th} cycle of training. Meanwhile, the addition of nHAP particles improved the proliferation of cells by 13% after 7 days of culture which indicated that the larger the porosity of scaffold was, the easier it was for the cell to adhere to and proliferate on the scaffolds. These results revealed that in minimally invasive surgery and bone repair surgery, this porous composite scaffold could significantly reduce the operative time, promote the bone cell growth and precisely match the irregular boundaries of bone defects. Therefore, this porous SMPU/nHAP composite scaffold design has potential applications for the bone tissue engineering.

References

[1] P.X. Ma. Scaffolds for tissue fabrication. Mater. Today, 2004, 7 (5): 30-40.

[2] J.Y. Ding and A.M. Ji. Advances in biological scaffold material in bone tissue engineering. Orthopedic Journal of China, 2006, 14 (1): 56-58.

[3] C. Liu, H. Qin and P.T. Mather, Review of progress in shape-memory polymers. J. Mater. Chem., 2007, 17: 1543-1558.

[4] T. Xie. Recent advances in polymer shape memory. Polymer, 2011, 52 (22): 4985-5000.

[5] Y. Yang, J. Chen and S. Qu. TEM study of calcium phosphate precipitation on HA/TCP ceramics. Biomaterials, 2003, 24 (13): 2125-2131.

[6] H. Cao, X. Chen and J.R. Yao. Fabrication of an alternative regenerated silk fibroin nanofiber and carbonated hydroxyapatite multilayered composite via layer-by-layer. J. Mater. Sci., 2013, 48 (1): 150-155.

[7] P. Venkatesan, N. Puvvada, R. Dash, *et al*. The potential of celecoxib-loaded hydroxyapatite-chitosan nanocomposite for the treatment of colon cancer. Biomaterials, 2011, 32 (15): 3794-3806.

[8] M.J. Gorbunoff and S.N. Timasheff. The interaction of proteins with hydroxyapatite: III. Mechanism, Anal. Biochem., 1984, 136 (2): 440-445.

[9] M.E. Roy and S.K. Nishimoto. Matrix Gla protein binding to hydroxyapatite is dependent on the ionic environment: calcium enhances binding affinity but phosphate and magnesium decrease affinity. Bone, 2002, 31 (2): 296-302.

[10] S.V. Dorozhkin and M. Epple. Biological and Medical Significance of Calcium Phosphates, Angew. Chem. Int. Edit., 2002, 41 (17): 3130-3146.

[11] T. Matsumoto, M. Okazaki, M. Inoue, *et al*. Hydroxyapatite particles as a controlled release carrier of protein. Biomaterials, 2004, 25 (17): 3807-3812.

[12] Y.S. Pek, S. Gao, M.S.M. Arshad, *et al*. Porous collagen-apatite nanocomposite foams as bone regeneration scaffolds. Biomaterials, 2008, 29 (32): 4300-4305.

[13] E. Landi, F. Valentini and A. Tampieri. Porous hydroxyapatite/gelatine scaffolds with ice-designed channel-like porosity for biomedical applications. Acta Biomaterialia, 2008, 4 (6): 1620-1626.

[14] T. Kawasaki. Theory of chromatography of rigid molecules on hydroxyapatite columns with small loads: IV. Estimation of the adsorption energy of nucleoside polyphosphates. Journal of Chromatography A, 1978, 151 (2): 95-112.

[15] T. Kawasaki. Theory of chromatography on hydroxyapatite columns with small loads: V. Determination of the adsorption energy of the ε-amino group of poly-l-lysine and the manner of adsorption of the molecule. Journal of Chromatography A, 1978, 157 (21): 7-42.

[16] T. Kawasaki, S. Takahashi and K. Ideda. Hydroxyapatite high-performance liquid chromatography: column performance for proteins. Eur. J. Biochcm., 1985, 152 (2): 361-371.

[17] G.Q. Li and M. John. A self-healing smart syntactic foam under multiple impacts. Composites Science and Technology, 2008, 68 (15-16): 3337-3343.

[18] Q.Q. Ni, C.S. Zhang, Y.Q. Fu, *et al*. Shape memory effect and mechanical properties of carbon nanotube/shape memory polymer nanocomposites. Composite Structures, 2007, 81 (2): 176-184.

Chapter 6

Conclusions

6 Conclusions

This dissertation has included the investigation of porous SMPU scaffolds and porous SMPU/nHAP composite scaffolds for the application of bone tissue engineering. Their physical characteristics, mechanical properties, shape recovery behaviors and biological performance have been discussed. Furthermore, the contribution of nHAP particles on porous scaffolds also has been studied. The purpose of these investigations is to design a three-dimensional porous nanocomposite scaffold which possesses high compression resistance, good shape memory recovery ratio and high biocompatibility.

First, in Chapter 1, general introduction of bone defects repair and bone tissue engineering has been presented. Brief summary related to hydroxyapatite and polyurethane has been included. Accordingly, brief outline of preparation and application of hydroxyapatite and polyurethane also has been reviewed.

In Chapter 2, characterization method in this dissertation has been summarized. Apparent density, porosity, shape fixity ratio and shape recovery ratio of scaffold also have been listed out.

In Chapter 3, four SMPU scaffolds (SMPU-200, SMPU-200-100, SMPU-100-50, and SMPU-50) with the three-dimensional porous structure were fabricated via a salt-leaching-phase inverse technique, a unique method to fabric porous structure. The use of different size of NaCl particles to obtain scaffolds with different apertures was investigated. With increasing of the aperture, the porosity of the scaffolds increased from 77.13% to 83.13% and their compression recovery ratio increased from 97.77% to 99.30% at room temperature, but their shape recovery ratio decreased from 95.0% to 91.1% at 55 °C higher than T_g. Moreover, all SMPU

scaffolds promoted cell proliferation on their surface, and the ability increased with the aperture of the scaffold.

In Chapter 4, nHAP particles were fabricated by the liquid phase precipitation method with a rod-like shape and their sizes were ca. 30-40 nm in length and ca. 10 nm in width. Four controllable porous SMPU/nHAP composite scaffolds (SMPU/nHAP-200, SMPU/nHAP-200-100, SMPU/nHAP-100-50 and SMPU/nHAP-50) with three-dimensional structure, which was important for cell growth, were fabricated via the salt leaching-phase inverse technique, a unique method to fabric porous structure. Their physical characteristics, mechanical properties and shape recovery behaviors were investigated. With the increase of the aperture of scaffolds, the porosity, the compression strain (at the strength of 0.12 MPa) and compression recovery ratio of the porous SMPU/nHAP composite scaffolds were increased at room temperature, but their shape recovery ratio was decreased at 55 ℃ higher than T_g. Moreover, these four porous composite scaffolds had a cell proliferation promoting ability and the ability was increased with the increase of the aperture of the scaffolds.

Finally, in Chapter 5, Five-step thermo-mechanical cycle test was used to investigate the shape recovery properties and the contribution of HAP particles was clarified. The effect of nHAP particles in porous SMPU/nHAP composite scaffold was found to enhance the compression resistance by 37%, shorten the compression recovery time by 41% and reduce the tensile resistance by 78%. From the thermo-mechanical cycle test, SMPU/nHAP composite scaffold had good shape fixity property which was more than 97% and higher shape recovery ability which reached more than 99% after 3^{th} cycle of training. Meanwhile, the addition of nHAP

particles improved the proliferation of cells by 13% after 7 days of culture which indicated that the larger the porosity of scaffold was, the easier it was for the cell to adhere to and proliferate on the scaffolds. These results revealed that in minimally invasive surgery and bone repair surgery, this porous composite scaffold could significantly reduce the operative time, promote the bone cell growth and precisely match the irregular boundaries of bone defects. Therefore, this porous SMPU/nHAP composite scaffold design has potential applications for the bone tissue engineering.

Accomplishments

List of publications

Journal publications

[1] **Juhong Yu**, Hong Xia, Akira Teramoto and Qing-Qing Ni. Fabrication and characterization of shape memory polyurethane porous scaffold for bone tissue engineering. Journal of Biomedical Materials Research: Part A, 2017, 105 (4): 1132-1137.

[2] **Juhong Yu**, Hong Xia, Akira Teramoto and Qing-Qing Ni. The effect of hydroxyapatite nanoparticles on mechanical behavior and biological performance of porous shape memory polyurethane scaffolds. Journal of Biomedical Materials Research: Part A. (2018), 106 (1): 244-254.

[3] **Juhong Yu**, Hong Xia and Qing-Qing Ni. A three-dimensional porous hydroxyapatite nanocomposite scaffold with shape memory effect for bone tissue engineering. Journal of Materials Science. (2018), 53: 4734-4744.

Conferences

International

[1] **Juhong Yu**, Hong Xia, Qing-Qing Ni. Fabrication and properties of shape memory polyurethane sponge scaffold for bone tissue engineering. 5th International Conference on Nano and Materials Science, ICNMS 2017 (January 2017, San Diego, USA).

[2] **Juhong Yu**, Hong Xia, Qing-Qing Ni. Fabrication and properties of shape memory polyurethane sponge scaffold for bone tissue engineering (Poster). 4th International Symposium on Advanced Textile Science and Technology cum the International Seminar on Silk Fashion Design and Development Trend, ZSTE (October 2016, Hangzhou, China).

Domestic (Japan)

[1] **Juhong Yu**, Qing-Qing Ni. Fabrication and properties of porous shape memory polyurethane/nano-hydroxyapatite composite scaffold. The 8th Japan Composite Materials Conference, JCCM8 (March 2017, Tokyo, Japan).

[2] **Juhong Yu**, Hong Xia, Qing-Qing Ni. Fabrication and properties of shape memory polyurethane sponge scaffold for bone tissue engineering. The 7th Japan Composite Materials Conference, JCCM7 (March 2016, Kyoto, Japan).

[3] **Juhong Yu**, Hong Xia, Qing-Qing Ni. Development of shape memory polyurethane sponge scaffold for bone tissue engineering. The 53th Japan Society of Mechanical Engineer Conference, JSME (March 2016, Nagano, Japan).

Acknowledgements

It is my pleasure to write this message and express my gratitude to all those who have directly or indirectly contributed to the creation of this work.

First and foremost, I would like to express my sincere gratitude to my supervisor, Prof. Qing-Qing Ni, for giving me the opportunity to do this study in his group and for his exemplary guidance, valuable advice, and constant encouragement throughout my PhD course.

I am also grateful to Prof. Toshiaki Natsuki in the same group as my co-supervisor for his continuous guidance and advice to this work.

I am particularly grateful to Prof. Akira Teramoto for accepting to be a co-supervisor of this work and for the discussion and helpful suggestions and comments for the cell experiments. I also want to thank Mr. Kou Kobayashi in Prof. Akira Teramoto's laboratory for his help on the biological test to this work.

I also want to forward my deepest gratitude to Dr. Hong Xia for her guidance, extensive advises and comments for this research work.

I also want to take this opportunity to express my gratitude to Ministry of education, culture, sports, science and technology (MEXT, Japan) and Global COE of Shinshu University for financial support.

I also want to forward my gratitude to various people, Ms. Makiko Shinotsuka, Ms. Ayako Nishida, Mr. Mitsuhiko Hayashi, Ms. Etsuko Adachi, for their valuable technical support and extensive guidance of experimental equipments on this work.

Special thanks also to all my graduate friends, especially my research group members (Mr. Jinxing Shi, Mr. Yi Wang, Mr. Takuisamu Hashizume, Mr. Melvin Gan Jet Hong, Mr. Yubing Dong, Mr. Ran Li, Mr. Hairong Chen, Mr. Xiaoyu Guan)

of their general advice and input on various things related to research, as well as things not related.

Finally, I dedicate this work to my beloved families, for their understanding and support through the duration of my study. I also would like to thank all my friends at Shinshu University for their help and encouragement.

Thank you

Juhong Yu